Investigation of Rhenium (I) Tri-, Di- , Tetra-Carbonyl Diimine Complexes

Ngai Sum Wong MSci

School of Chemistry

University of Nottingham

Supervisor: Michael George

Thesis submitted to the University of Nottingham for the degree of Master of Research

December 2022

Declaration

I hereby declare that this Thesis and the work presented in it are my own, unless acknowledged otherwise.

Ngai Sum Wong

December 2022

Abstract

Chapter 1

This Chapter provides an introduction to the photophysical and photochemical properties of the complexes of interest in this Thesis highlighting their different excited-states. A brief background of well-studied rhenium (I) tricarbonyl diimine complex is presented to allow comparison to the much less explored rhenium (I) di- and tetra-carbonyl diimine complex which are the subject of this work. A brief outline is given of techniques used within this Thesis namely UV-visible, luminescence and time-resolved infrared (TRIR) spectroscopy. The latter technique is a pump-probe method that has been utilised to investigate the photophysical and photochemical properties of the complexes of interest.

Chapter 2

This chapter focuses on Rhenium dicarbonyl bis-diimine complex and presents new complexes with the form of $[Re(CO)_2(dppp2)_2]^+$. $[Re(CO)_2(dppp2)_2]PF_6$ which have been characterized by FTIR, ^1H NMR, and HRMS. During the synthesis of $[Re(CO)_2(dppp2)_2]^+$, four new tricarbonyl complex intermediates have been synthesized which are $[(OTf)Re(CO)_3(dppp2)]$, $[(CH_3CN)Re(CO)_3(dppp2)]OTf$, $[(OTf)Re(CO)_3(phdo)]$ and $[(CH_3CN)Re(CO)_3(phdo)]OTf$ and have been characterized by FTIR, ^1H NMR, ^{19}F NMR and HRMS. Preliminary emission measurements are reported. Two completely new synthetic routes/methodologies for the synthesis of Rhenium (I) dicarbonyl bis-diimine complex are reported namely to facial-meridianal isomerization and direct CO substitution route. Both methods have been developed and demonstrated that both routes can be used to synthesise bis-diimine complexes.

Chapter 3

This chapter presents the study of temperature effect on photochemistry and photophysics of the Rhenium tetracarbonyl diimine complexes. Five complexes $[Re(CO)_4(4,4'\text{-}R_2\text{-}bpy)]PF_6$ (R= NH_2, CH_3, H, Br or CF_3) have been prepared and probed by temperature-dependent emission measurement. The photophysics and photochemistry of these complexes are governed by the formation of two mixed excited states, namely State I and State II. The State II excited-state, decays on the microsecond timescale and results in the photodissociation of a CO ligand and the interplay between these states governs both the decay. The result suggests that the temperature effect that the CO photodissociation reaction of the complexes may have two reaction barriers, the first barrier is in between state II ^{3}ILCT and ^{3}MLCT state and the second barrier is in the ^{3}MLCT state and the photoproduct. The temperature effect and the solvent effect affected both barriers. The substituents on the bpy ligand affected the energy of ^{3}MLCT state which will enhance or inhibit the temperature effect and CO dissociation.

Chapter 4

The experimental methods and spectroscopic techniques used throughout this Thesis are described in this Chapter. This includes detailed descriptions of the equipment used, along with procedures and materials used.

Acknowledgement

First and foremost, I like to thank my supervisor, Professor Mike George, for all his help and support throughout my MRes. During the year, he gave his bigger support when I got surgery and showed me how to learn from negative results. Thank you so much. I am so glad you be my supervisor.

I owe a tremendous amount of thanks to Natalia Dyachenko. In the lab, she helped me a lot with synthesizing, without her I would never have learnt how to synthesise the compounds. Also, she gave me a lot of advice for my lab skill and Thesis. Thank you. I would like to thank Dr Katherine Reynolds. She showed me a lot of knowledge of rhenium complex photophysics. Also, she taught me how to use the spectroscopy equipment in the lab, especially for running temperature-dependent emissions. Thank you. I would also like to thank Dr. Ashley Love and Matthew Pratley for helping me to set up the photoreactor, without them I am not able to run the reaction. Thank you. I also need to give a big thanks to Dr. Rodolfo Teixeira for helping me to proofread my thesis, without him my thesis would be full of mistakes and very raw. Thank you

I also need to thank the people (too many names) helping me throughout this year in the lab and outside. Also, I thank all members of the George group, thank you for all the tea in Sue's, for the jokes in the Fort. I have been studying in Nottingham for nearly five years, from undergrad (MSc) to MRes. Without all the people who I met and helping me, I wouldn't be able to get this far. Thank you.

Finally, a very special thank you to all my friends and family, who have supported me all the time. Especially to my girlfriend and my parents. Without their support, I don't think I would have done it this far. Thank you so much.

Abbreviations

Commonly used abbreviations in this report are defined below. Abbreviations that are not listed below are used infrequently and therefore defined within the body to text.

bpy	2,2-bipyridine
dppz	dipyrido-[3,2-a:2’,3’-c]-phenazine
dppp2	pyrido[2',3′:5,6]pyrazino[2,3-f][1,10]phenanthroline
DFT	density functional theory
CT	charge transfer
CH_2Cl_2 (DCM)	dichloromethane
CH_3CN (MeCN)	acetonitrile
ILCT	intra-ligand charge transfer
IR	infrared
LF	Ligand Field
MLCT	metal-to-ligand charge transfer
^{3}MLCT	triplet metal-to-ligand charge transfer
NMR	nuclear magnetic resonance
OTf	Triflate ion
phdo	1,10-Phenanthroline-5,6-dione

phen	1,10-phenanthroline
py	pyridyl
TRIR	time-resolved infrared spectroscopy
THF	tetrahydrofuran
UV-vis	ultraviolet-visible
ν(CO)	carbonyl stretching frequency

Contents

1. Chapter 1

Introduction

The properties and reactivity of excited states have been exploited in many applications including photocatalysis,[1-4] solar energy conversion,[5-9] organic light-emitting diodes[10, 11] and luminescent probes.[12-14]

Many transition metal complexes possess long-lived excited states. The chemical environment is important as it affects which states are accessible to photochemical processes. This is particularly important as in such systems as the nature of the metal and ligands can mean that there are a number of closely lying states and the interplay between them is strongly dependent on the environment.[15]

The most well-studied type of the excited state is metal-to-ligand charge transfer (MLCT) which involves the transfer of an electron from the dπ system of the metal to one of the π^*L orbitals of the ligand, resulting in oxidation of the metal and reduction of the ligand. Depending on the ligand, one of several π^*L molecular orbitals (MOs) can be populated, potentially resulting in a mixture of different MLCT states. A ligand-to-metal charge transfer (LMCT) occurs when an electron occupying a ligand πL' or πL orbital is promoted to the metal dπ* system. Electronic transitions centred on one or more ligands can also occur. Transitions centred on a single ligand are generally referred to as ($\pi \rightarrow \pi^*$). If the donor and acceptor MOs are situated over spatially similar regions the associated change in dipole is small; if the electron is transferred to a spatially distinct part of the ligand the change in dipole tends to be larger. The latter is also referred to as a ligand-centred charge transfer (LCCT) transition. Electronic

transitions involving a formal oxidation of one ligand and reduction of another are referred to as intraligand charge transfer (ILCT) transitions or sometimes ligand-to-ligand charge transfer. While the metal is not formally involved in these transitions, it can play a significant role in their mediation. Metal-centred d-d transitions are often present but at low intensities, as they are Laporte forbidden, and thus tend to be masked by stronger transitions in the same spectral region. It should be noted that these transitions represent limiting cases; in reality, mixed-character transitions comprising two or more states are often encountered. One of the key features for many applications is for charge-separation to occur and thus the natures of the excited states present are crucial with considerable attention has been directed to understanding and controlling them.[14] Charge-separated excited states of transition metals are both good oxidants and reductants. For example, photoexcited $[Ru(bpy)_3]^{2+}$ is commonly used as a photoredox catalyst and a further advantage is the fact that it can exist and shows stability in multiple oxidation states, and this is important for the prolonged operation of photocatalytic systems or light-harvesting systems such as dye sensitized solar cells, where electronically reduced or oxidized intermediates can persist for a significant amount of time.[16, 17]

This Thesis focusses on studying the synthesis and photophysics of Rhenium diimine carbonyl complexes. Tricarbonyl complexes containing the (diimine)$Re(CO)_3$ moiety are widely investigated and this Thesis explores the less studied dicarbonyl and tetracarbonyl analogues. This introduction focuses on the background of complexes containing the (diimine)$Re(CO)_3$ moiety together with a brief outline of the techniques used in this work.

1.1. Rhenium carbonyl diimine complexes

The Rhenium (I) provides a d^6 metal centre which has ideal properties for photosensitive.[18-20] Carbonyl Ligands are well-known reporting groups for probe processes by FTIR Spectroscopy.[21] Finally, diimine ligands provide a platform for modification of the structure allowing to tune the photophysics of the complex.

1.1.1. Diimines ligands

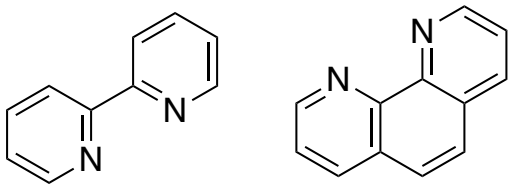

Figure 1.1 The structure of 2,2'-bipyridine (bpy)(left) and 1,10-phenanthroline (phen)(right).

Different diamine ligands can affect the photophysics and photochemistry of metal complexes.[22] These ligands, such as 2,2'-bipyridine (bpy) and 1,10-phenanthroline (phen) (Figure 1.1), can have unique photophysical properties. They show in different emission states, redox potentials, and excited states, as well as relaxation pathways.[23] Some ligands provide unique photophysical properties and the hydrophobic DNA intercalator dipyridophenazine (Figure 1.2) is an example relevant to this work.

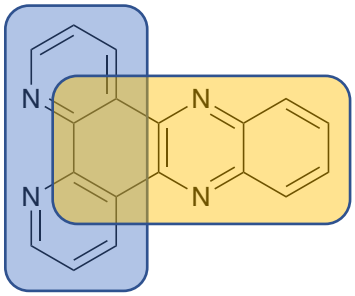

Figure 1.2 The structure of dipyridophenazine (dppz) ligand with indicated phenanthroline (phen) system (blue) and a phenazine (phz) system (yellow)

The dipyridophenazine (dppz) ligand can be considered as a fusion of two systems, phenanthroline (phen) (Figure 1.2, blue) and phenazine (phz) system (Figure 1.2, shown in yellow). Metal complexes with dipyridophenazine are characterized by two or three close energy excited states, and such are able to act as sensors because of the interplay between these states. There are two MLCT states for $[Ru(bpy)_2(dppz)]^{2+}$ with different acceptor MOs on the dppz ligand namely MLCT(phen) and MLCT(phz) state $[Ru(bpy)_2(dppz)]^{2+}$ show the so-called light switch effect caused by the excited states associated with the dppz.[16] The complex is non-emissive in an aqueous solution, but in the presence of DNA the system becomes emissive. The reasons for this are that the excited states present are modulated by environmental effects and, as such, complexes using this ligand are well-known for intercalation with double-helical DNA and other biomolecules.[24]

1.1.2. Rhenium(I) tricarbonyl diimine complexes

Rhenium(I) tricarbonyl diimine complexes have been extensively reported in the literature due to their strong emission and photocatalytic properties, which makes them suitable components for photophysical applications and photochemical catalytic reactions.[25] One of the most common and stable complex structures is *fac*-$[(L)Re(CO)_3(N,N)]^n$ shown in Figure 1.3 where N,N is a diimine ligand; L is a halogen, an alkyl group, or a pyridyl ligand; n is the charge of the complex. Based on different L ligands, the complex could be having charge, for example, L= pyridyl ligand, *fac*-$[(py)Re(CO)_3(N,N)]^+$.

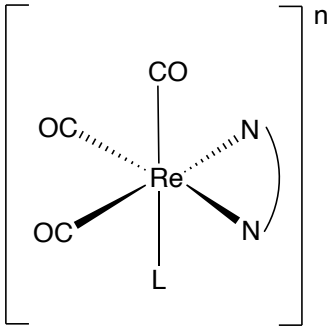

Figure 1.3 The general structure of Rhenium(I) tricarbonyl diimine complexes where N,N is a diimine ligand; L is a halogen, an alkyl group, or a pyridyl ligand; n is the charge of the complex.

1.1.2.1. Synthesis of *fac*-[(L)Re(CO)$_3$(N,N)]^n

The general synthetic route of *fac*-[(L)Re(CO)$_3$(N,N)]^n is shown in Scheme 1.1. Re(CO)$_5$X, where X is halogen (Cl or Br), and the target diimines chromophore both are added to toluene for four hours reflux in the dark, under Ar or N_2 condition to get *fac*-[(X)Re(CO)$_3$(N,N)].[26] For further modification, use silver salt such as AgOTf, $AgBF_4$ or $AgPF_6$ to react with *fac*-[(X)Re(CO)$_3$(N,N)] and the L ligands, where L is the ligands wanting to substitute the X position such as pyridyl, added in one pot or in separate step to produce *fac*-[(L)Re(CO)$_3$(N,N)]^n.[26, 27]

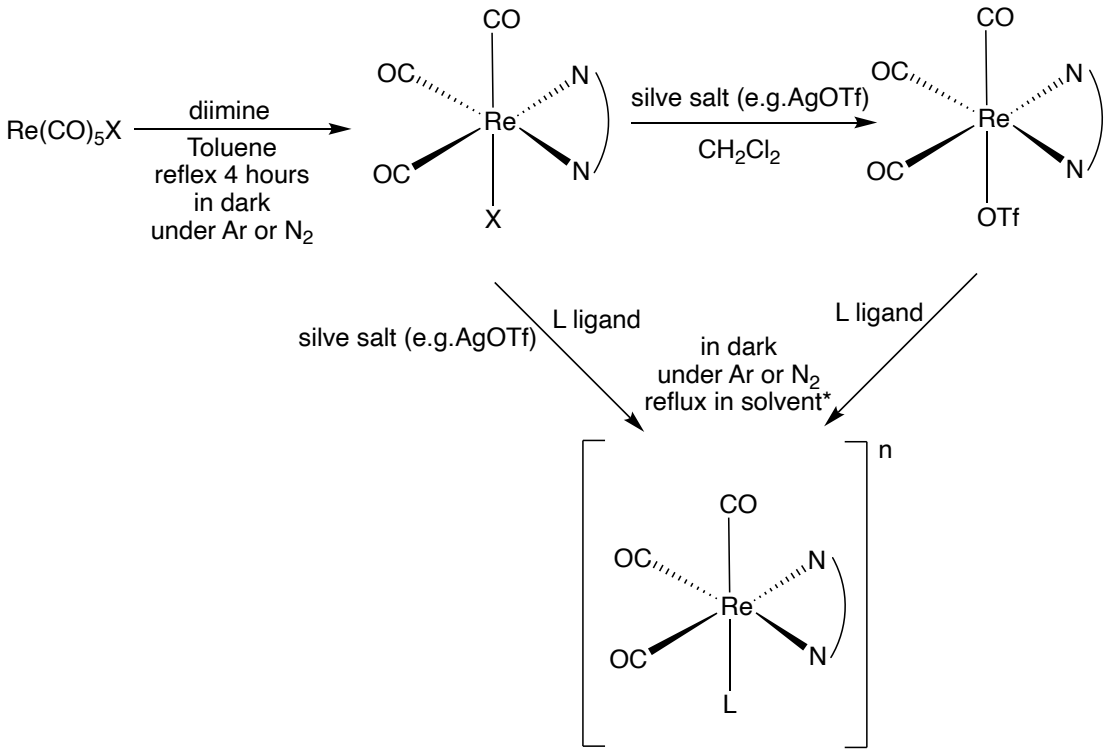

Scheme 1.1 The general synthetic route of *fac*-[(L)Re(CO)$_3$(N,N)]^n. X is halogen (Cl or Br). L is the ligand that wants to substitute the X position. n is the charge of the complex. *The solvent could be any, based on the solubility of the complex and ligand.

1.1.2.2. FTIR spectra of *fac*-[(L)Re(CO)$_3$(N,N)]^n

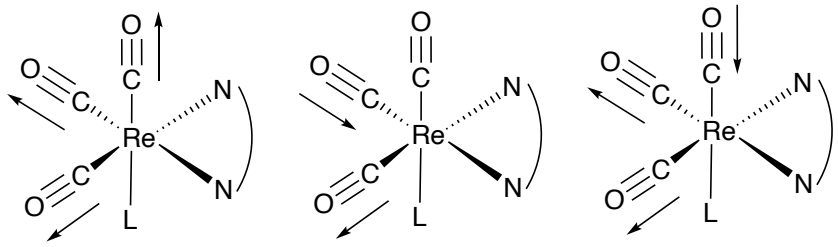

A'(1) A'' A'(2)

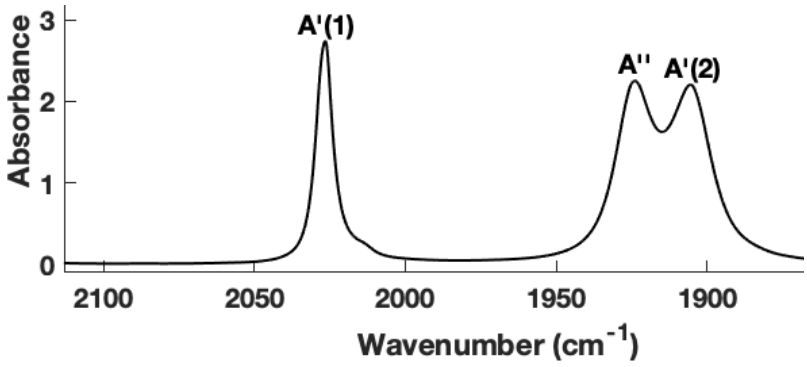

Figure 1.4 The schematically FTIR spectra of *fac*-[(L)Re(CO)$_3$(N,N)]^n.[28]

FTIR spectra of *fac*-[(L)Re(CO)$_3$(N,N)]^n saw three IR bands due to CO stretching vibrations, ν(CO) in the range of about 1900-2040 cm^{-1} which are schematically shown in Figure 1.4. The highest band corresponds to a totally symmetric in-phase ν(CO) vibration, denoted A'(1). The two lower bands belong to the out-of-phase totally symmetric A'(2) vibration and the asymmetric vibration of the equatorial CO ligands, A''. These two vibrations occur at similar energies, and the corresponding bands' separation depends on the axial ligand L. The comparison of the CO stretching vibration frequencies between complexes can be correlated to the electron donating ability of each ligand bound to the metal centre. Two well-developed bands are observed in complexes with halide-, O- or P-coordinated ligands. On the other hand, the A'(2) and A'' bands are merged into one broad band if L is N-coordinated.[28, 29]

1.1.2.3. ^{1}H NMR spectra of *fac*-[(L)Re(CO)$_3$(N,N)]^n

The ^{1}H NMR of the diimine ligand will shift to a higher position but remain similar in pattern comparable to the chromophore ligand itself because the electron density is donating to the metal centre, which will deshell the protons. Also, the facial-complex will not affect the ligand symmetry too much, and the ^{1}H NMR will show the peak symmetry as a pure ligand. [30, 31]

1.1.2.4. Photophysic of Rhenium(I) tricarbonyl diimines complexes

The photophysic of rhenium(I) tricarbonyl diimines complexes is elaborate. Usually, they can separate from their lowest excited state, a ligand field (LF), metal-to-ligand charge transfer (MLCT), ligand-to-ligand charge transfer (LLCT), sigma-bond-to-ligand charge transfer ($\sigma \rightarrow \pi^*$), and intraligand (IL) excited states. However, density functional theory (DFT) and time-dependent density functional theory (TD-DFT) have provided shed light on these states and show that the excited state may not be 'pure'. For example, $[(Cl)Re(CO)_3(bpy)]$, by the calculation, shows the highest occupied molecular orbital (HOMO) contained 50% or greater Re d-orbital character along with about 20% contributions each from CO and Cl. Also, the lowest unoccupied molecular orbital (LUMO) consists of 80% or greater diimine ligand π^* character. Therefore, the lowest energy optical transition was assigned as a metal-ligand-to-ligand charge transfer transition (MLLCT).[22]

Furthermore, by different diimines ligands, the photophysics is tunable and provides unique photophysical properties, for example, rhenium(I) tricarbonyl dipyridophenazine complexes.

1.1.2.4.1. Photophysics of Rhenium(I) Tricarbonyl Dipyridophenazine Complexes

The photophysics of $[(L)Re(CO)_3(dppz)]^n$ complexes are similar to those of other rhenium tricarbonyl diimine analogues; however, it is not possible to simplify the electronic structure because the dppz ligand is made up of several close-lying orbitals that inevitably forms chromophores with metal. The possible excited states of $Re(CO)_3$-

dppz complexes can be MLCT and π-π*IL(dppz) in nature. Due to dppz ligands two-system, the ^{3}MLCT can either be 'phen' in nature, ^{3}MLCT(phen) which is emissive or 'phz' in nature,^{3}MLCT(phz) which is non-emissive and is referred as a dark state.[21, 32] The emissive ^{3}MLCT(phen) should be the lowest-lying state. However, following variable temperature emission measurements, it indicated that the non-emissive ^{3}MLCT(phz) was observed to be the lowest state in all solvent investigated. However, the state is characterized by having low entropy, which means its population in an organic solvent at ambient temperatures is redecided because of the dominance of TΔS. The population between energetic factors favours the–dark ^{3}MLCT(phz) and entropic factors favour–higher-lying emissive ^{3}MLCT(phen) states that can be changed by either temperature or solvent. This is also referenced as a light switch effect and described above. [33]

The UV-vis absorption spectra of $Re(CO)_3$-dppz complexes usually show ^{1}π-π* IL(dppz) and ^{1}MLCT(phen) transition states.[21] The two states are close in energy, so they are populated simultaneously. However, in some cases having substitutions in dppz ligand such as dppz-$PhNMe_2$, results in singlet intra-ligand charge transfer (^{1}ILCT).[34, 35] Therefore, after the absorption of light, the singlet excited state is only short-lived before it undergoes ICS to the triplet state or other excited states.[21]

According to the emission study, the spectra usually shows that the lowest excited have ^{3}MLCT(phen/phz) or ^{3}π-π*IL character. The $Re(CO)_3$-dppz complexes can be separated into two extreme cases: ^{3}MLCT can be lowest excited state or ^{3}π-π*IL can be a lowest excited state. However, because ^{3}MLCT(phen/phz) and ^{3}π-π*IL are close lying in energy, it has to consider the interplay between ^{3}π-π*IL(dppz), ^{3}MLCT(phen) and ^{3}MLCT(phz).[21]

Using TRIR measurement and of *fac*-$[Re(CO)_3(dppz)(py)]^+$, *fac*-$[Re(CO)_3(dppz)(Cl)]$ and *fac*-$[Re(CO)_3(dppz\text{-}F_2)(Cl)]$ as an example to show the possible interplay cases between $^3\pi$-π^*IL(dppz), ^{3}MLCT(phen) and ^{3}MLCT(phz). The case of *fac*-$[Re(CO)_3(dppz)(py)]^+$ in CH_3CN solvent shows the interplay between $^3\pi$-π^*IL(dppz) and ^{3}MLCT(phz) state by ns-TRIR measurement (Figure 1.5). From 50ps after excitation, the TRIR shows the v(CO) stretching region at 2023, and 1914 cm-1 confirmed as the $^3\pi$-π^*IL(dppz) state, and up to 1000 ps, the $^3\pi$-π^*IL(dppz) state is the only species present with no observed decay. However, in ns-TRIR measurement show that 600 ns after excitation, the formation of three net v(CO) band at 2016, 2060 and 2120 cm-1 is observed. The band shift show $^3\pi$-π^*IL(dppz) state partially decays to a relaxed equilibrium of $^3\pi$-π^*IL(dppz) and ^{3}MLCT(phz) excited states. By 77K ns-TRIR measurement, there is no MLCT band formation, so it is confirmed that $^3\pi$-π^*IL(dppz) state is the lowest excited state. In this case shows, there is equilibrium happening between $^3\pi$-π^*IL(dppz) and ^{3}MLCT(phz) excited states on a nano-timescale.[36]

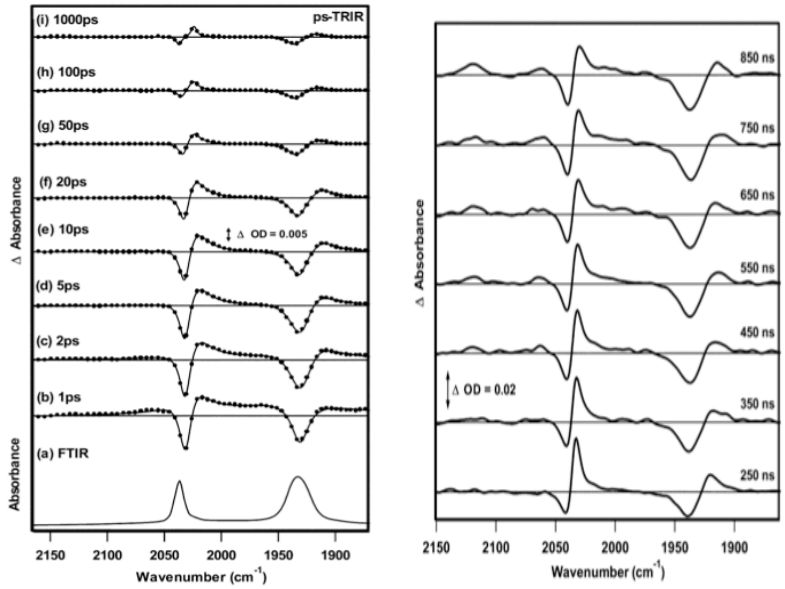

Figure 1.5 FTIR spectrum of fac-$[Re(CO)_3(dppz)(py)]$ and ps-TRIR spectra obtained between 1 and 1000 ps following 400 nm excitation in CH_3CN(left) A series of step-scan FTIR spectra of fac-

[$Re(CO)_3(dppz)(py)$] in CH_3CN obtained from 250 to 850 ns following 355 nm excitation(right). It is adapted from the reference [36]

The lowest excited state of *fac*-[$Re(CO)_3(dppz)(Cl)$] is also $^3\pi$-π^*IL(dppz) but shows a different case. In ps-TRIR measurement in CH_3CN show that appears $^3\pi$-π^*IL(dppz) and ^{3}MLCT(phen) after excitation. About ten ps after excitation, the $^3\pi$-π^*IL(dppz) remind unchanged, but ^{3}MLCT(phen) band shows shifting that means ^{3}MLCT(phen) excited state partially decays to the relaxed equilibrium of ^{3}MLCT(phen) and ^{3}MLCT(phz) states. Also, the emission study in CH_3CN shows the emission from ^{3}MLCT characters. Because the lowest state is $^3\pi$-π^*IL(dppz) but an emission from ^{3}MLCT(phen) state, it is possible that happen an interaction between ^{3}MLCT(phen) and $^3\pi$-π^*IL(dppz) states. In this case, it shows the possibility to have either equilibrium or conversion between ^{3}MLCT(phen) and $^3\pi$-π^*IL(dppz) states and equilibrium between ^{3}MLCT(phen) and ^{3}MLCT(phz) states.[33]

The case of *fac*-[$Re(CO)_3(dppz\text{-}F_2)(Cl)$] has shown another situation. The ps-TRIR measurement in CH_3CN solvent only show ^{3}MLCT(phz) excited states; however, in ps-TRIR measurement in CH_2Cl_2 solvent show ^{3}MLCT(phz) state decays to the relaxed equilibrium of ^{3}MLCT(phen) and ^{3}MLCT(phz) states. Also, the $^3\pi$-π^*IL(dppz) states are not shown in the TRIR measurement. Compare with the case of *fac*-[$Re(CO)_3(dppz\text{-}Br_2)(Cl)$] in CH_2Cl_2 solvent that has a similar situation, but ps-TRIR show *fac*-[$Re(CO)_3(dppz\text{-}Br_2)(Cl)$] happen $^3\pi$-π^*IL(dppz) state convert to ^{3}MLCT(phz) states within few picoseconds. Maybe, the case of *fac*-[$Re(CO)_3(dppz\text{-}F_2)(Cl)$] can cause conversion between $^3\pi$-π^*IL(dppz) states and ^{3}MLCT(phz) states in faster timescale.[37, 38]

In conclusion, the case above has shown the possible activities that the interplay

between $^3\pi$-π^*IL(dppz), ^{3}MLCT(phen) and ^{3}MLCT(phz). Between them equilibrium can happen or conversion. Also, it needs to be noted that all of the triplet states can be populated directly from the singlet state. Moreover, to conclude all the cases above, it is good to know that different substrates on dppz ligand, different ancillary ligands and different solvents may affect the population and interplay between different lowest triplet excited states.

1.1.2.4.1.1. Manipulation of $Re(CO)_3$-dppz Complexes Excited States

To tune the excited states in dppz complexes, there is mainly three-way to achieve it. First, it is the substitution of dppz on 11 and 12 positions. The second one is to change the ancillary ligands, and the final is the solvent effect and biomolecule intercalation on the $Re(CO)_3$-dppz complexes. The effect on the excited state is shown in Figure 1.6.

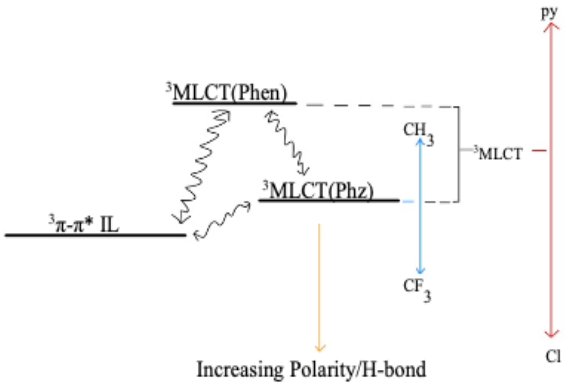

Figure 1.6 The relatively energy the coordinate base on different substrate at 11 and 12 positions in the dppz ligands(blue), different ancillary ligands(red) and different medium(yellow). (not in scale).[21]

By putting different substituents at position 11 and 12 of the dppz ligand, will result in a change to the phz ring system. As a result, when dppz-X_2 (X= CH_3, H, Br~F, Cl, CF_3 and NO_2), has the most electron-donating group on dppz, there is an increase in the energy on ^{3}MLCT(phz) states. On the other hand, when the most electron-withdrawing

group is on dppz, there is decreased in the energy on ^{3}MLCT(phz) states (Figure 1.6, shown in blue arrow). Using a *fac*-[Re(CO)$_3$(dppz-X$_2$)(py)]$^+$ (X=CH$_3$, H and F) and *fac*-[Re(CO)$_3$(dppz-X$_2$)(Cl)] (X=CH$_3$, H, F, Cl and CF$_3$) as examples, the ns-TRIR of *fac*-[Re(CO)$_3$(dppz-X$_2$)(py)]$^+$ in with different substituents on the dppz shows different time delay on the equilibrium between ^{3}MLCT and ^{3}π-π*IL(dppz). For the electron-donating group (X=CH$_3$), the equilibrium appears 850 ns after excitation, but when it is an electron-withdrawing group (X=F), the equilibrium appears 450 ns after excitation. Whereas for the non-substituted complex (X=H), the equilibrium appears 600 ns after excitation. The closer in energy, the ^{3}MLCT(phz) excited states are to ^{3}π-π*IL(dppz) the faster the equilibrium appears. In the other example, *fac*-[Re(CO)$_3$(dppz-X$_2$)(Cl)] (X = CH$_3$, H, F, Cl and CF$_3$), the ps-TRIR spectra, shown in Figure 1.7, showed the 100 ps time delay for all the different substituents on the dppz ligand. In electron-donating group (X=CH$_3$) that is show ^{3}MLCT(phen) and ^{3}π-π*IL(dppz); however, the electron-withdrawing group (X=CF$_3$) only shows the ^{3}MLCT(phz) excited state to be the lowest. In this case, it shows the energy gap between ^{3}MLCT(phz) and ^{3}MLCT(phen) becomes larger, and it is more likely that the ^{3}MLCT(phz) state is populated. In conclusion, these two cases have shown that the ^{3}MLCT(phz) excited states will become lower in energy or higher in energy based on the electronic effect of the substrate. Also, note that the ^{3}MLCT(phen) excited is not affected.[33, 38]

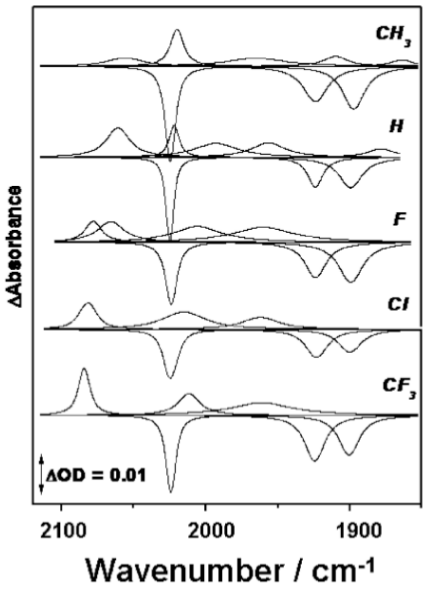

Figure 1.7 TRIR spectra of fac-[$ReCl(CO)_3(dppz\text{-}X_2)$] obtained 100 ps following 400 nm excitation of CH_2Cl_2 solutions at room temperature. It is adapted from the reference [33].

The other way to manipulate the excited states is to change the ancillary ligands. As a result, L= py, 4-Me_2N-py and Cl, this will affect the energy of ^{3}MLCT. In weak-field ligand, e.g. L =Cl, the energy of ^{3}MLCT state will be decreased, which $^3\pi$-π^*IL(dppz) is more close in laying with ^{3}MLCT. On the other hand, in the strong-field ligand, e.g. py, the energy of ^{3}MLCT will be increased, which $^3\pi$-π^*IL(dppz) is less close in laying with ^{3}MLCT (Figure 1.6, shown in red arrow). Using *fac*- [$Re(CO)_3(dppz\text{-}Cl_2)(L)$] (L= py, 4-$Me_2$N-py and Cl) as example. According to the ps-TRIR measurement, as shown in Figure 1.8, the lowest excited state of the complexes (L= py) is $^3\pi$-π^*IL(dppz). However, on the increase the electron donating on py ligand (4-Me_2N-py), the lowest excited state becomes ^{3}MLCT and $^3\pi$-π^*IL(dppz) in close lying. Moreover, the L=Cl, the lowest excited state shows only ^{3}MLCT excited state. As the case shows, on changing the ancillary ligands will move the energy coordinates of ^{3}MLCT (phen/phz) more toward or far way $^3\pi$-π^*IL(dppz) excited state.[32]

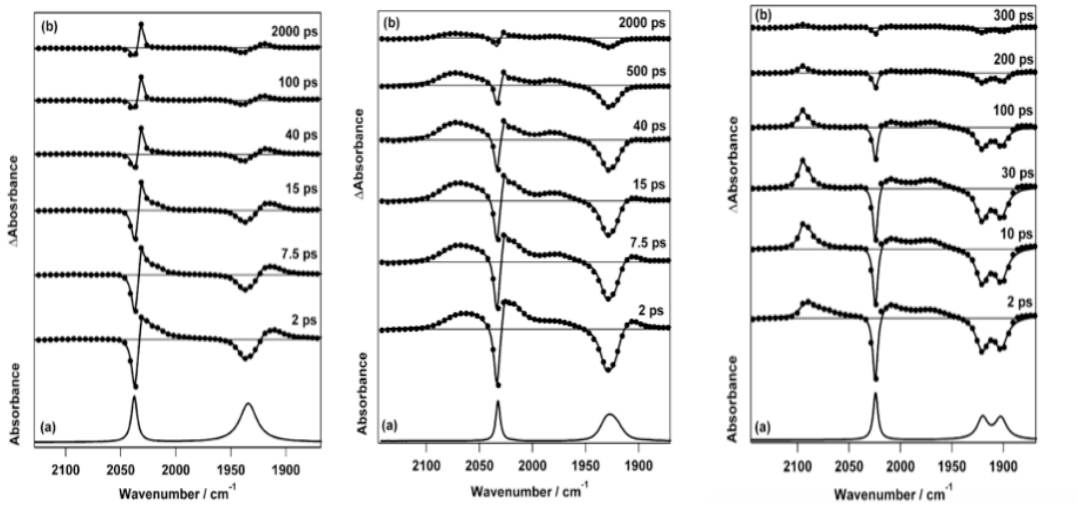

Figure 1.8 FTIR spectra of *fac*-[$Re(CO)_3$(dppz-Cl_2)(py)]$^+$ (left), *fac*-[$Re(CO)_3$(dppz-Cl_2)(4-Me_2N-py)]$^+$ (middle) and *fac*-[$Re(CO)_3$(dppz-Cl_2)(Cl)](right) in CH_3CN at room temperature. (b) Series of TRIR spectra obtained between 2 and 2000 ps after 400 nm excitation of this solution. It is adapted from the reference[32].

The third way to tune the excited state of $Re(CO)_3$-dppz complexes is the solvent effect. For example, when the *fac*-[$Re(CO)_3$ dppz-F_2)(py)]$^+$ complex in non-protic solvents, the complex shows the ^{3}π-π*IL(dppz) is in the lowest excited state and having equilibrium between ^{3}MLCT(phz) and ^{3}π-π*IL(dppz) states on a nanosecond timescale; however, in aqueous solution, the properties change. The complex exhibits a ^{3}MLCT(phz) and ^{3}π-π*IL(dppz) excited state on a picosecond timescale. The solvent change from non-polar to polar or having hydrogen bond interaction with the free N atom in dppz ligands will change the photophysics properties of $Re(CO)_3$-dppz complexes. They usually lower the ^{3}MLCT (phz) state in lower energy when the polarity and hydrogen bond incensing in the solvent(Figure 1.6, shown in yellow arrow).[38, 39]

1.1.2.5. Photochemistry of Rhenium(I) tricarbonyl diimines complexes

In this section will focus on Photochemical Ligand Substitution (PLS) and Facial-Meridianal Isomerization (FMI) and this introduction is given as the section below is used to develop a new synthetic route to highly substituted rhenium diimine complexes.

1.1.2.5.1. Facial-Meridianal Isomerization (FMI)

In 2007, Sato *et al*. reported first time for photochemical synthesis of mer-[(Cl)Re(CO)$_3$(bpy)]. They reported that *fac*-[(Cl)Re(CO)$_3$(bpy)] was irradiated under a CO atmosphere by high energy UV light (313nm) and, even under an Ar atmosphere in the absence of CO, synthesis of *mer*-[(Cl)Re(CO)$_3$(bpy)] is working. Also, they point out that irradiation using 366 nm instead of 313 nm light did not give any meridianal product. This shows the excited state for the FMI is not the same as PLS (will more detail in Section 1.1.2.5.2). Nevertheless, they isolated *mer*-[(Cl)Re(CO)$_3$(bpy)] and analyse the complex by FTIR and NMR. Also, they point out that the meridianal isomer is not stable in the solvent, but still is useful starting material for the synthesis of *cis,cis*-[(L)(Cl)Re(CO)$_2$(bpy)]-type complexes.[40]

fac-[(Cl)Re(CO)$_3$(bpy)] and *mer*-[(Cl)Re(CO)$_3$(bpy)] show very different in FTIR and ^{1}H NMR measurement. Sato et al. reported that eight aromatic proton signals are observed for *mer*-[(Cl)Re(CO)$_3$(bpy)], but only four are observed for *fac*-[(Cl)Re (CO)$_3$(bpy)] because there is a mirror plane between the two pyridine rings of the bpy ligand. Moreover, the CO stretching bands in the IR spectrum of *mer*-[(Cl)Re(CO)$_3$(bpy)] have three peaks with different strengths, but *fac*-[(Cl)Re(CO)$_3$(bpy)] have three peaks with same strengths. Figure 1.9 shows the different in FTIR and ^{1}H NMR measurement adapted from Sato et al. paper.[40]

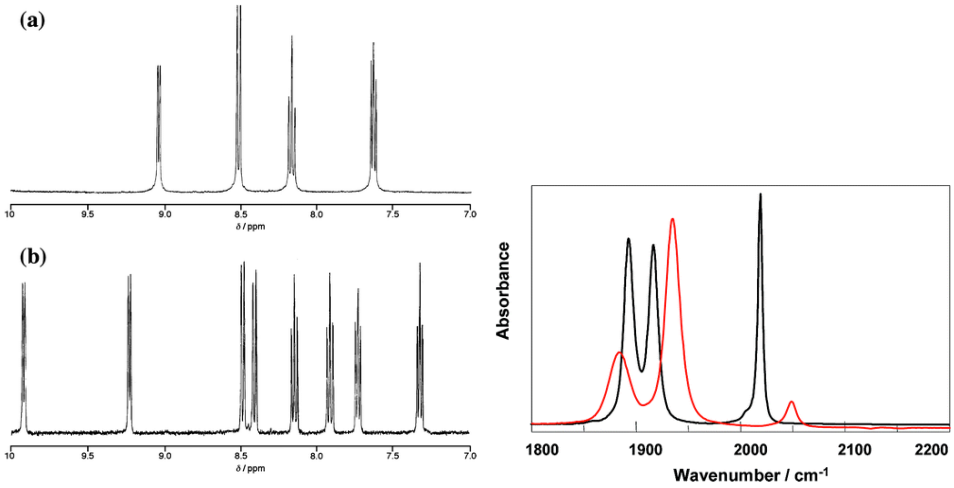

Figure 1.9 The different of *fac*-[(Cl)Re(CO)$_3$(bpy)] (top left, black) and *mer*-[(Cl)Re(CO)$_3$(bpy)] (bottom left, red) in FTIR(right) and ^{1}H NMR(left) spectra, adapted from the reference[40]

1.1.2.5.2. Photochemical Ligand Substitution (PLS)

Photochemical ligand substitution (PLS) reactions of many transition-metal complexes are known to proceed via a ^{3}LF excited state that is thermally accessible from a ^{3}MLCT state, especially when the photosubstitution involves dissociative mechanisms.[22, 28]

Koike *et al.* in 2002 reported a type of *fac*-[(L)Re(CO)$_3$(N,N)]^n which is *fac*-[(PR$_3$)Re(CO)$_3$(4,4'-X$_2$-bpy)]^n (4,4'-X$_2$-bpy is 4,4'-X2 −2,2'-bpy, where X is H, CF$_3$, OEt or Ph, and PR$_3$ is a tertiary phosphine or phosphite) has efficient photochemical ligand substitution. They found the complex to yield substitution trans to the axial PR$_3$ group by CO loss and the Rhenium(I) dicarbonyl diimine complexes, cis, trans-[(PR3)(L)Re(CO)$_2$ (4,4'-X$_2$-bpy)]^n, were formed with chloride, py or CH$_3$CN as the entering group. Labelling (^{13}CO) studies demonstrated that the axial CO, which is trans to the phosphorus ligand, was indeed labilized, consistent with a dissociative mechanism and an associated excited state kinetic trans-effect.[22, 28, 41]

On the other hand, Sato *et al.* reported that the PLS reactions of *fac*–[(Cl)Re(4,4'-X$_2$-

bpy)$(CO)_3$] (X = H, MeO, NH_2, CF_3) are induced by high-energy (UV light) photoexcitation and yielded solvato complexes, *cis,cis-/cis,trans*-[(solvent)(Cl)Re(4,4'-X_2-bpy))$(CO)_2$]. Mechanistic studies, including TRIR measurements, clearly reveal that the PLS reaction does not proceed via the lowest ^{3}MLCT state, but instead it occurs via higher vibrational levels of the ^{1}MLCT or higher electronic states, such as $^1\pi$ - π *, and higher-lying Re→bpy and Re→CO ^{1}MLCT states. The TRIR measurements have indicated that the CO ligand dissociates with sub-picosecond rates after excitation, leading to vibrationally hot CO-loss photoproducts after 1 ps of excitation and the relaxed photoproduct forms during 50–100 ps after excitation.[22, 28, 41, 42]

Nevertheless, Sato *et al.* in 2012 reported that the photochemistry of *fac*–[(Cl)Re(bpy)$(CO)_3$] to yield *mer*-[(Cl)Re(bpy)$(CO)_3$], *cis*, *cis*-[(solvent)(Cl)Re(bpy)$(CO)_2$] or *cis*, *trans*-[(solvent)(Cl)Re(bpy)$(CO)_2$] dependent on the concentration or combination of solvent, the effect of the presence of CO, and the temperature dependence. Also, they found that the mechanism of the photochemical reactions for all three products are different.[43] The mechanism is shown in Figure 1.10.

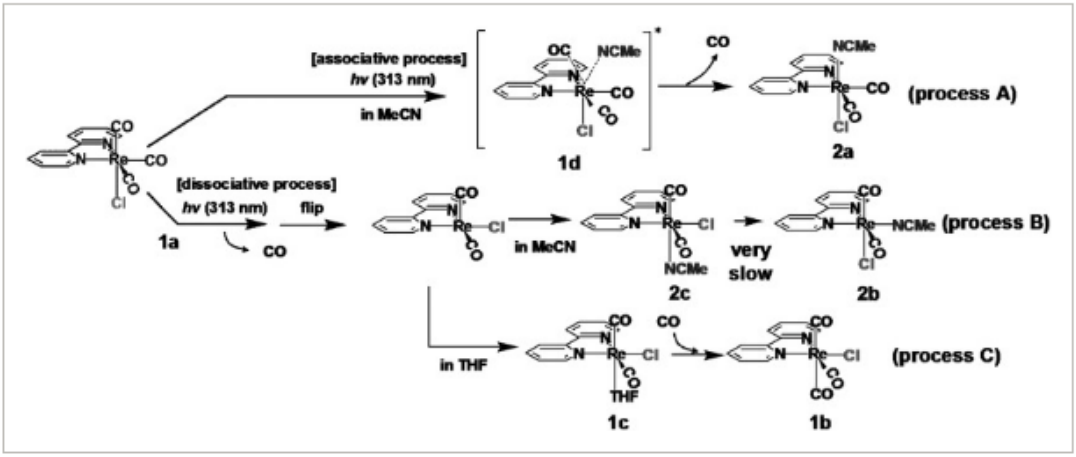

Figure 1.10 Mechanism of the photochemical reactions of fac–[(Cl)Re(bpy)$(CO)_3$] using 313nm light in MeCN (processes A and B) or THF (process C). It is adapted from the reference[43]

1.2. Spectroscopy tools

To study the chemistry and photophysics of the complexes and their reactions, the application of different spectroscopic tools becomes significant. They produce different insights into the nature of the excited state and insight into the subsequent dynamics and reactivity.

Fourier-transform Infrared (FTIR) spectroscopy and nuclear magnetic resonance (NMR) spectroscopy were used in this Thesis, especially in Chapter 2, which was used to investigate the new synthesis complexes and new synthetic route. They can provide the complex and ligand structure in which orientation and isomer.

UV-vis Absorption (UV-vis) and Luminescence spectroscopy were used in Chapters 2 and 3, showing the electronic transition and emission states, respectively.[36] Furthermore, in Chapter 3, temperature-dependent emission and lifetime were applied, which gave more insights into different excited states and how temperature affects them.

Time-resolved Infrared (TRIR) spectroscopy was not used in any chapter; however, Chapters 2 and 3 have to compare results with previous work in the group, which they used to monitor the movement of electrons in different excited states or reaction coordinates.[44] Therefore, including some basic information on TRIR can better understand the Chapters.

1.2.1. UV-vis absorption and luminescence spectroscopy

1.2.1.1. UV-vis absorption spectroscopy

The ultraviolet region of the spectrum is generally considered to range from 200 to 400 nm, and the visible region from 400 to 800 nm. Transition metal complexes commonly exhibit absorption in the various d-electron states arising from the electron interaction of coordinated ligands. Absorption bands can also arise from a certain complex where the energy required to remove an electron from one atom and place it on another falls within the UV-vis region, which the process is known as charge transfer excitation.[45] A mercury (Hg) Arc lamp provide the light source, sent to a wavelength isolation device to provide 200 to 800 nm wavelength. Then passes through the sample, resulting in light absorption, which is sent to the detector.[45]

1.2.1.2. Luminescence spectroscopy

Luminescence spectroscopy allows for detecting the emission of a complex following excitation, which can then be further probed to measure the lifetime of that emission. Also, spectroscopy can be used in different temperatures if a heater-chiller and thermocouple are applied. A Xenon (Xe) Arc lamp provides the light source sent to the monochromator set at the desired wavelength for excitation. Then passes through the sample, which results in light emission, and the emission from the sample goes to the emission monochromator. The emission monochromator scans on a chosen wavelength

range, and the light is detected by the photomultiplier tube detector. [45-47]

1.2.1.3. Application of the absorption and emission spectroscopy

The absorption spectroscopy uses UV and visible light to excite the complex, which indicates the major absorption transition of the complexes.[36, 48, 49] For example, the UV-vis absorption spectra of *fac*-$[Re(CO)_3(dppz)(py)]^+$ and *fac*-$[Re(CO)_3(phen)(py)]^+$ can be seen in Figure 1.11. The UV-vis spectrum of *fac*-$[Re(CO)_3(dppz)(py)]^+$ shows both a $^1\pi$-π^* IL and ^{1}MLCT transition, but for *fac*-$[Re(CO)_3(phen)(py)]^+$ show only a ^{1}MLCT transition is observed.[36]

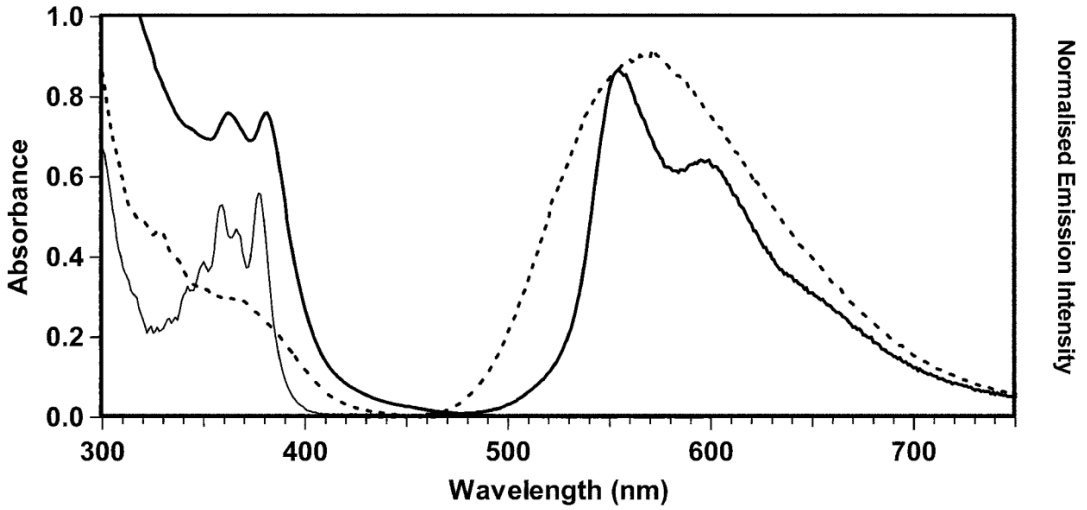

Figure 1.11 UV-vis absorption spectra (left axis) and normalized emission spectra (right axis) of *fac*-$[Re(CO)_3(dppz)(py)]^+$(solid line), *fac*-$[Re(CO)_3(phen)(py)]^+$(dashed line) and dipyridophenazine (dppz) (thin line) in CH_3CN. It is adapted from the reference[36].

Emission spectroscopy measures the radiation and light produced by a molecule that can locate the major emission states of the molecule, using the same complexes as above as an example (Figure 1.11).[36, 48, 49] The emission measurement of *fac*-$[Re(CO)_3(dppz)\ (py)]^+$ shows π-π^* IL characters which are structured; however,

emission measurement of *fac*-$[Re(CO)_3(phen)(py)]^+$ show MLCT emission indicated by the broad structureless emission.[36]

1.2.2. Time-resolved infrared spectroscopy

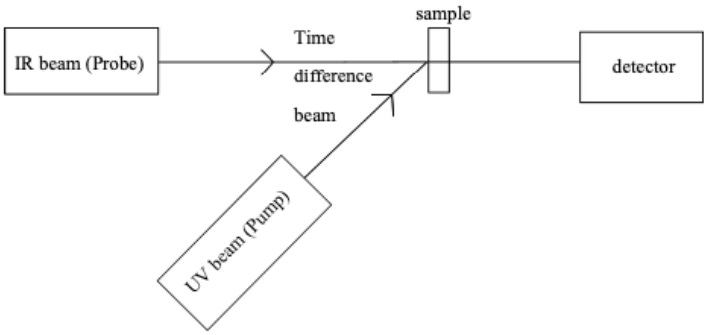

Figure 1.12 Illustration of the pump-probe technique. Showing the IR beam (probe) and UV beam (pump) arrive the sample cell with time difference [50-52]

Time-resolved infrared (TRIR) spectroscopy has a long history of identifying and assigning reaction coordinates or excited states. TRIR uses a pump-probe technique where the system is pumped with UV-vis light (initiating reactions or exciting molecules). Then IR radiation is used to probe the system (monitoring reaction intermediate or tracking excited state relaxation), as shown in Figure 1.12. It combines UV flash photolysis and different types of infrared (IR) spectrometers, such as IR grating, IR laser-based, step-scan FTIR and ultrafast IR laser pulses, with fast (or ultrafast) IR detection. The time resolution can be detected from milliseconds to femtoseconds timescale.[50-52]

The benefit of using TRIR is that the electronic excitation of a molecule alters the spatial distribution of the electron structure, resulting in changes in vibronic structure. The shifts can be interpreted as structural or electronic changes in the excited molecules. It provides significant insight into the molecule's transient structure. Moreover, to

enhance the maximum benefit for TRIR measurements, the reporting group in the metal complex plays an important role.[21, 32]

1.2.2.1. Reporting group

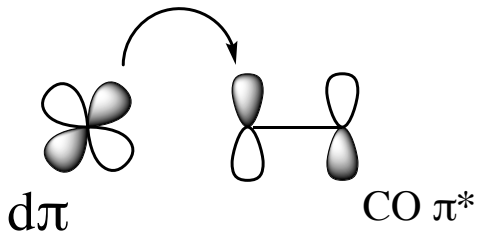

Figure 1.13 Illustration of the π-back bonding. Showing the metal dπ electron donate to CO anti π orbital. It is adapted from the reference[53].

Reporting groups are species with a back-donation from the filled metal orbitals to empty ligand orbitals of π symmetry (M → L π back-donation) and having well-defined stretching frequencies in otherwise quiet parts of the spectral region, such as CO or CN ligands.[21, 44, 54] Use CO ligands as an example, the driving force of changing the CO stretching response to the interplay between π back-donation and the electrostatic effect exerted by the metal-ligand fragment, as shown in Figure 1.13. In particular, metal-ligand fragments polarise the π CO bonding orbitals in the C ← O direction, thus shortening the bond and enhancing the covalency. On the other hand, π back-donation shifts charge in the opposite direction (C → O), extending the bond and decreasing the covalency. The net direction C ← O or C → O of the polarization of π CO bonding orbitals is found to invariably determine whether the CO bond is strengthened or weakened, respectively. These phenomena showed their spectrum shifts upon correlating with electron density changes.[53] It provides a helpful tag for TRIR probing of the character of the excited states. It can provide information that can be used to interpret the orbital origin, metal oxidation states and degree of back-bonding in metal

carbonyl complexes.[44]

1.2.2.2. Probing excited states

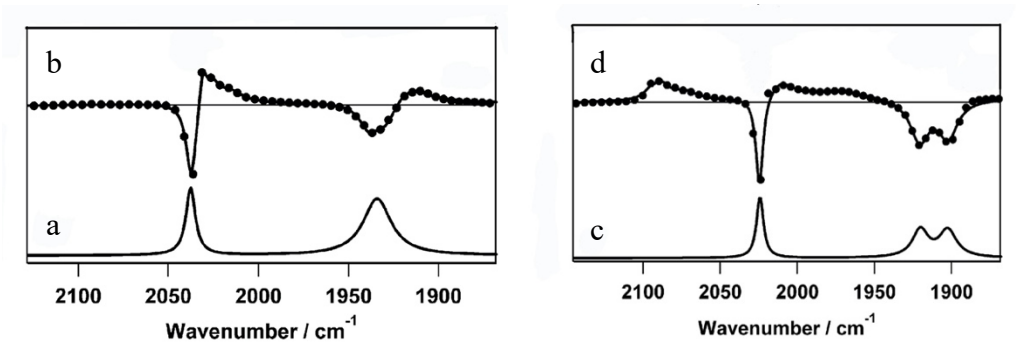

Figure 1.14 FTIR spectrum of (a) *fac*-[Re(CO)$_3$(dppz-Cl$_2$)(py)]$^+$ and (c) *fac*-[Re(CO)$_3$(dppz-Cl$_2$)(Cl)] in CH3CN at room temperature. TRIR spectra of (b) *fac*-[Re(CO)$_3$(dppz-Cl$_2$)(py)]$^+$ and (d) *fac*-[Re(CO)$_3$(dppz-Cl$_2$)(Cl)] at 2ps after 400 nm excitation in CH$_3$CN. It is adapted from the reference[28].

An excited states processes associated with the metal centre will directly cause a change in the electron density of the complex. The excited state of metal carbonyl complexes, for example, *fac*-[Re(CO)$_3$(bpy)(Cl)], can be probed by TRIR due to the CO reporter ligands the complex possesses. An MLCT excited state decreases the electron density at the metal centre, shifting the ν(CO) band to higher energy (Figure 1.14, spectrum d), and the size of the shift is a direct measure of the degree of charge transfer (CT) in the excited states. Whereas, for a π-π* IL excited state, which neither transfers nor accepts electron density from the metal, there are changes in electron density with the population of the antibonding orbital relative to the ground state. The ν(CO) bands are shifted to lower energy, and the shift is expected to be small because this is a secondary effect (Figure 1.14, spectrum b).[28, 44] Therefore, some excited states (MLCT, π-π* IL etc.) have a unique signal in their TRIR measurement, which can help assign the nature of the excited state is observed. Following the ν(CO) band change with time, that could

know the kinetic of the excited state whether it undergoes emission, intersystem crossing (ISC) or internal crossing (IC). It also shows how long the electron will populate in the excited state before they relax.[28, 32, 44] TRIR can indicate the nature of the different excited states and provide kinetic information about interconversion between excited states and excited-state relaxation.

2. Chapter 2

Synthesis and Investigation of the Chemistry and Photophysics of $[Re(CO)_2(diimine)_2]^+$ complexes

2.1. Introduction

Chapter 1 focused on the photophysics and photochemistry of rhenium tricarbonyl diimine complexes. Rhenium(I) dicarbonyl complexes usually have four types of complex, *cis*-$[Re(CO)_2(N,N)_2]^+$, *cis*,*cis*-$[(L)(L')Re(CO)_2(N,N)]^n$, *cis*,*trans*-$[(L)(L')Re(CO)_2(N,N)]^n$ and *cis*-$[(L)\ Re(CO)_2(N,N,N)]^n$ (where N,N is diimine ligand, N,N,N is terpyridine ligand, Land L' are solvent ligand, halide or pyridine, and n is the charge of the complex). The complex structure is shown in Figure 2.1. This chapter will focus more on bis-diimine ligand complex.[40, 42, 55-60]

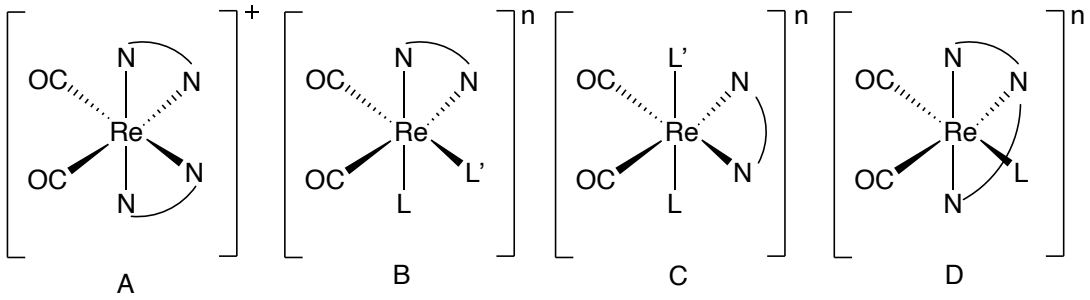

Figure 2.1 The Rhenium(I) dicarbonyl complex *cis*-$[Re(CO)_2(N,N)_2]^+$(A), *cis,cis*-$[(L)(L')Re(CO)_2(N,N)]^n$ (B), *cis,trans*-$[(L)(L')Re(CO)_2(N,N)]^n$ (C) and *cis*-$[(L)\ Re(CO)_2(N,N,N)]^n$(D) (where N,N is diimine ligand, N,N,N is terpyridine ligand, Land L' are solvent ligand, halide or pyridine, and n is the charge of the complex.

2.1.1. *cis*,*cis*- and *cis*,*trans*-[(L)(L')Re(CO)$_2$(N,N)]^n complexes

For the purposes of this work, this introduction will focus on the *cis*,*cis* type and *cis,trans* type (Figure 2.1, B and C). The literature is mainly focused on studies of *cis,trans* type (C), having only few reports on the *cis*, *cis* type (B).[40, 42] The synthesis of *cis,cis* type is more challenging than for *cis,trans* type. Their synthesis is focused on the photoreaction by using their tricarbonyl analogous as precursors to then attach the target ligand by Photochemical Ligand Substitution (PLS) (see chapter 1 Section 1.1.2.5.2). This strategy is based on using different solvent and axial ligands to direct the reaction mechanism to change from *cis,cis*-type to *cis,trans*-type. The synthesis of *cis,cis*-type requires careful choice of solvent, axial ligand and temperature.[40-42, 60] In addition, it is reported an alternative route to the synthesis of *cis,trans*-type complexes using a thermal reaction.[61, 62]

The *cis,cis*-type and *cis,trans*-type isomer can be identified by NMR. A, due to the lack of symmetry of the cis,cis-type, that will show more signals than the isomer *cis,trans*-type complex, as shown in Figure 2.2.[40-42, 60]

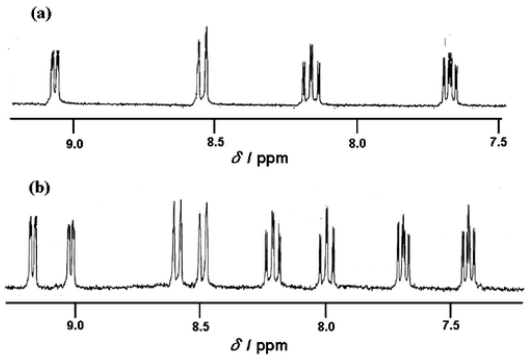

Figure 2.2 The NMR different of *cis*,*cis* type of [(Cl)(MeCN)Re(CO)$_2$(bpy)] (b) and *cis,trans* type of [(Cl)(MeCN)Re(CO)$_2$(bpy)] (a). It is adapted from the reference[42].

The photophysics of *cis,trans* type have been reported in the literature.[57, 63] Shakirova et al. reported a series of structurally analogous *cis*,*trans*-$[Re(N,N)(CO)_2(L)_2]^+$ (where L is N-donor ligands) complexes by substitution of acetonitrile with various aromatic N-donor ligands. The complexes obtained show unusually strong absorption in the visible spectral region, which are determined by MLCT charge transfer processes from the rhenium centre to the diimine and axial N-donor ligands. Also, they reported that all complexes, except for the methylated derivative, which is non-emissive, display phosphorescence in the NIR area with the band maxima ranging from 711 to 805 nm that are the record values for rhenium complexes.[57]

2.1.2. *cis*-[(L) $Re(CO)_2(N,N,N)]^n$ (N,N,N=terpyridine, n = 0 or 1^+)

In recent years, *cis*-[(L) $Re(CO)_2(N,N,N)]^n$ complexes (Figure 2.1 D) have been reported in the literature, focusing on their NIR-emissive and panchromatic absorption properties.[56, 64] The complexes can be prepared from the conversion of κ^2N-tricarbonyl complex to the κ^3N coordination mode under high temperature. The absorption profiles of the κ^3N complexes cover the whole visible spectra and can be finely tuned by changing the ancillary ligand L (where L = pyridine. PPh_3). Such complexes have near-infrared emission (780−950 nm) with unusually high quantum yields (0.02−0.7%) for this class of compounds.[56, 64]

2.1.3. *cis*-$[Re(CO)_2(N,N)_2]^+$

Rhenium(I) dicarbonyl bis-diimine complexes that have not been widely reported in the literature, with the focus being on the bipyridine and phenazine dicarbonyl analogues.

2.1.3.1. Synthesis of *cis*-$[Re(CO)_2(N,N)_2]^+$

The synthesis of rhenium(I) dicarbonyl complexes has been reported via a variety routes including trimethylamine N-Oxide decarbonylation,[63, 65] photo-decarbonylation,[40-42, 57] redox-mediated decarbonylation,[66, 67] nitrosylation[68] and thermal decarbonylation.[58, 59] Although, we have different methods for decarbonylation, for the type *cis*-$[Re(CO)_2(N,N)_2]^+$ only thermal decarbonylation so called "melting method" has been reported in the literature.[55]

In 2006, Smithback *et al.* reported the synthesis of *cis*-$[Re(CO)_2(P,P)(N,N)]^+$ and *cis*-$[Re(CO)_2(N,N)_2]^+$ (where P,P is a chelating diphosphine and N,N is a diimine ligand).[58] They reported four synthetic routes that rely on either reactive triflate displacement or abstraction of labile chloro ligands, followed by use the strong *trans*-labilizing effect of phosphine donors or direct use of the trans effect of phosphine donors. The reaction scheme is shown in Scheme 2.1

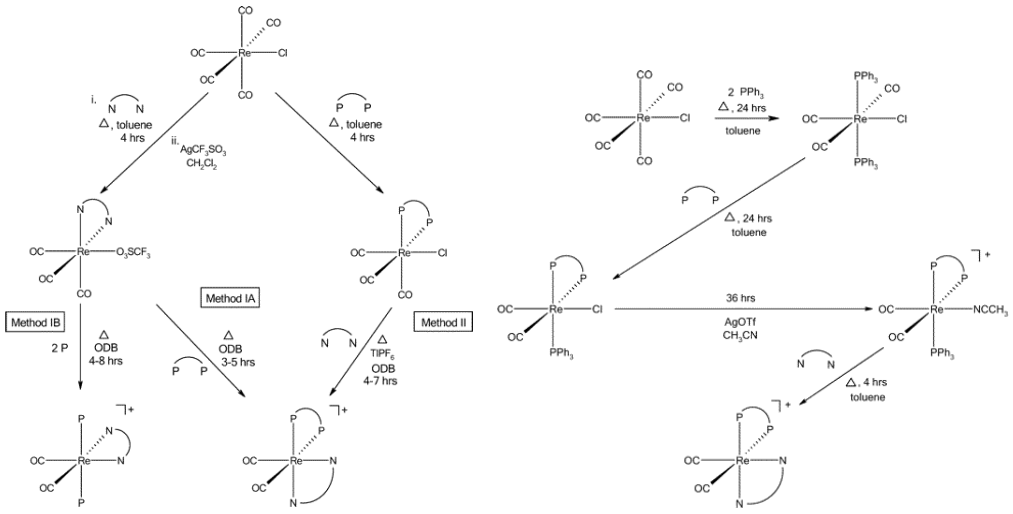

Scheme 2.1 The reaction scheme of use the strong trans-labilizing effect of phosphine donors (right) or direct use of the trans effect of phosphine donors (left). It is adapted from the reference[59]

In their research, they also reported the synthesis *cis*-$[Re(CO)_2(N,N)_2]^+$ using the

melting method, which is a type of decarbonylation reaction mainly performed in the solid state, starting from *fac*-$[(OTf)Re(CO)_3(diimine)]^+$ complexes, and it involves activation of the core with high temperature (e.g., 275–300 °C), under either vacuum or a constant flow of an inert gas. [58, 59]

In 2020, Atallah *et al* used a similar method. They used $[(OTf)Re(CO)_3(N,N)]$ and $[(CH_3CN)Re(CO)_3(N,N)]^+$ as precursor developed novel *cis*-$[Re(CO)_2(N,N)_2]^+$ with bipyridine and phenazine analogues. The yield of those complexes around 30 to 60 %. The reaction scheme is shown in Scheme 2.2.[58, 59]

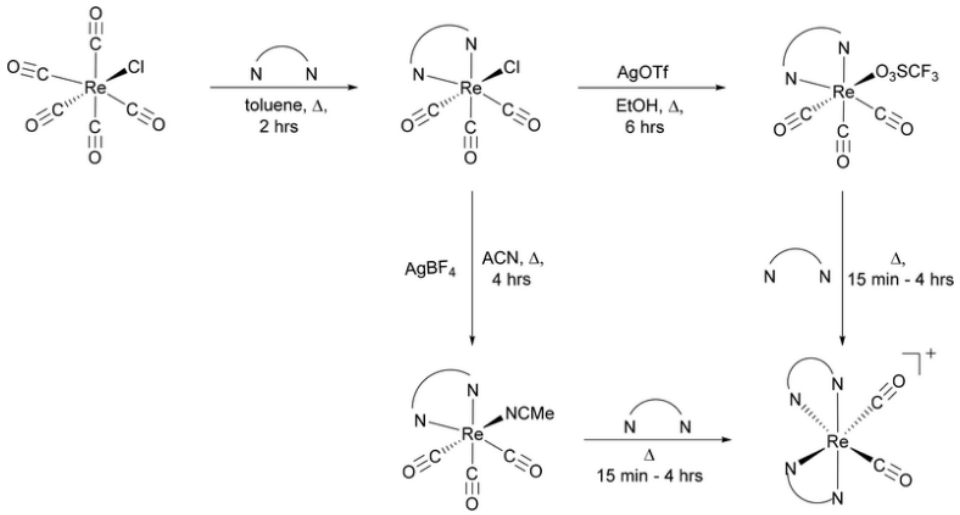

Scheme 2.2 The reaction scheme of the Melting method for synthesis *cis*-$[Re(CO)_2(N,N)_2]^+$. It is adapted from the reference[58].

2.1.3.2. FTIR spectra of *cis*-$[Re(CO)_2(N,N)_2]^+$

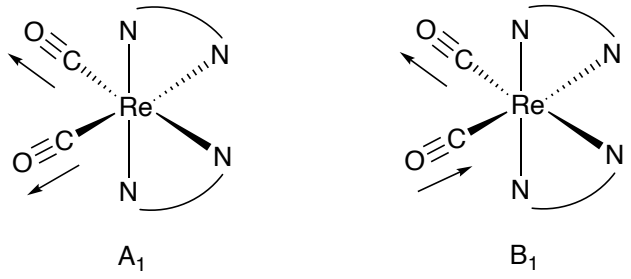

Figure 2.3 The schematic IR vibrations of *cis*-$[Re(CO)_2(N,N)_2]^+$.[56-58]

FTIR spectra of *cis*-$[Re(CO)_2(N,N)_2]^+$ shows two IR bands, due to CO stretching vibrations. The ν(CO) in the range of about 1800-1950 cm^{-1} is schematically shown in Figure 2.3. The two bands belong to the symmetric vibration and the antisymmetric vibration of the equatorial CO ligands. These two vibrations occur at similar strength. Usually, the higher frequency one will have more strength than lower frequency one. The carbonyl stretching frequencies are significantly lower than the corresponding *fac*-$[Re(CO)_3]^+$ tricarbonyl species. The comparison of the CO stretching vibration frequencies between complexes can be correlated to the electron donating ability of each ligand bound to the metal center.[56-58]

2.1.3.3. ^{1}H NMR spectra of *cis*-$[Re(CO)_2(N,N)_2]^+$

The ^{1}H NMR spectra of the complexes shows diimine ligand resonances will shift to a higher position relative to the free ligand because the electron density is donating to the metal centre, which will deshell the protons. Also, due to the symmetry of the complex, the ^{1}H NMR will show all proton signals of the diimine ligand (one of them) and the other one will show as in peak symmetry(double the integration).[58] For example, *cis*-$[Re(CO)_2(bpy)_2]^+$, the NMR will show bpy ligand in eight proton signals in different position and double the integration (two bpy ligands).

2.1.3.4. Photophysics of Rhenium(I) dicarbonyl *bis*-diimine complexes

Photophysics of Rhenium dicarbonyl diimine complex is a group of Rhenium carbonyl complexes that have not been widely reported in the literature. Rhenium dicarbonyl diimines complex shows MLCT and π-π*IL transition in electronic absorption spectroscopy. Complexes having the form *cis*-$[Re(CO)_2(N,N)(L,L)]^+$ and *trans*, *cis*-$[(P)_2Re(CO)_2(N,N)]^+$ (where N,N is diimine ligand; L,L is either a chelating diphosphine or another diimine ligand and P is a monodentate phosphine ligand) can attenuate nonradiative decay processes. Electrochemical measurements can probe the oxidation of the Re(I) metal to become Re(II). This occurs in the MLCT charge transfer to the N,N ligand. The lowest excited states are ^{3}MLCT, which is shown by TRIR and luminescence spectroscopic measurements.[58, 59, 69-72]

Atallah *et al*. reported the bpy and phen dicarbonyl analogue complexes, having the form *cis*-$[Re(CO)_2(N,N)_2]^+$ (N,N = various 2,2'-bipyridine (bpy) or 1,10-phenanthroline (phen) derivatives) where the photophysical and redox properties were explored. The absorption spectrum of those complexes shows π-π* band around 260 to 300 nm and shows MLCT absorption around 400-500 nm. The emission measurements reported the complexes showed ^{3}MLCT excited state emission. Those both complexes show absorption around 680 to 720 nm. Also, the emission lifetime of cited complexes is within the nanosecond timescale decay between 23 – 512 ns. The emission and absorption data show in Table 2.1

Complex	Absorption (nm)		Emission (nm)
cis-[Re(3,4,7,8-Me_4phen)$_2$(CO)$_2$]OTf	271,300 (π-π*)	391,449, 521(MLCT)	681
cis-[Re(4,7 -Me_2phen)$_2$(CO)$_2$]PF_6	265,286,305 (π-π*)	400,474,543(MLCT)	698
cis-[Re(5,6-Me_2phen)$_2$(CO)$_2$]PF_6	272,317 (π-π*)	408,483,555(MLCT)	703
cis-[Re(phen)$_2$(CO)$_2$] OTf	266,293 (π-π*)	410,485,554(MLCT)	704
cis-[Re(4,7-Ph_2phen)$_2$(CO)$_2$]PF_6	279,298 (π-π*)	429,493,572(MLCT)	722
cis-[Re(5,5'-Me_2bpy)$_2$(CO)$_2$]PF_6	294 (π-π*)	364,394,475,545(MLCT)	695
cis-[Re(4,4'-dtbbpy)$_2$(CO)$_2$] PF_6	287 (π-π*)	362,400,483,552(MLCT)	706
cis-[Re(bpy)$_2$(CO)$_2$]PF_6	289 (π-π*)	361,402,494,564(MLCT)	714
cis-[Re(4,4'-Me_2bpy)$_2$(CO)$_2$] PF_6	286 (π-π*)	362,399,486,554(MLCT)	715

Table 2.1 Showing the table of emission and absorption data for *cis*-[Re(CO)$_2$(N,N)$_2$]$^+$ (N,N = various 2,2'-bipyridine (bpy) or 1,10-phenanthroline (phen) derivatives). It is adapted from the reference[58].

This study detailed nine complexes and showed that electron donating groups, such as methyl substituents, induced a blue shift in both electronic absorption and emission energies with a concomitant decrease in the k_{nr} value with respect to the parent

compounds. On the other hand, electron delocalizing substituents, such as phenyl groups, cause a red shift in electronic absorption and emission energy with a corresponding decrease in the k_{nr} value with respect to the parent compound. [58]

The time-resolved infra-red (TRIR) and transitions absorption (TA) measurement were performed and showed a ^{3}MLCT state population in those complexes. The TRIR shown below (Figure 2.4), where two υ(CO) bands of the ^{3}MLCT are seen at 1875 and 1985 cm^{-1} following a 532 nm excitation, *cis*-[Re(5,5'-Me_2bpy)$_2$(CO)$_2$]PF_6 in CH_2Cl_2. Two new blue shifted vibrations appeared, consistent with the Re(I) metal centre becomes transiently oxidized to Re(II), leading to a reduction in π-backbonding and a concomitant increase of the CO bond order is observed in both the symmetric and antisymmetric vibrational modes. Also, the excited state features are long lived, with little decay occurring over the entire 4 ns delay line in the experiments, which is consistent with the exclusive formation of ^{3}MLCT excited states in all instances.[58]

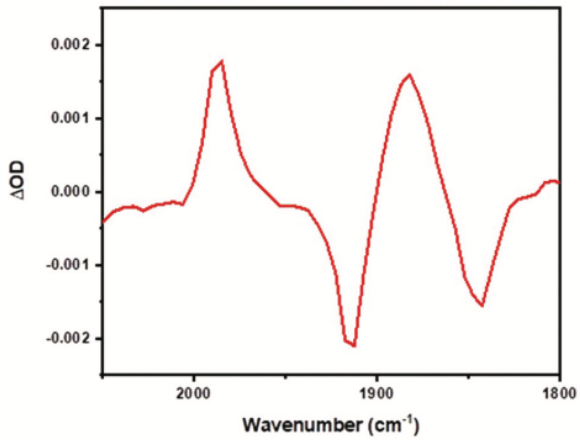

Figure 2.4 TRIR spectra of *cis*-[Re(5,5'-Me_2bpy)$_2$(CO)$_2$]PF_6.It is adapted from the reference[58]

2.1.4. Recent Studies on *cis*-$[Re(CO)_2(N,N)_2]^+$

The work in this project follows unpublished work[73] studying complexes such as *cis*-$[Re(bpy)_2(CO)_2]PF_6$, $[Re(dppz)_2(CO)_2]PF_6$, and $[Re(dppz)(bpy)_2(CO)_2]PF_6$. Dyachenko reported new $[Re(dppz)_2(CO)_2]PF_6$ and can be synthesis by the melting method with similar precursor as Atallah *et al*.[58, 73] Dyachenko also reported,[73] mixed diimine ligands $[Re(dppz)(bpy)_2(CO)_2]PF_6$ can be synthesized by the melting method; however, synthesis of the mixed diimine ligands complex $[Re(dppz)(bpy)_2(CO)_2]PF_6$ by melting method will get by-product of $[Re(bpy)_2(CO)_2]PF_6$ and $[Re(dppz)(bpy)_2(CO)_2]PF_6$ which the mass spectrometry will show the mass of three of those complexes and the reported yield of $[Re(dppz)(bpy)_2(CO)_2]PF_6$ became very low.

The characterization of $[Re(dppz)_2(CO)_2]PF_6$ has been measured by FTIR, NMR and HRMS. The report shows that $[Re(dppz)_2(CO)_2]PF_6$ has shown two bands of CO stretching vibrations, ν(CO) in the range of about 1800-1950 cm^{-1} which match the range of the literature. Also, the ^1H NMR spectra shows one of their dppz ligand all proton signals and the other one ligand will show as in peak symmetry. There are showing dppz ligand of ten proton signals with the requisite amount of integration. The HRMS shows the mass of 807.1269 (M^+) which is consistent with the mass of $[Re(dppz)_2(CO)_2]^+$.[73]

The work reported in this Thesis builds upon studies of dppz complexes such as $[Re(dppz)_2(CO)_2]^+$ and the Melting method was investigated to try and synthesise new complexes with analogous ligands to dppz such as dppp2.[73]

2.1.5. Dppp2 ligand complex

In Chapter 1, we mention the tricarbonyl rhenium dppz complexes have special

properties such as the DNA light switch effect together with the ability tune the photophysics of the resulting complexes by attaching different EDGs or EWGs at 11, 12 position (see chapter 1 Section 1.1.2.4.1.1).[33] This work investigates another way to tune the dppz ligand which is fuse N atom at para and ortho position in the phz part. This makes the dppz have a pyridine end of the ring. According to the literature, the pyridine is lower the ^{3}MLCT(phz) energy. Summers et al. reported that [(Cl)Re(CO)$_3$(dppp2)] and [(Cl)Re(CO)$_3$(dppp3)] mostly populated in ^{3}MLCT((phz) by TRIR measurement. Also, the complexes show solvent effect and keep the dppz light switch effect.[74] They also report that due to the population of ^{3}MLCT((phz) and having pyridine which provide the ability to do CO_2 reduction via pyridine position. However, they also pointed out the CO at the axial position may make the non-emission state have shorter lifetimes, which could have implications for the subsequent bimolecular photochemistry needed for CO_2 reduction.[74].

2.2. Aim

The aim of the work described in this Chapter is to synthesize and investigate the photochemistry and photophysics of [Re(CO)$_2$(diimine)$_2$]$^+$ complexes and compare them to analogous tricarbonyl complexes, particularly focusing on complexes related to the dppz ligand using the pyrido[2',3′:5,6]pyrazino[2,3-f][1,10]phenanthroline (dppp2) and pyrido[3',4′:5,6]pyrazino[2,3-f][1,10]phenanthroline (dppp3) ligand. We have used the following strategy to address the aims above:

- Synthesis of the dppp2 ligand and use these to form [(Cl)Re(CO)$_3$(dppp2)].
- Converting [(Cl)Re(CO)$_3$(dppp2)] to form [(CH$_3$CN)Re(CO)$_3$(dppp2)]$^+$ and [(OTf)Re(CO)$_3$(dppp2)] precursors.

- To Synthesize $[Re(CO)_2(dppp2)_2]^+$ from $[(CH_3CN)Re(CO)_3(dppp2)]^+$ and [(OTf)Re(CO)$_3$(dppp2)] precursors via melting method with excess of dppp2.
- To investigate alternative routes to synthesize $[Re(CO)_2(dppp2)_2]^+$.
- To Probe the photophysics and photochemistry of $[Re(CO)_2(dppp2)_2]^+$ using emission and time-resolved spectroscopy.

2.3. Results and Discussion

2.3.1. Synthesis of dppp2 Ligand and Formation of [(Cl)Re(CO)$_3$(dppp2)].

The synthesis of dppp2 has been reported in the literature and it has been demonstrated that it can be successfully synthesized.[75, 76] However, the reported purification process using $CHCl_3$ to recrystallize causes yield loss. The procedure is detailed in the experimental section 4.2.1. Initially, it was investigated whether changing the reaction solvent from methanol (CH_3OH) to acetonitrile (CH_3CN) could aid the synthesis, due to the product being insoluble in CH_3CN and it would precipitate out. However, under that condition, a pale beige precipitate was produced during the reaction, which was attributed to an intermediate formed during the reaction (see characterization at section 2.3.1.1.1.). The precipitate was collected and redissolved into CH_3OH and further refluxed for 3 hours. After this time, the solvent was evaporated to afford a brownish solid that was confirmed to be dppp2 (see characterization at section 2.3.1.1.). The procedure is detailed in the experimental Section 4.2.1. After completing the synthesis of dppp2, [(Cl)Re(CO)$_3$(dppp2)] prepared by the procedure described in the literature and detailed in the experimental section 4.2.2.[74]

2.3.1.1. Analysis and Characterization of dppp2 and [(Cl)Re(CO)$_3$(dppp2)]

The dppp2 ligand was characterized by ^{1}H NMR and HRMS techniques and the measurements are consistent with the literature.[75, 76] The HRMS shows a peak at 284.0933 m/z ($M+H^+$), which is consistent with the mass of the dppp2 ligand (calc. 284.0931). Figure 2.5 is shown the spectrum is similar to the reported on the literature.[75, 76] It is possible to observe in the NMR spectrum, the distinct signals for H^E, H^F and H^C on the pyridine ring, as well as the split on H^A and H^B due to the lack of symmetry on the ligand.

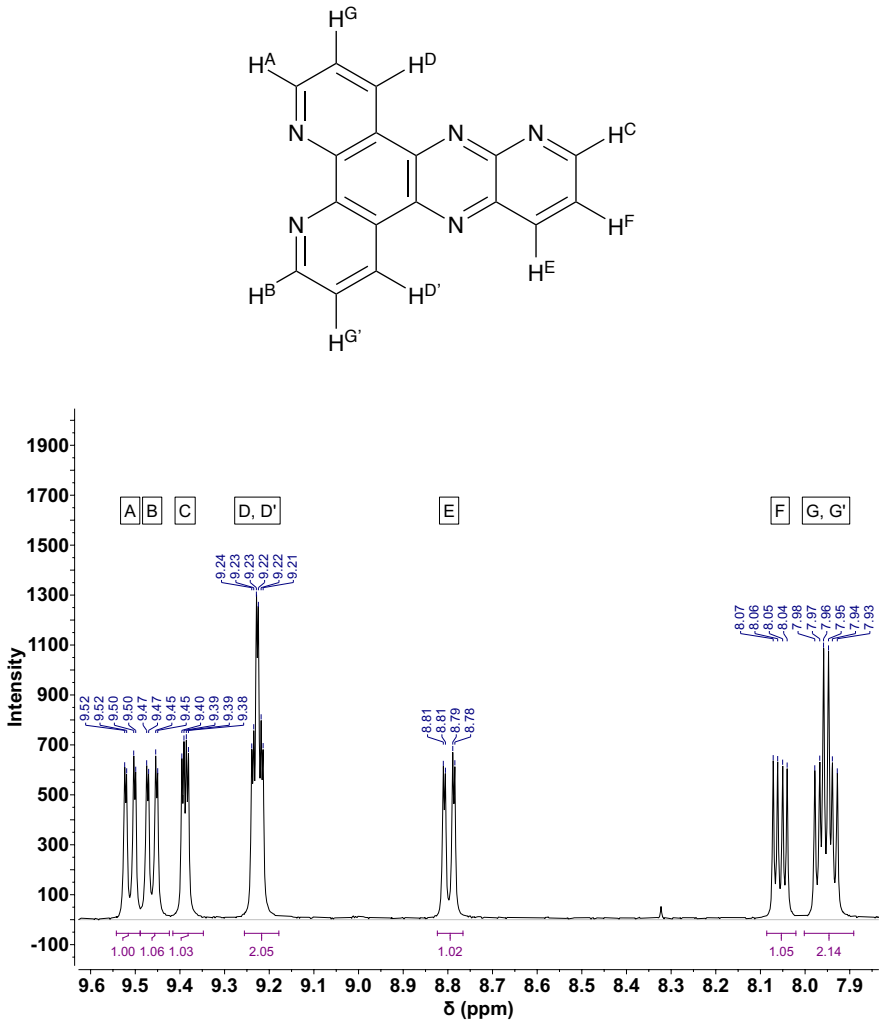

Figure 2.5 The ^{1}H NMR spectrum of dppp2 molecule and obtained in DMSO.

The [(Cl)Re(CO)$_3$(dppp2)] complex was characterized by FTIR, ^{1}H NMR and HRMS measurement and the results are consistent with the literature.[74] The HRMS result shows a peak at 611.9811 m/z (M+Na$^+$) (calc. 611.9844), for [(Cl)Re(CO)$_3$(dppp2)]. The ^{1}H NMR spectrum was assigned as shown in Figure 2.6-a. The result shows deshielding of the proton signals, confirming the coordination of the dppp2 ligand in the complex. The extension of the shift was higher in the signals of H^A, H^B, $H^{D, D'}$ and $H^{G, G'}$, consistent with direct coordination to the phenanthroline ring, shifting the electron density from the ring to the metal centre. The FTIR measurement (Figure 2.6-b) shows a sharp absorption peak and one broad absorption attributed to two overlapped stretches with A′(1), A″, and A′(2) symmetry. These three strong CO bands indicate a facial structure and match the molecular symmetry of the complex.

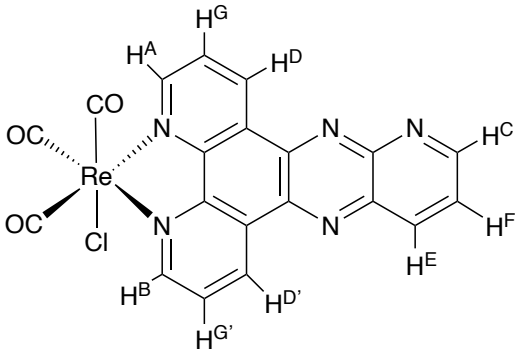

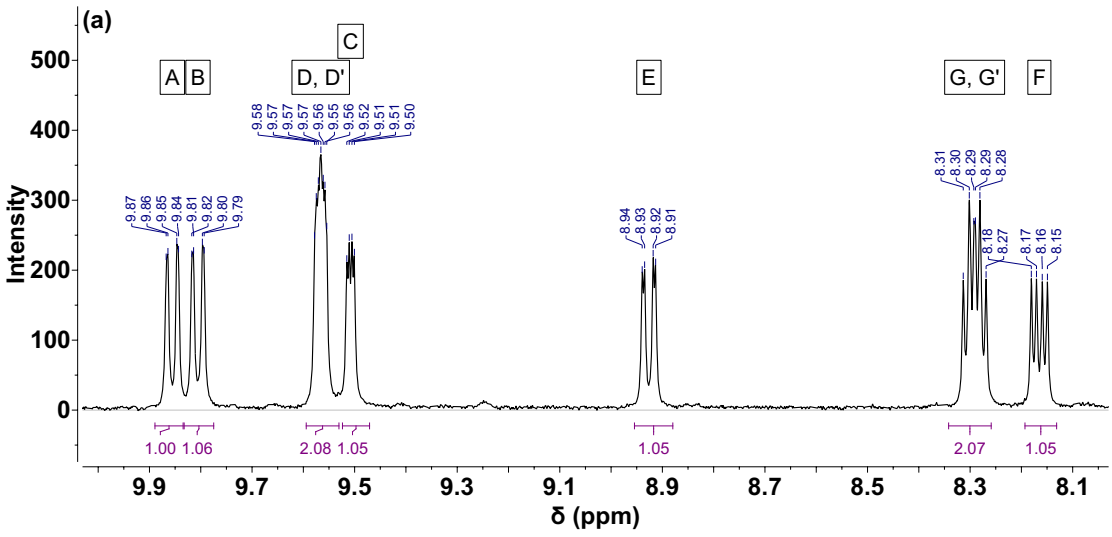

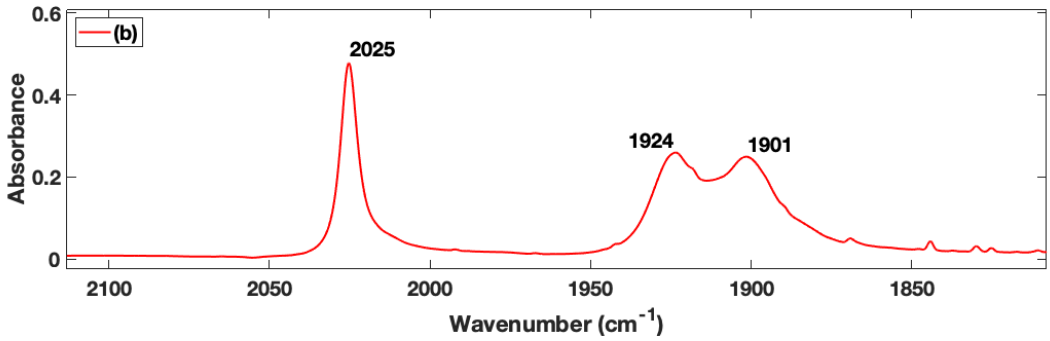

Figure 2.6 The spectra of [(Cl)Re(CO)$_3$(dppp2)]. ^{1}H NMR (a) in DMSO; FTIR (b) in CH_2Cl.

2.3.1.1.1. Characterisation of the intermediate — the pale beige precipitate

Characterization of the intermediate was carried out by HRMS and ^{1}H NMR techniques. The HRMS measurement shows a mass of 320.1141 m/z ($M+H^+$), indicating that the intermediate molecular formula is $C_{17}H_{13}N_5O_2$. Figure 2.7 The proposed structure of the precipitate. This shows the proposed structure based on the starting materials (1,10-phenanthroline-5,6-dione and 2,3-diaminopyridine) and the molecular weight obtained by HRMS.

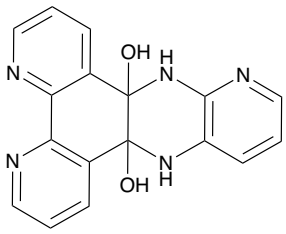

Figure 2.7 The proposed structure of the precipitate.

To further verify the structure of the intermediate, NMR spectroscopy was performed. The ^{1}H NMR spectrum is shown in Figure 2.7. The ^{1}H NMR spectrum of the pale yellow-white precipitate obtained in DMSO, shows the H^I and H^J shift at 5.96 and 5.90 ppm, which indicated that the proton disproportion of the hydroxyl protons, due the lack of symmetry. The amine protons H^E and H^F shift at 7.31 and 6.80 ppm. The shift

separation is due to the deshielding, because of the proximity of the pyridine nitrogen atom.[77] The proton of $H^{A,\ A'}$, $H^{B,\ B'}$ and $H^{C,\ C'}$ have similar patterns to 1,10-phenanthroline-5,6-dione (phdo). Particularly to the $H^{A,\ A'}$ is possible to observe a non-resolved double dd splitting. The signal for H^{D}, H^{G} and H^{F} shows a similar coupling pattern in 2,3-diaminopyridine. This proposed structure is further corroborated by the ^{13}C NMR that does not show any carbonyl signal.

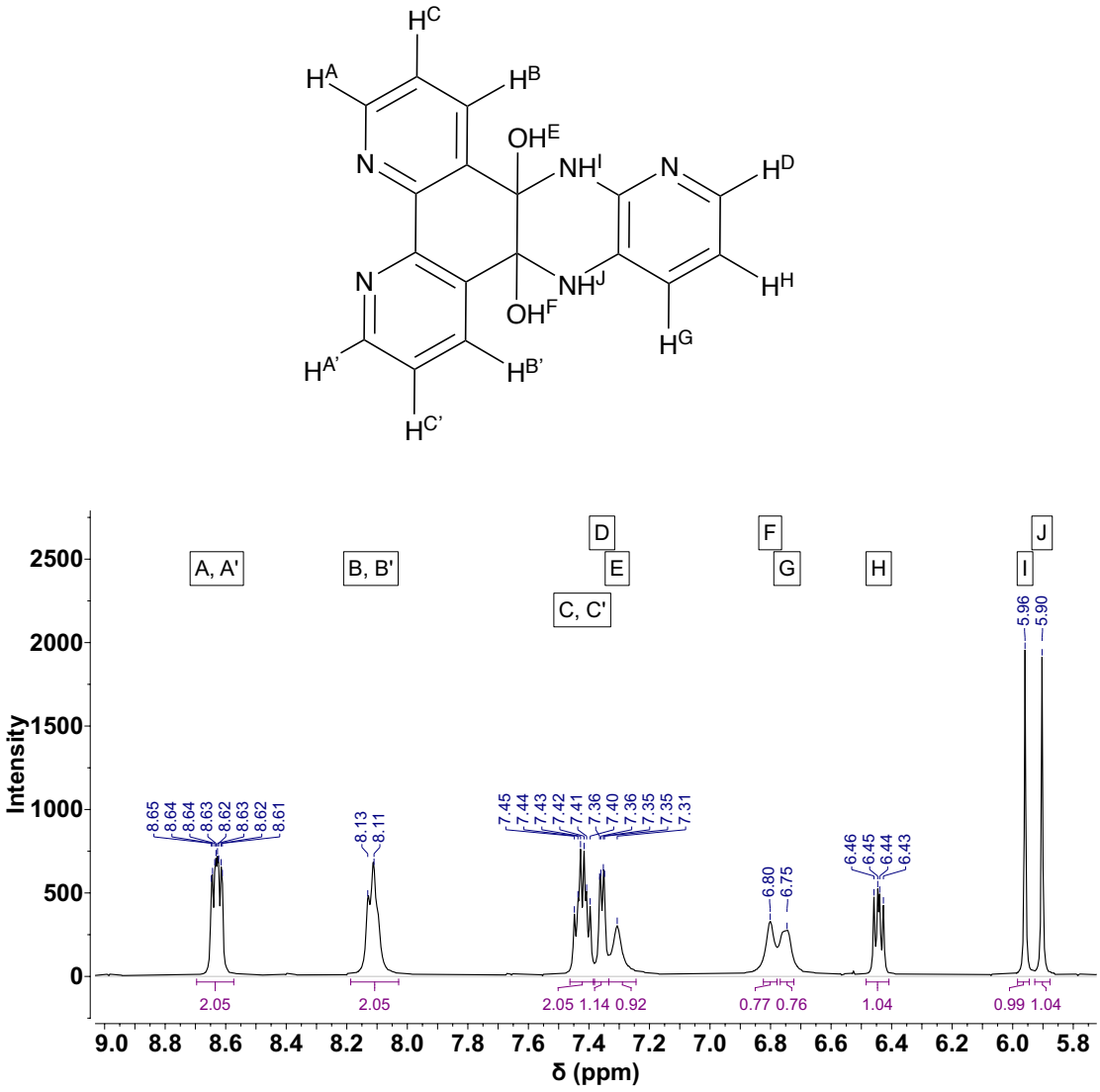

Figure 2.8 The ^{1}H NMR spectrum of the pale beige precipitate obtained in DMSO.

2.3.2. Formation of $[(CH_3CN)Re(CO)_3(dppp2)]^+$ and

[(OTf)Re(CO)$_3$(dppp2)]

Having prepared the ligand dppp2 and the [(Cl)Re(CO)$_3$(dppp2)] precursor, the synthesis of [(OTf)Re(CO)$_3$(dppp2)] and [(CH$_3$CN)Re(CO)$_3$(dppp2)]OTf, was performed by using a procedure adapted in the literature.[27] The details are given in the experiment Sections 4.2.3 and 4.2.4. The [(Cl)Re(CO)$_3$(dppp2)] reacted with AgOTf to give [(OTf)Re(CO)$_3$(dppp2)]. CH_2Cl_2 was the solvent for the purification process to avoid ligand exchange and the [(OTf)Re(CO)$_3$(dppp2)] was obtained with 72% yield. Attempts of using CH_3CN for the purification were made, but the OTf ligand was exchanged to CH_3CN ligand at room temperature to immediately give [(CH$_3$CN)Re(CO)$_3$(dppp2)]OTf. The reaction scheme is shown in Scheme 2.3.

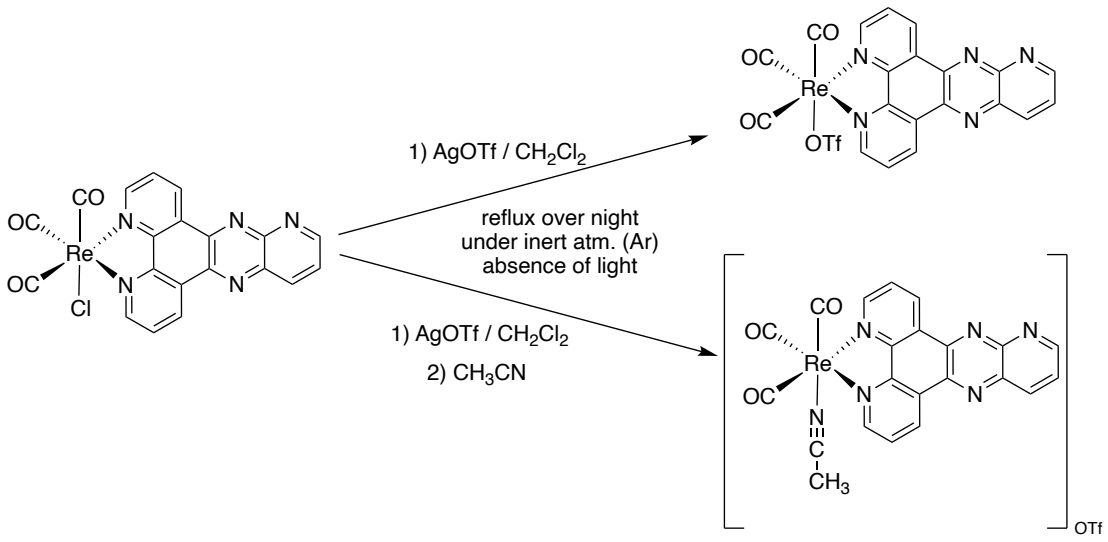

Scheme 2.3 The reaction scheme formation of [(L)Re(CO)$_3$(dppp2)]^n (L = OTf, CH_3CN; n=0, 1+).

2.3.2.1. Analysis and Characterization of $[(L)Re(CO)_3(dppp2)]^n$ (L = OTf, CH_3CN; n=0, 1+)

2.3.2.1.1. $[(OTf)Re(CO)_3(dppp2)]$

The identification of $[(OTf)Re(CO)_3(dppp2)]$ was confirmed by FTIR, UV-Vis, ^1H NMR and ^{19}F NMR spectroscopy. The spectroscopy characterization of $[(OTf)Re(CO)_3(dppp2)]$ is shown in Figure 2.9. The FTIR measurement of the complex shows that it has three strong CO bands (2038, 1938 and 1919 cm^{-1}), which indicates its facial structure and matches its molecular symmetry, similar to what was observed to the $[(Cl)Re(CO)_3(dppp2)]$. The ^1H NMR spectrum shows its dppp2 ligand pattern and de shielding the signals due to the OTf ligand's poor coordinating ability and weak field effect. Like what was observed for the coordination, the phenanthroline shifts are more affected by the ligand exchange. Moreover, the ^{19}F NMR spectrum shows the OTf ligand shift at -77.71 ppm, which agrees with the literature.[78] The UV-Vis measurement shows a similar result to $[(Cl)Re(CO)_3(dppp2)$,[74] but with the absorption blue shifted to 365 nm. The HRMS was not obtained for the complex due to the low stability of the complexes in polar solvents.

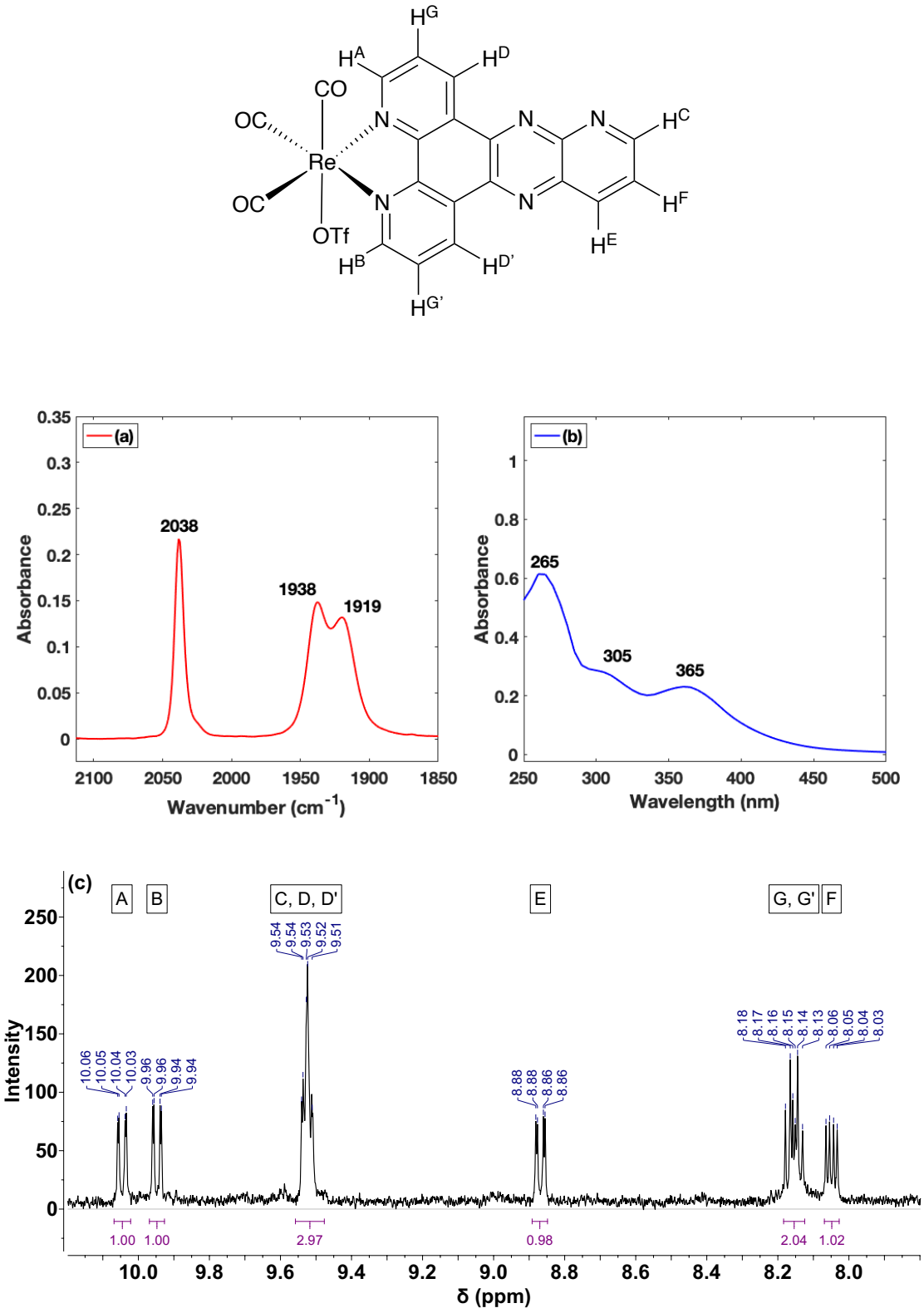

Figure 2.9 The spectra of [(OTf)Re(CO)$_3$(dppp2)]. FTIR (a) and UV-vis (b) in CH_2Cl; ^{1}H NMR (c) in CD_2Cl_2.

2.3.2.1.2. [(CH$_3$CN)Re(CO)$_3$(dppp2)]OTf

The complex [(CH$_3$CN)Re(CO)$_3$(dppp2)]OTf, or other solvent coordinated complexes, can be prepared based on the equilibrium of the triflate ion in solution. In more polar solvents, the triflate tends to leave the coordination sphere of metal complexes, to form the non-coordinated triflate ion,[78, 79] as shown in Scheme 2.4.

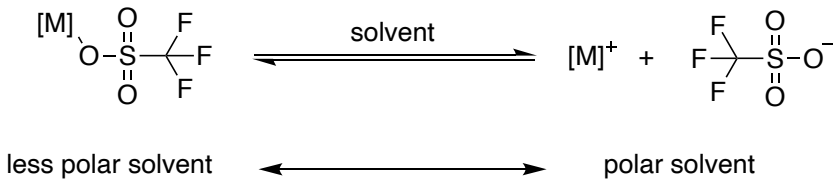

Scheme 2.4 The equilibrium reaction between OTf ligand and OTf ion with the polarity of the solvent.

Therefore, upon addition of the complex [(OTf)Re(CO)$_3$(dppp2)] in CH$_3$CN, the OTf ligand becomes the OTf counter ion forming the [(CH$_3$CN)Re(CO)$_3$(dppp2)]OTf, as can be seen in the FTIR measurement is shown in Figure 2.10.

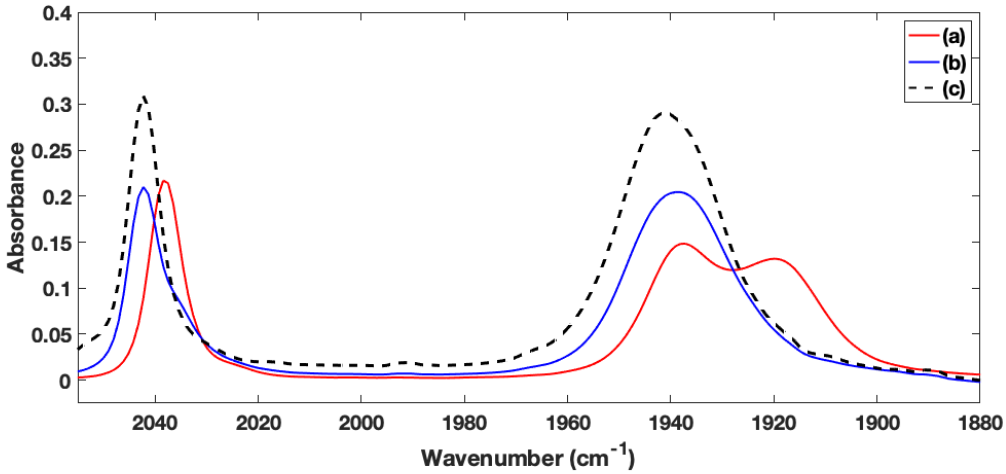

Figure 2.10 FTIR measurement showing the OTf ligand and OTf ion exchange. The IR measurement of [(OTf)Re(CO)$_3$(dppp2)] complex in CH$_2$Cl$_2$ (a). IR measurement of [(OTf)Re(CO)$_3$(dppp2)] complex in CH$_3$CN (b). The IR measurement of isolated [(CH$_3$CN)Re(CO)$_3$(dppp2)]OTf complex in CH$_3$CN (c).

The identification of [(CH_3CN)Re(CO)$_3$(dppp2)]OTf was confirmed by FTIR, UV-Vis, ^{1}H NMR, ^{19}F NMR and HRMS. The spectroscopic data of [(CH_3CN)Re(CO)$_3$(dppp2)]OTf is shown in Figure 2.11. The FTIR measurement of the complex shows that a sharp CO absorption and broad signal at 2024 and 1948 cm^{-1}, respectively. This is probably due to two overlapping bands. The spectrum is in agreement with its facial structure. The ^{1}H NMR spectrum shows its dppp2 ligand pattern and is possible to observe the peak of the CH_3CN ligand at 2.11 ppm. Moreover, the ^{19}F NMR spectrum shows the OTf counter ion forms at -78.93 ppm.[78] The HRMS measurement of [(CH_3CN)Re(CO)$_3$(dppp2)]OTf shows a peak with a mass of at 595.0535 m/z corresponding to the [(CH_3CN)Re(CO)$_3$(dppp2)]$^+$ (calc. 595.0523, error 0.6ppm). The UV-Vis measurement of [(CH_3CN)Re(CO)$_3$(dppp2)]$^+$ shows an absorption at 370 nm, that is blue shifted in comparison to [(Cl)Re(CO)$_3$(dppp2)],[74] but red shifted compared to [(OTf)Re(CO)$_3$(dppp2)].

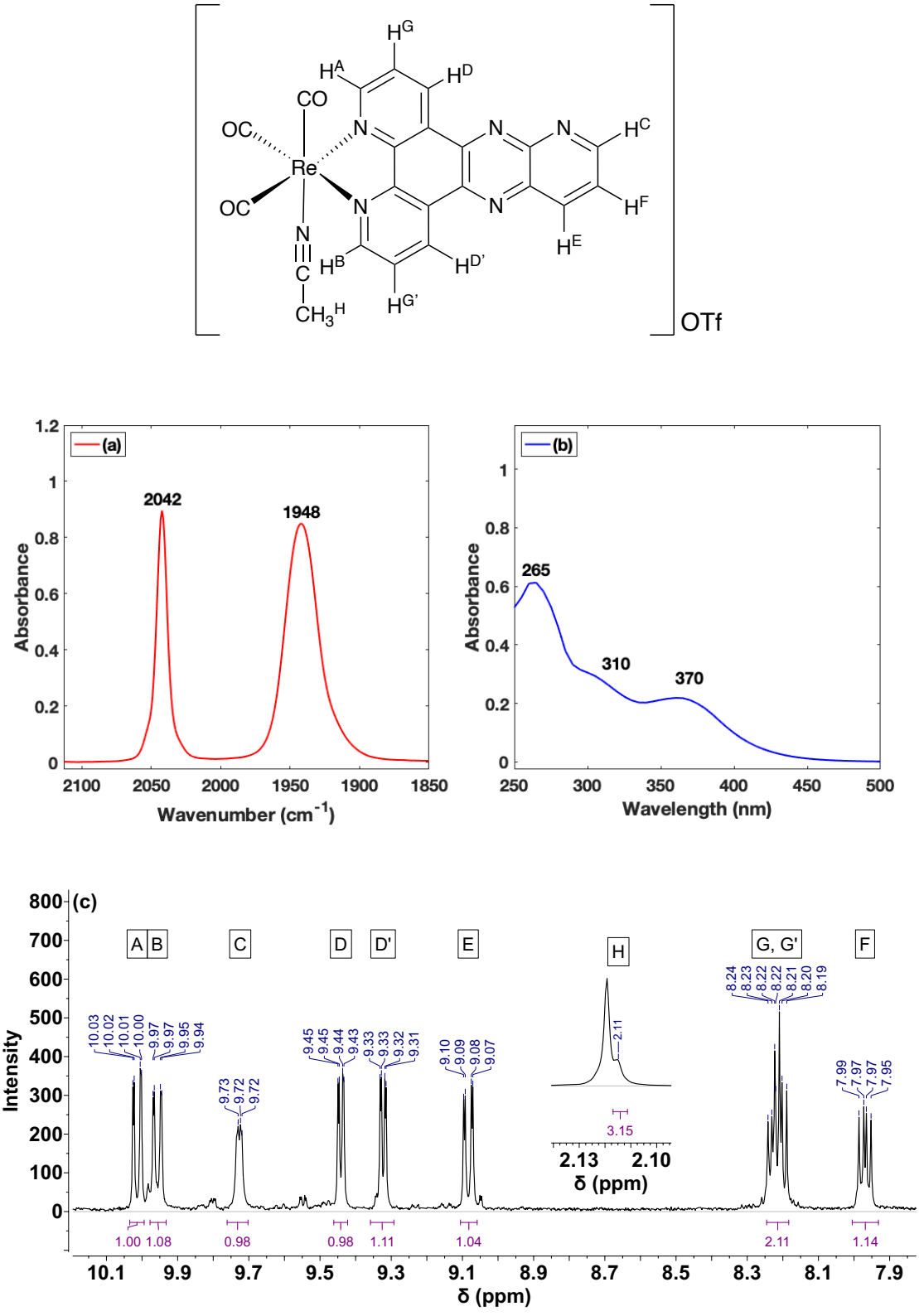

Figure 2.11 The spectra of [(CH$_3$CN)Re(CO)$_3$(dppp2)]OTf. FTIR (a) and UV-vis (b) in CH_2Cl; ^{1}H NMR (c) in CD_2Cl_2.

2.3.2.1.3. The Emission Measurement of [(OTf)Re(CO)$_3$(dppp2)] and [(CH$_3$CN)Re(CO)$_3$(dppp2)]OTf

Emission spectra were obtained for all the compounds in CH_2Cl_2 and are shown in Figure 2.12. For the complex [(Cl)Re(CO)$_3$(dppp2)] no emissions were observed. This is consistent with the population of the in ^{3}MLCT(phz) as previously reported by TRIR measurements, as the ^{3}MLCT(phz) is reported as a non-emission state.[74] The spectra of [(OTf)Re(CO)$_3$(dppp2)] shows a broad emission centred at 600nm, probably due to the ^{3}MLCT(phen) state. In addition, the emission of [(CH$_3$CN)Re(CO)$_3$(dppp2)]OTf shows broad signals with maximum at 570nm with a shoulder at 504 nm.

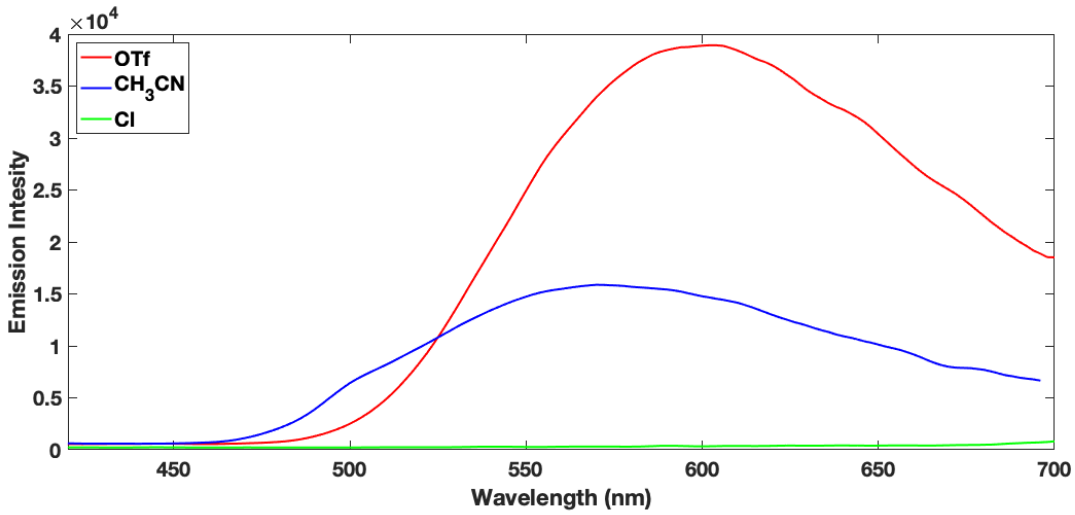

Figure 2.12 The emission spectra of [(L)Re(CO)$_3$(dppp2)]^n in CH_2Cl_2 (L = OTf, Cl, CH_3CN; n=0, 1+).

By changing from OTf ligand to CH_3CN ligand is also possible to observe a 30 nm blue shift in the emission. This can be due to the coordinating ability of the ligands. The ligand CH_3CN is a stronger field compared to the OTf ligand. Therefore, the orbitals energy splitting tends to be higher, increasing the energy gap, and shifting the emission to higher energy.

2.3.3. The preparation of $[Re(CO)_2(dppp2)_2]PF_6$ via the melting method

The preparation of $[Re(CO)_2(dppp2)_2]PF_6$ was attempted using a melting method following those reported in the literature[58, 59] and is detailed in the experiment Section 4.2.5. The melting method using $[(OTf)Re(CO)_3(dppp2)]$ with excess of dppp2 ligand did not yield $[Re(CO)_2(dppp2)_2]PF_6$. However, the reaction using $[(CH_3CN)Re(CO)_3(dppp2)]OTf$ afforded a black power, that after extraction using CH_3OH gave the desired $Re(CO)_2(dppp2)_2]PF_6$ with low yield (<5%). The product was characterized by FTIR, ^1H NMR, ^{19}F NMR spectroscopy and HRMS spectrometry.

2.3.3.1. Analysis and Characterization of $Re(CO)_2(dppp2)_2]PF_6$

The FTIR in Figure 2.14 shows CO bands corresponding to a mixture of the target $[Re(CO)_2(dppp2)_2]PF_6$ and possibly to the complex $[(CH_3CN)Re(CO)_3(dppp2)]PF_6$, due to FTIR absorptions (Figure 2.14-a). The ^{19}F NMR spectrum shows PF_6 ion peak only. The desired complex $[Re(CO)_2(dppp2)_2]^+$ can have three different isomers (Figure 2.13). However, the ^1H NMR spectrum suggests that only one isomer was synthesized (Figure 2.14). In the ^1H NMR spectrum is possible to observe the presence of 18 protons in the structure, indicating that the two ligands experience different chemical environments. This corresponds to isomer B. Unfortunately, the reaction using the melting method led to a very low yield, and the reaction may be isomer selective. Therefore, alternative methods for preparing $[Re(CO)_2(dppp2)_2]PF_6$ complex will be investigated.

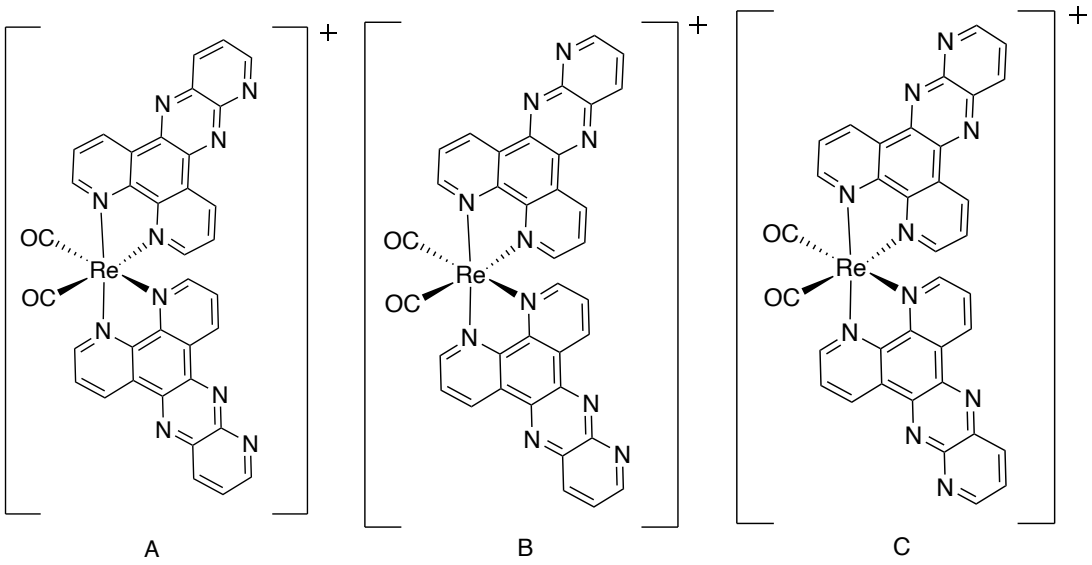

Figure 2.13 The possible isomer structures of $[Re(CO)_2(dppp2)_2]^+$

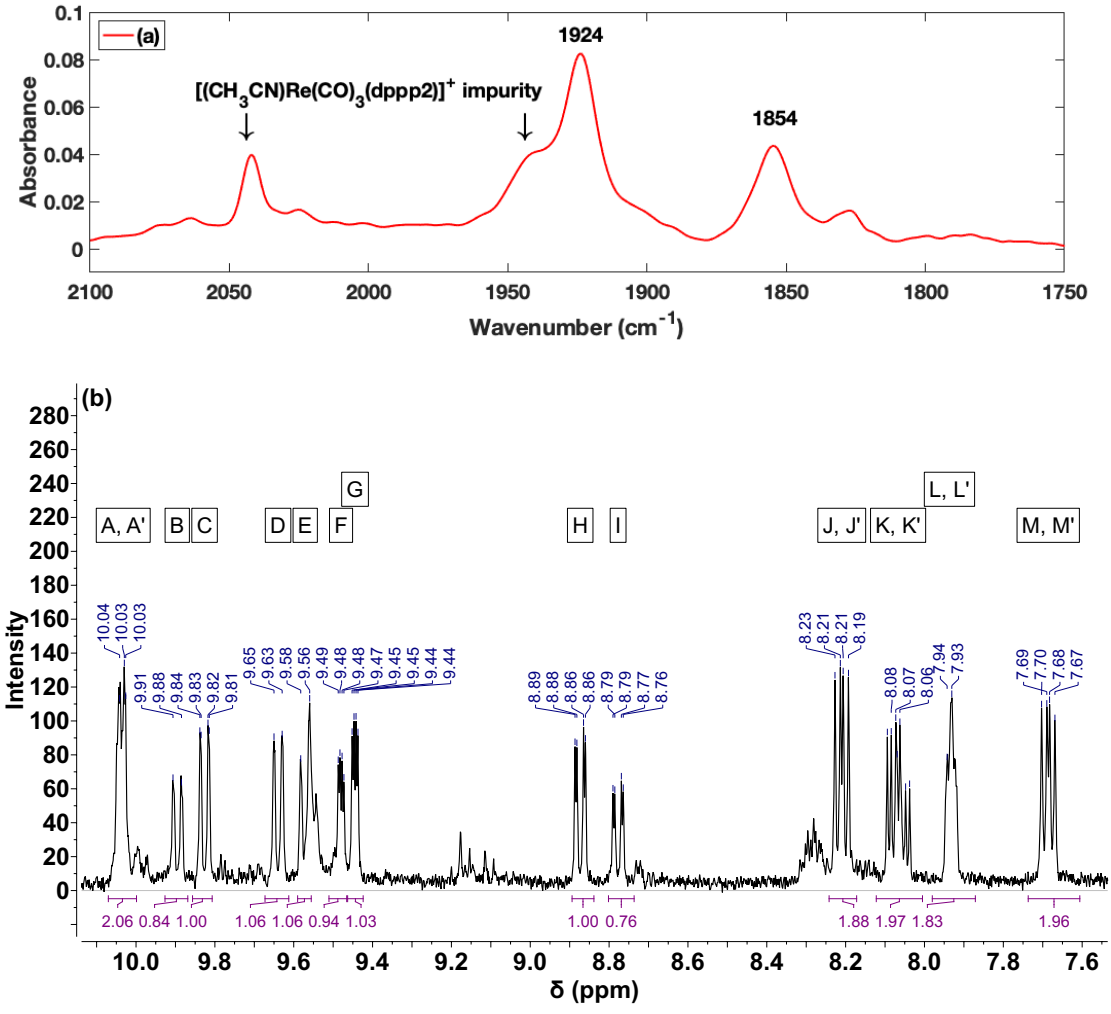

Figure 2.14 The spectra of $[Re(CO)_2(dppp2)_2]PF_6$. IR (a) in CH_2Cl; ^1H NMR (b) in CD_3CN.

2.3.4. Alternative Route for Rhenium dicarbonyl bis-diimine complexes via late-stage condensation of 1,10-phenanthroline-5,6-dione (phdo)

The first alternative route to prepare $[Re(CO)_2(dppp2)_2]PF_6$ is based on changing the condensation reaction of phdo to form dppp2 to the end of the synthetic route. The proposal is based on the preparation of $[(Cl)Re(CO)_3(phdo)]$, the ligand exchange to form $[(CH_3CN)Re(CO)_3(phdo)]^+$ and $[(OTf)Re(CO)_3(phdo)]$ precursors. Then, applying the previous melting method to form $[Re(CO)_2(phdo)_2]PF_6$, and, finally, performing the condensation reaction to make $[Re(CO)_2(dppp2)_2]PF_6$. The proposed reaction is shown in Scheme 2.5.

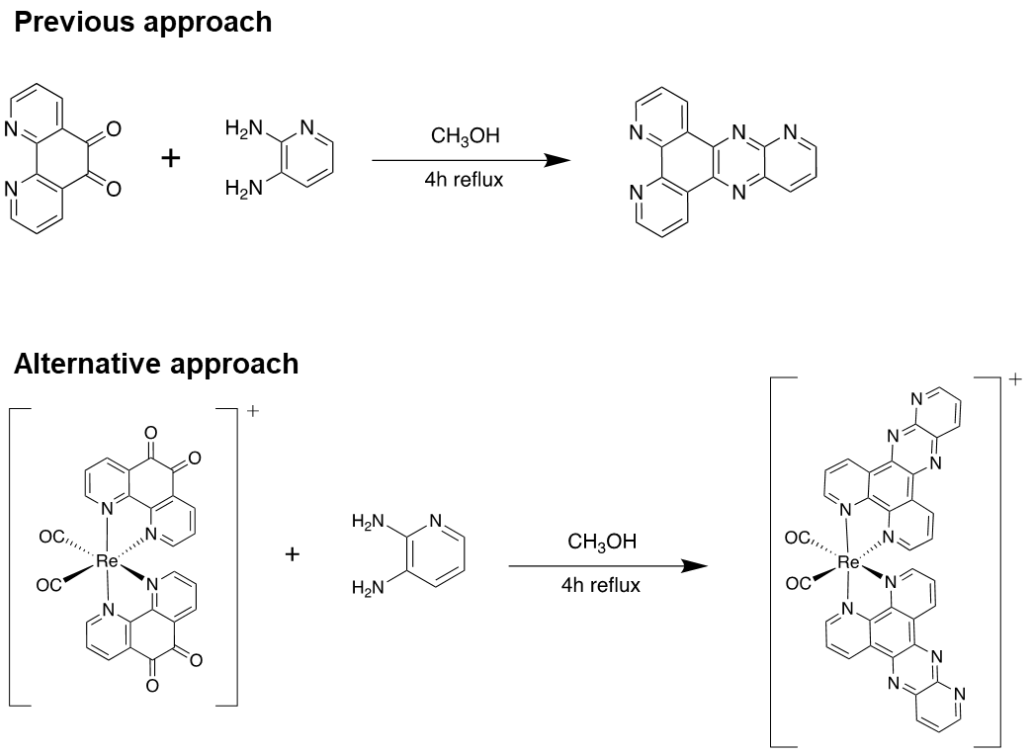

Scheme 2.5 The proposed condensation reaction using $[Re(CO)_2(phdo)_2]^+$

2.3.4.1. Formation of $[(Cl)Re(CO)_3(phdo)]$, $[(CH_3CN)Re(CO)_3(phdo)]^+$ and $[(OTf)Re(CO)_3(phdo)]^+$

The complex $[(Cl)Re(CO)_3(phdo)]$ was prepared following literature procedure[80] and is detailed in the experiment Section 4.2.6.

The synthesis of two new complexes, $[(OTf)Re(CO)_3(phdo)]$ and $[(CH_3CN)Re(CO)_3(phdo)]OTf$, were prepared by a similar procedure described in the literature[27] and details are given in the experiment Sections 4.2.7 and 4.2.8. $[(Cl)Re(CO)_3(phdo)]$ reacted with AgOTf to give $[(OTf)Re(CO)_3(phdo)]$ in CH_2Cl_2. By applying the same experimental procedures and adding CH_3CN instead, the OTf ligand exchanges with CH_3CN at room temperature to deliver $[(CH_3CN)Re(CO)_3(phdo)]OTf$ complex. The reaction scheme is shown in Scheme 2.6.

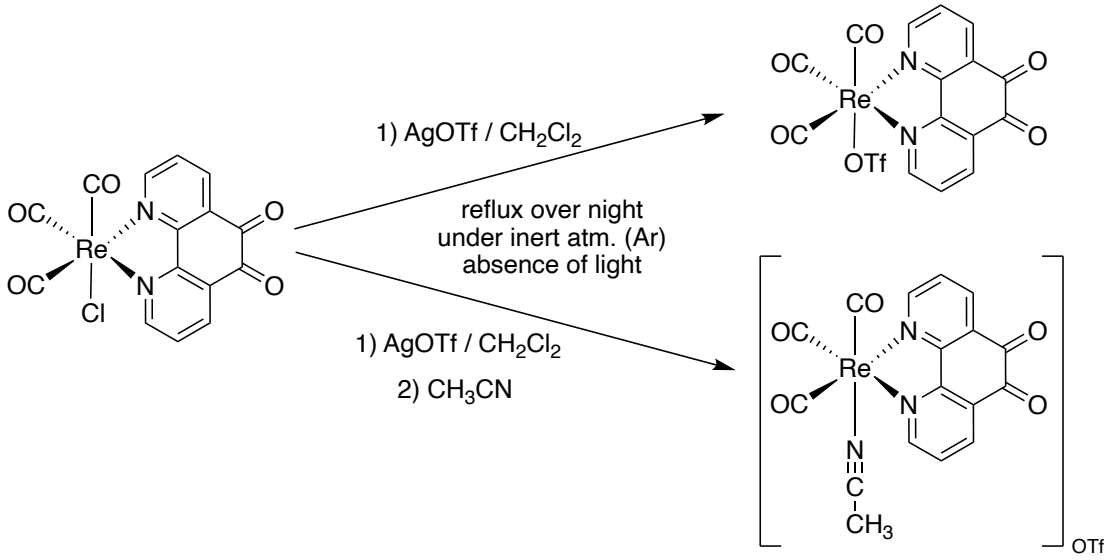

Scheme 2.6 The reaction scheme of synthesis $[(L)Re(CO)_3(phdo)]^n$ (L= OTf, CH3CN ; n=0, 1+).

2.3.4.1.1. Analysis and Characterization of $[(L)Re(CO)_3(phdo)]^n$ (L= Cl, OTf, CH3CN ; n=0, 1+).

2.3.4.1.1.1. $[(Cl)Re(CO)_3(phdo)]$

The $[(Cl)Re(CO)_3(phdo)]$ was characterized by FTIR and ^1H NMR techniques (Figure 2.15), and is in agreement with previously reported data.[80] The FTIR spectrum shows four CO bands and three of them in equal strength (2024, 1924 and 1905 cm^{-1}) which indicates its facial structure and matches its molecular symmetry as shown in Figure 2.15. The CO band with different strength (1709 cm^{-1}) is the ketone form phdo ligand. The ^1H NMR spectrum was assigned as shown in Figure 2.15 and confirmed the presence of the coordinated phdo, causing the deshielding of the signals due to the electron density of phdo shifted to the metal centre.

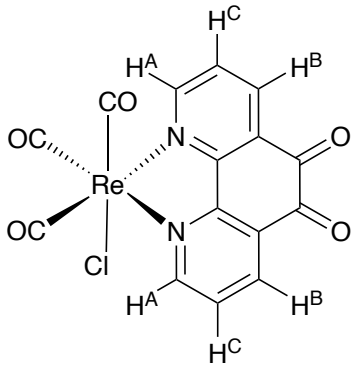

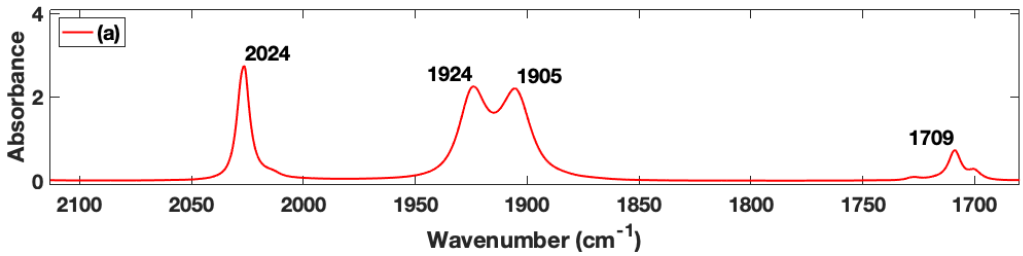

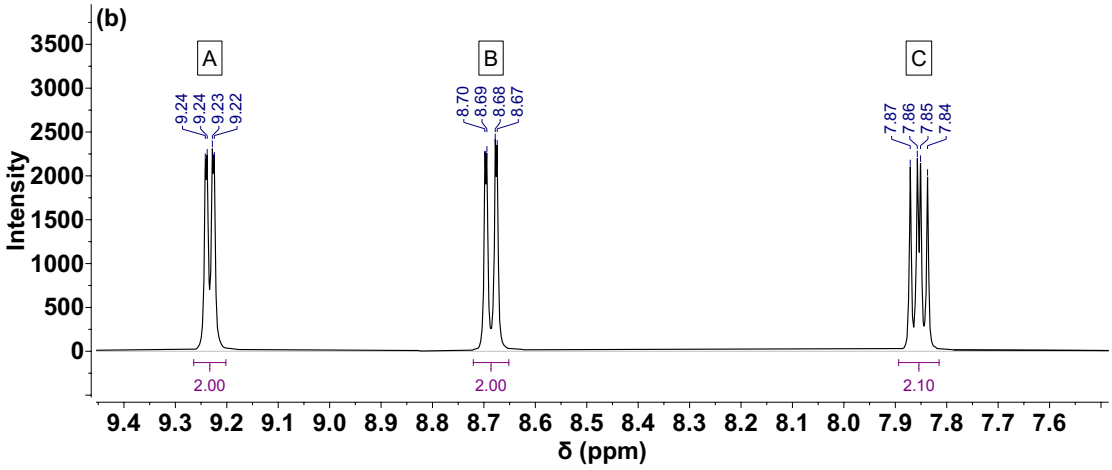

Figure 2.15 The spectra of [(Cl)Re(CO)$_3$(phdo)]. IR (a) in CH_3CN; ^{1}H NMR (b) in CD_3CN.

2.3.4.1.1.2. [(OTf)Re(CO)$_3$(phdo)]

The characterization of novel [(OTf)Re(CO)$_3$(phdo)] was confirmed by FTIR, UV-Vis, ^{1}H NMR, and ^{19}F NMR (Figure 2.16). The FTIR spectrum shows that it has four CO bands and three of them have equal strength (2041, 1944, and 1924 cm^{-1}) which indicates its facial structure and matches its molecular symmetry and the CO band with different strength (1705 cm^{-1}) from the phdo ligand. The ^{1}H NMR shows its phdo ligand pattern, and some peaks shift upward due to the OTf ligand's poor coordinating ability and weak field effect. Moreover, the ^{19}F NMR shows the OTf ligand form at -77.51 ppm, which matches with the literature.[78] The UV-Vis measurement shows a similar result to [(Cl)Re(CO)$_3$(phdo)],[81] but [(OTf)Re(CO)$_3$(phdo)] is blue shifted. The HRMS was not obtained for the complex due to the low stability of the complexes on polar solvents.

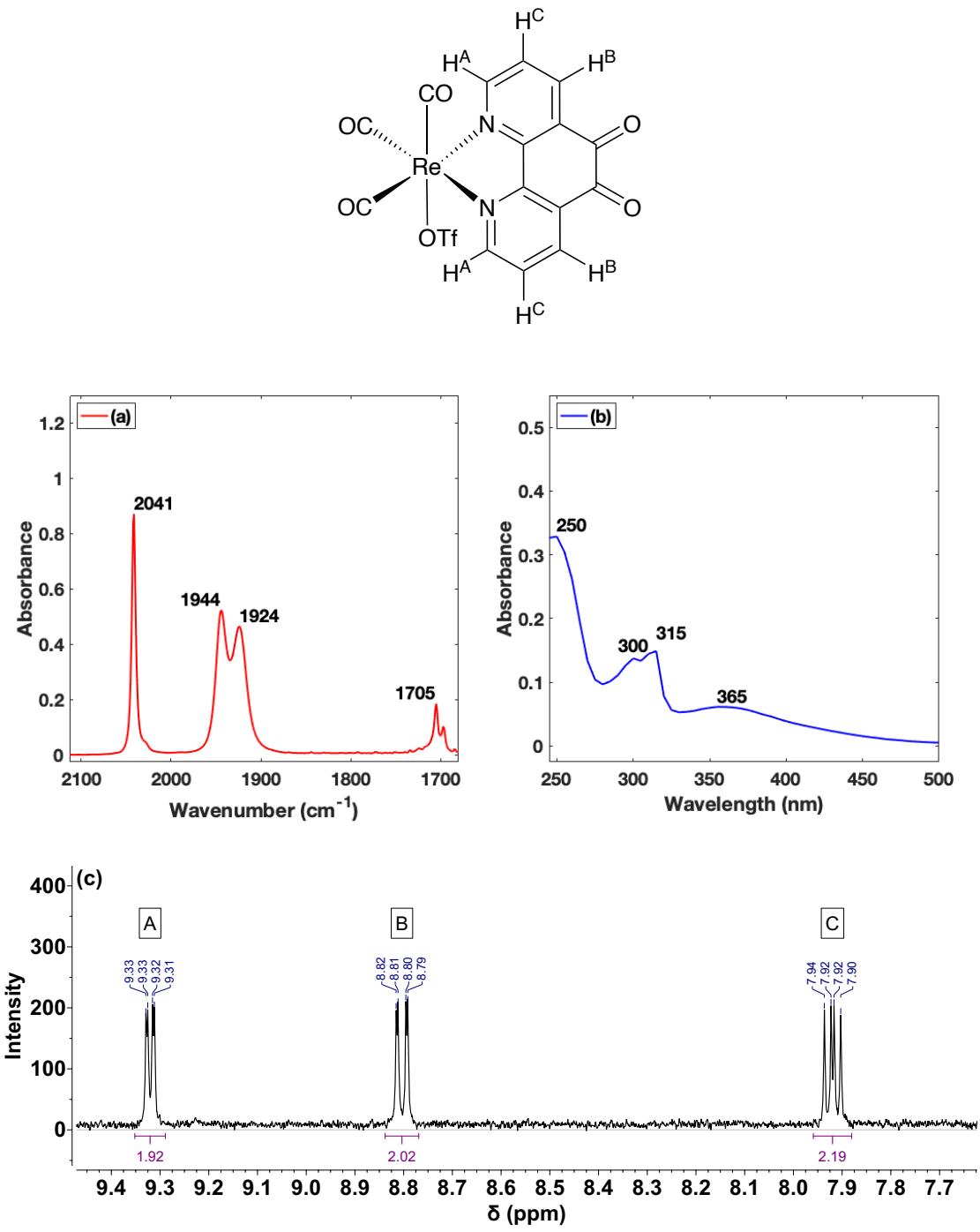

Figure 2.16 The spectra of [(OTf)Re(CO)$_3$(phdo)]. IR (a) and UV-Vis (b) in CH_2Cl_2; ^{1}H NMR (c) in CD_2Cl_2.

2.3.4.1.1.3. [(CH$_3$CN)Re(CO)$_3$(phdo)]OTf

The characterization of novel [(CH$_3$CN)Re(CO)$_3$(phdo)] was confirmed by FTIR, UV-Vis, ^{1}H NMR, ^{19}F NMR and HRMS (Figure 2.17). The FTIR spectrum of the complex shows that it has three CO bands, a sharp band at 2043 cm^{-1} and a broad band at 1944 cm^{-1}, which corresponds to the complex with its facial structure, and a CO band with different strength (1712 cm^{-1}) is tentatively assigned to the is the ketone in the phdo ligand although it should be noted that the intensity is extreme and is unexplained one possibility is enhancement due to fermi resonance, but the presence of an impurity cannot be ruled out. The ^{1}H NMR shows its phdo ligand pattern, and some peaks shift downward (H^A) consistent with the CH$_3$CN ligand's better coordinating ability and strong field effect. Also, it is possible to observe the peak of the CH$_3$CN ligand at 2.25 ppm. Moreover, the ^{19}F NMR shows a signal at -79.29 ppm, that matches the value for the triflate acting as a counter ion.[78] The HRMS measurement of [[(CH$_3$CN)Re(CO)$_3$(phdo)]OTf shows a signal at 522.0089 m/z (M$^+$). It matches the [(CH$_3$CN)Re(CO)$_3$(phdo)]$^+$ (calc.522.0094). The UV-Vis measurement shows a similar result to [(Cl)Re(CO)$_3$(phdo)],[81] but with a blue shift in the spectral bands.

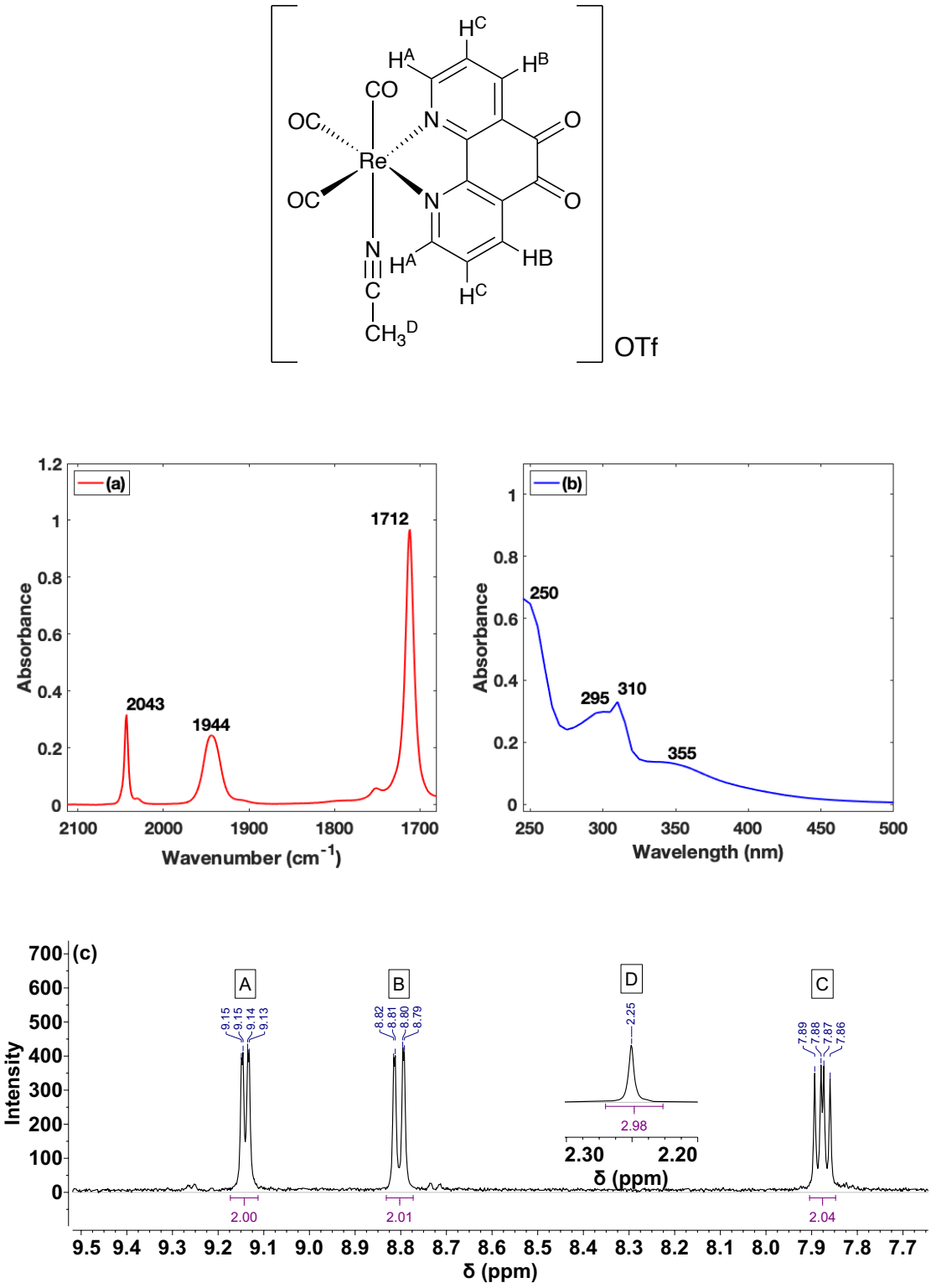

Figure 2.17 The spectra of $[(CH_3CN)Re(CO)_3(phdo)]OTf$. IR (a) and UV-Vis (b) in CH_2Cl_2; ^1H NMR (c) in CD_2Cl_2.

It is worth postulating that, due to the fast exchange of OTf and CH_3CN in polar solvents, an equilibrium could be in operation. To further confirm the equilibrium between [(OTf)Re(CO)$_3$(phdo)] and [(CH_3CN)Re(CO)$_3$(phdo)]OTf, the [(CH_3CN)Re(CO)$_3$(phdo)]OTf was dissolved in a more apolar solvent (ethyl acetate (EtOAc)), to observe if any [(OTf)Re(CO)$_3$(phdo)] was reformed. After 30 min of stirring, the mixture was analysed by ^{19}F NMR spectroscopy The ^{19}F NMR spectrum shows peaks at -77.51 ppm and -79.29 ppm which match the peaks with OTf ligand and OTf counter ion forms, respectively, providing evidence for the presence of an equilibrium (Figure 2.18).

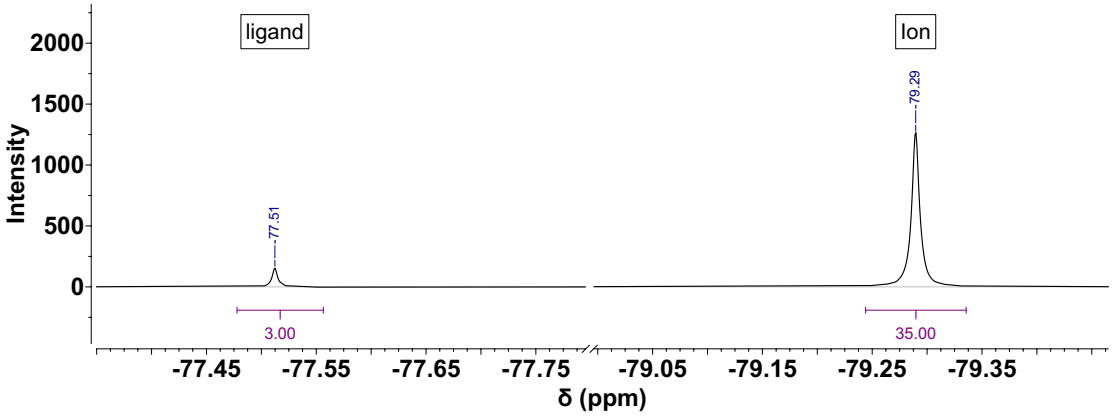

Figure 2.18 The ^{19}F NMR measurement of the reaction mixture of [(OTf)Re(CO)$_3$(phdo)] and [(CH_3CN)Re(CO)$_3$(phdo)]OTf in CD_2Cl_2.

2.3.4.1.1.4. The Emission Measurement of [(L)Re(CO)$_3$(phdo)]^n (L= Cl, OTf, CH3CN ; n=0, 1+).

The emission spectra were obtained for all compounds in CH_2Cl_2 and are shown in Figure 2.19. For the complex [(Cl)Re(CO)$_3$(phdo)] and [(OTf)Re(CO)$_3$(phdo)] no emission was observed. The [(Cl)Re(CO)$_3$(phdo)] in DMF was previously shown to be emissive.[81] However, in our measurement in CH_2Cl_2 no emission was observed, probably due to the solvent effects. The spectra of [(CH_3CN)Re(CO)$_3$(phdo)]OTf

shows a broad emission centred at 550nm, probably due to the ^{3}MLCT state. This might be since CH_3CN is a stronger field ligand compared to Cl or OTf, which may change the energy gap and the disfavouring the non-emissive relaxation pathway, therefore, the complex is emissive.

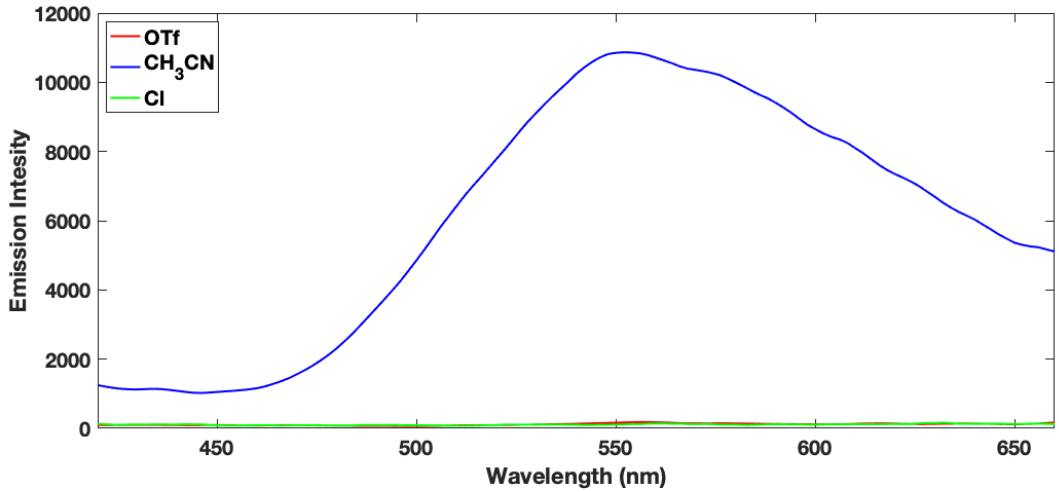

Figure 2.19 The emission spectra of $[(L)Re(CO)_3(phdo)]^n$ in CH_2Cl_2 (L = OTf, Cl, CH_3CN; n=0, 1+).

2.3.4.2. Synthesis of $[Re(CO)_2(phdo)_2]PF_6$ using the melting method

To afford the desired $[Re(CO)_2(phdo)_2]PF_6$, both $Re(CO)_3(phdo)OTf$ nor $[Re(CO)_3(phdo)(NCCH_3)]OTf$ were used in the presence of excess of phdo via previous described melting method.[58, 59] The melting reaction was attempted for $Re(CO)_3(phdo)OTf$ and $[Re(CO)_3(phdo)(CH_3CN)]OTf$ with phdo ligand, but did not yield the desired product. The phdo ligand was unstable in high temperatures, and it is reported that they undergo decomposition in temperature passing its meting point (258-260 °C). To avoid decompositions, the reaction temperature was lowered from 270 °C to 260 °C, and the reaction time was also reduced from 4 hours to 2 hours. However, even at these conditions, no product was detected, and decomposition of the ligand was

observed. Therefore, a new alternative method for the preparation of bis-diimine dicarbonyl complexes was attempted.

2.3.5. New and alternative synthesis route of for Rhenium dicarbonyl bis-diimine complexes via photochemical reaction

The second alternative method is based on photochemical isomerization, that can lead to CO loss to the solvent, forming a *cis*-dicarbonyl complex,[40-43, 57] that we propose that can undergo ligand substitution to form rhenium dicarbonyl bis-diimine complexes. The irradiation of a *fac* Rhenium complex using UV light formed the *mer* Rhenium complex isomer. The meridianal isomer of the complex can then undergo solvent exchange to form a cis complex, where both labile ligands are in a cis form, enabling exchange of a diimine ligand. If the same ligand exchange is performed and if the fac rhenium complex, the labile ligands go to a trans isomer form, that would not be able to do the coordination reaction of diimine.

As a proof of concept, [(Cl)Re(CO)$_3$(bpy)] and [(Cl)Re(CO)$_3$(phen)] was chosen to be used for investigation, because it is well known in the literature. In addition, their bis-diimine complexes are also reported in literature, allowing a comparison to verify if the proposed route can be used to synthetise rhenium dicarbonyl bis-diimine complexes. Two approaches are going to be tested: Facial-meridianal isomerization route and direct CO substitution route.

2.3.5.1. Analysis and Investigation of Facial-meridianal isomerization route

For the facial-meridianal isomerization route it was used [(Cl)Re(CO)$_3$(bpy)] (1a), due to the reaction to form the precursor for coordination of diimine ligand [(Cl)(CH$_3$CN)Re(CO)$_2$(bpy)] (**1c**) knowing in the literature. Therefore, the diimine

coordination step could take place with phdo ligand. The proposed reaction scheme is shown in Scheme 2.7.

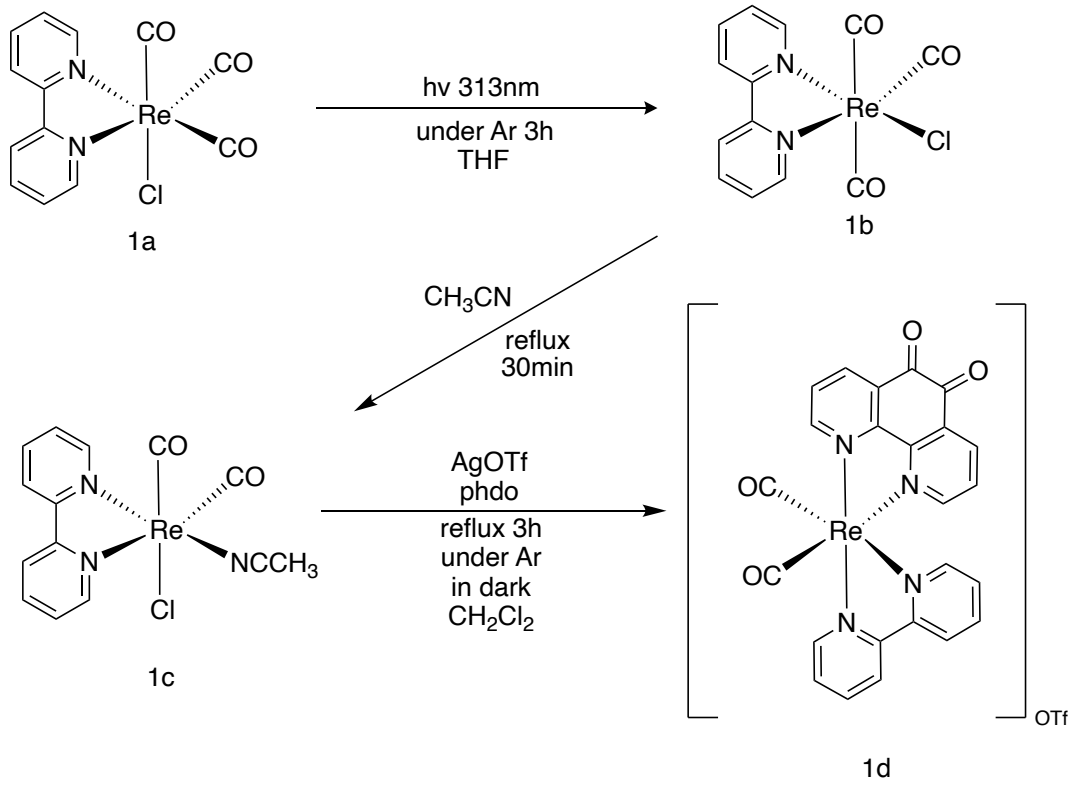

Scheme 2.7 The proposed reaction scheme for the Facial-meridianal isomerization route

The complexes *mer*-[(Cl)Re(CO)$_3$(bpy)] (**1b**) and *cis,cis*-[(Cl)(CH$_3$CN)Re(CO)$_2$(bpy)] (**1c**) were prepared following the conditions from literature,[40] and details are given in Section 4.2.9. The photolysis of *fac*-[(Cl)Re(CO)$_3$(bpy)] under UV irradiation formed the brown solid, that was analysed to be a mixture of the starting material and the desired *mer*-[(Cl)Re(CO)$_3$(bpy)] in low yield. The crude was then refluxed for 30 min in CH$_3$CN to give the *cis,cis*-[(Cl)(CH$_3$CN)Re(CO)$_2$(bpy)]. The mixture was then further reacted with AgOTf and phdo ligands in an attempt to obtain the desired *cis*-[Re(CO)$_2$(bpy)(phdo)]OTf. However, the reaction was found to yield bis-diimine dicarbonyl complex *cis*-[Re(CO)$_2$(bpy)$_2$]OTf (see below), indicating that some disproportionation reaction is operating. Attempts to purify other products of the

reaction mixture were unsuccessful.

2.3.5.1.1. FTIR measurements

FTIR measurements were taken for all three steps in the reaction (Figure 2.20). The FTIR spectrum for the photoisomerization step (Figure 2.20-a) shows the formation of the *mer*-[(Cl)Re(CO)$_3$(bpy)] (**1b)**, however, there are still strong absorptions the starting material **1a**, indicating a low yield for this step.

From the spectrum at Figure 2.20-b, it is possible to observe the appearance of absorption at 1913 and 1830 cm^{-1} relative to the formation of *cis,cis*-[(Cl)(CH$_3$CN)Re(CO)$_2$(bpy)], and the disappearance of the signal of *mer*-[(Cl)Re(CO)$_3$(bpy)]. Finally, upon the reaction of the phdo ligand, the FTIR spectrum (Figure 2.20 -c) shows only two strong absorptions in 1917 and 1848 cm^{-1}, missing the absorption due to the phdo carbonyl group. This absorption position matches the signals for *cis*-[Re(CO)$_2$(bpy)$_2$]OTf (**1d'**),[58] indicating that this complex of formed instead of *cis*-[Re(CO)$_2$(bpy)(phdo)]OTf.

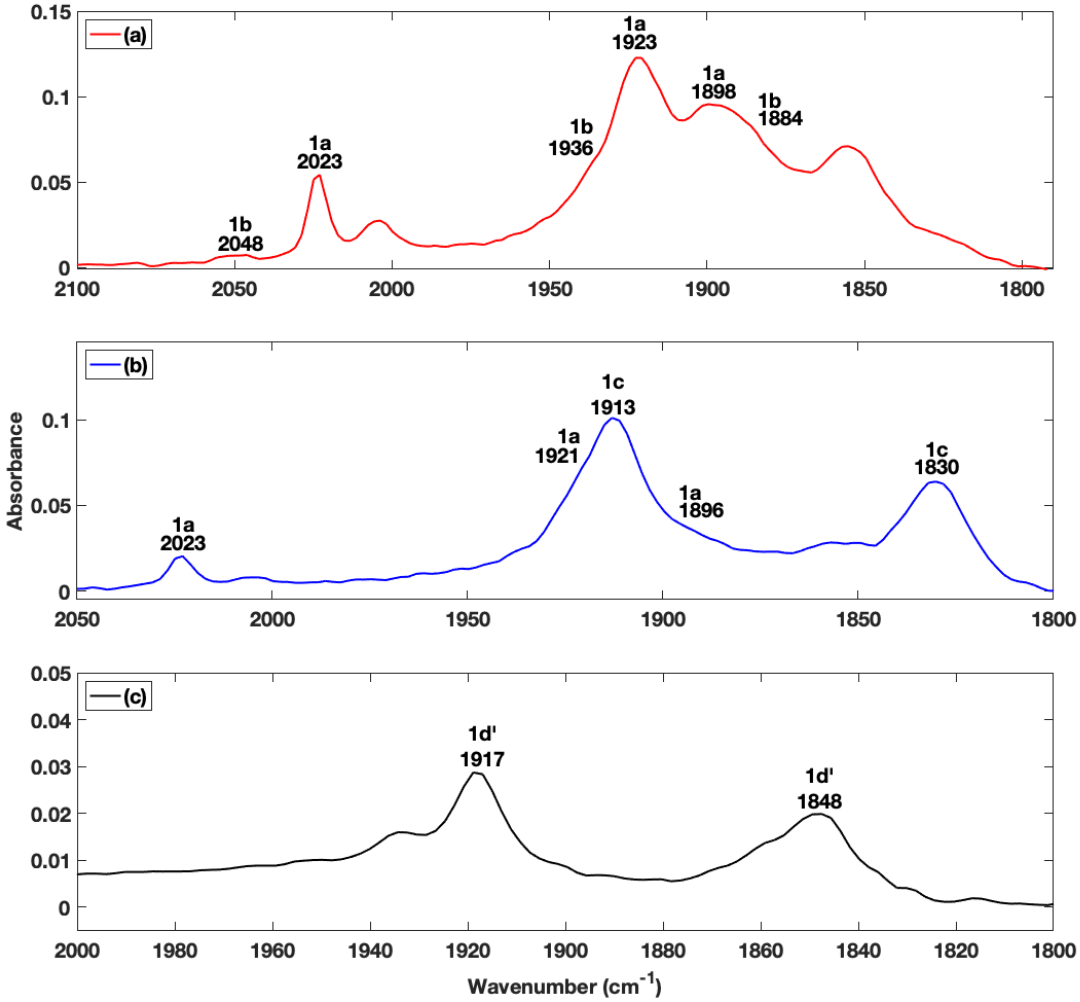

Figure 2.20 The IR spectra of Facial-meridianal isomerization route in each step. Formation of *mer*-[(Cl)Re(CO)$_3$(bpy)] (a). Formation of *cis, cis*-[(Cl)(CH$_3$CN)Re(CO)$_2$(bpy)] (b). Formation of bis-diimine complex (c).

2.3.5.1.2. ^{1}H NMR measurements

The ^{1}H NMR spectra for all compounds (Figure 2.21) was obtained and the results agree with the ones obtained by FTIR. The ^{1}H NMR spectrum for *mer*-[(Cl)Re(CO)$_3$(bpy)] (Figure 2.21-a) shows the 8 protons signals, due the lack of symmetry in the complex. The ^{1}H NMR spectrum for the *cis,cis*-[(Cl)(CH$_3$CN)Re(CO)$_2$(bpy)] (Figure 2.21-b) confirm the formation of the desired

complex, in agreement with previously reported data.[42] Finally, the ^{1}H NMR spectrum for *cis*-[Re(CO)$_2$(bpy)$_2$]OTf (Figure 2.21-c) is also consistent with result previously reported[58] and it is consistent with literature. Also, the spectrum shows unknown phdo ligand complex which the shift of the phdo ligand has a blue shift and the proton signal pattern did not separate.

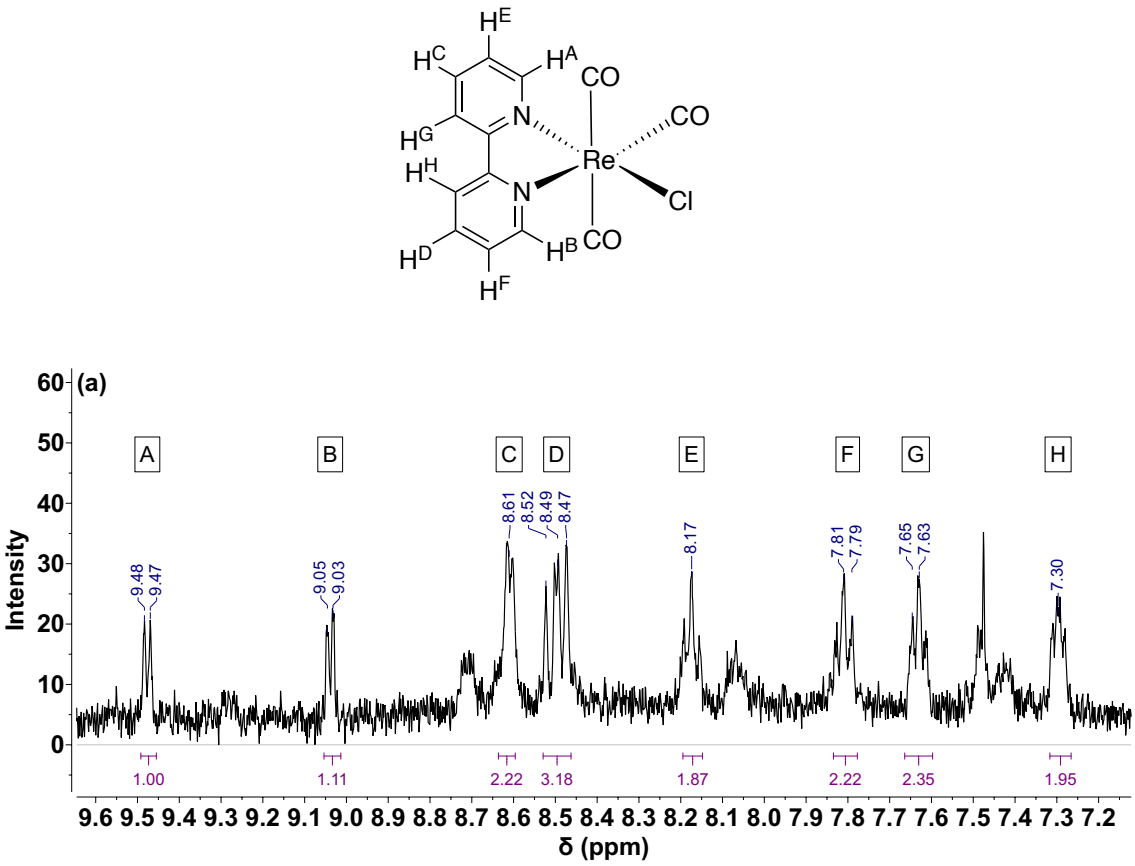

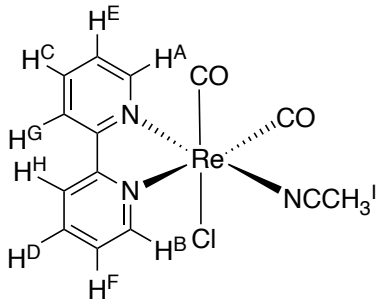
H^E
H^C
H^A
CO
N
CO
H^G
Re
H^H
N
NCCH3^I
H^D
H^B
Cl
H^F

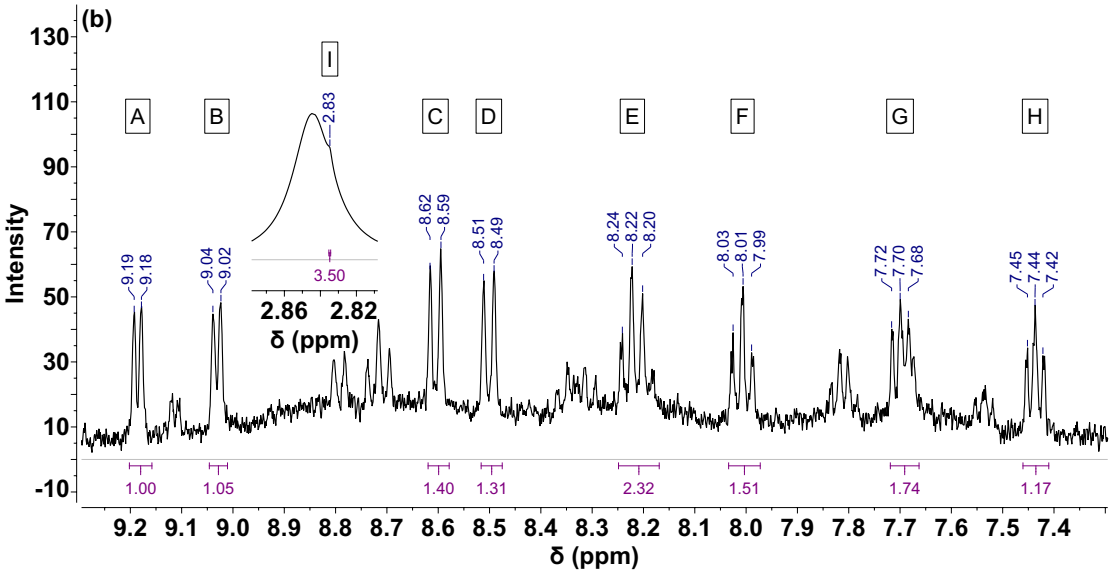
(b)
Intensity
A
B
I
C
D
E
F
G
H
2.83
3.50
2.86 2.82
δ (ppm)
9.19
9.18
9.04
9.02
8.62
8.59
8.51
8.49
8.24
8.22
8.20
8.03
8.01
7.99
7.72
7.70
7.68
7.45
7.44
7.42
1.00
1.05
1.40
1.31
2.32
1.51
1.74
1.17
δ (ppm)

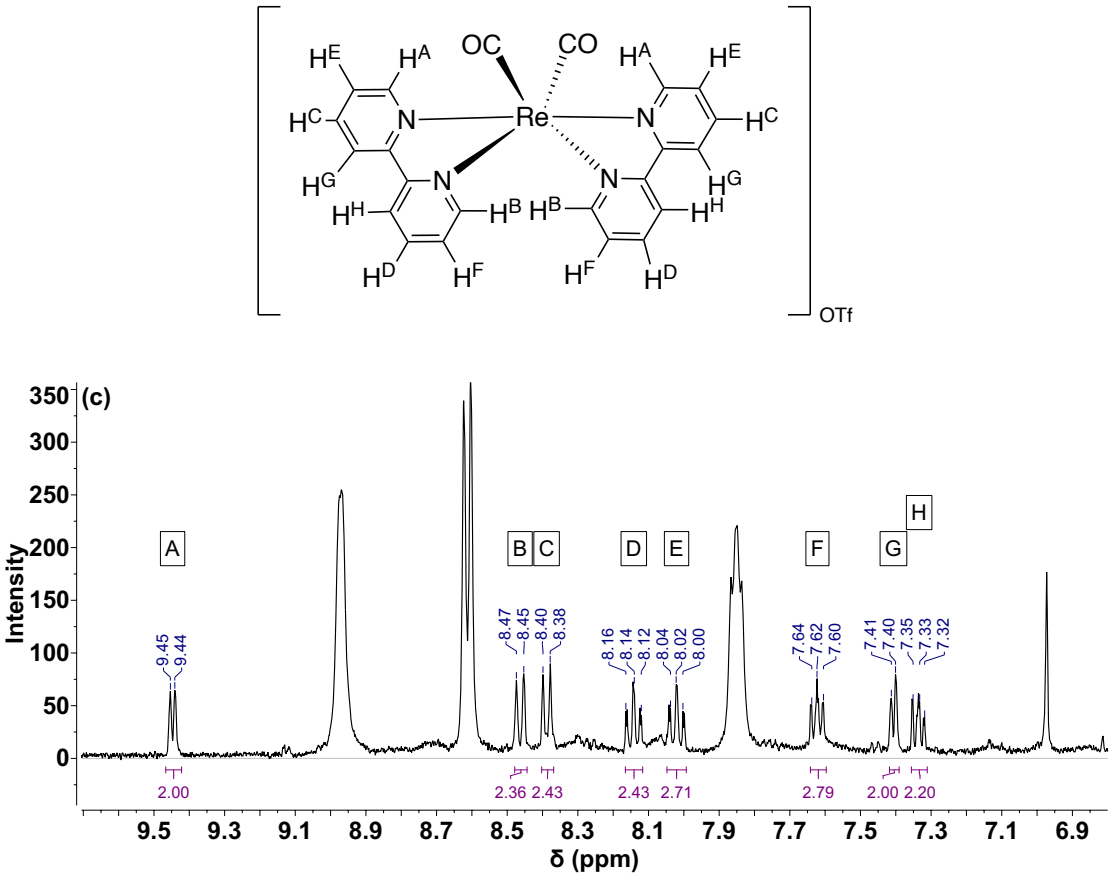

Figure 2.21 The ^{1}H NMR spectra of Facial-meridianal isomerization route in each step. Formation of *mer*-[(Cl)Re(CO)$_3$(bpy)](THF-d^8)(a). Formation of *cis, cis*-[(Cl)(CH$_3$CN)Re(CO)$_2$(bpy)] (acetone-d^6) (b). Formation of bis-diimine complex (CD$_3$CN) (c).

2.3.5.1.3. HRMS measurement

In order the further confirm the structure of the Rhenium bis-diimine dicarbonyl complex prepared, HRMS was obtained for *cis*-[Re(CO)$_2$(bpy)$_2$]OTf. The HRMS shows a peak of 555.0824 m/z relative to the ion (M^+) which matches the mass of [Re(CO)$_2$(bpy)$_2$]$^+$ (calc. 555.0825). The HRMS was not obtained for the other complex due the low stability of the complexes in polar solvents.

2.3.5.1.4. Conclusion of Facial-meridianal isomerization route

Several conclusions can be made from all the results above: the facial-meridianal isomerization route success to make rhenium dicarbonyl bis-diimine complexes form *cis*,*cis*-[(Cl)(CH_3CN)Re($CO)_2$(bpy)] precursor via formation of *mer*-[(Cl)Re($CO)_3$(bpy)]. However, the mixed ligands [Re($CO)_2$(bpy)(phdo)]$^+$ were not successfully made, instant by the route made by [Re($CO)_2$($bpy)_2$]$^+$ and what is currently an unknown phdo complex. The result might be interpreted that, if there are different ligands, the one more reactive will replace the one less reactive during the reaction. The step of the proposed route is the reaction of [(Cl)(CH_3CN)Re($CO)_2$(bpy)] with AgOTf to make [(OTf)(CH_3CN)Re($CO)_2$(bpy)] separate with ligand coordination which may make the reactive ligands easier to coordinate rather than replace the original ligand and clearly this needs to be further investigated. The result might also suggest that the unknown phdo ligand complex maybe *cis*,*trans*-[($CH_3CN)_2$Re($CO)_2$(phdo)]OTf because the ^{1}H NMR spectrum shows symmetry of the proton signal of the ligand and again this also need to be further investigated.

2.3.5.2. Analysis and Investigation of Direct CO substitution route

For the direct CO substitution route we investigated [(Cl)Re($CO)_3$(phen)] (**2a**), as the meridianal isomer of the complex was not present in the literature and the meridianal isomer may not stable in solvent. Therefore, direct CO substitution may be more promising to get *cis,cis*-[(Cl)(CH_3CN)Re($CO)_2$(phen)] (**2b**). As **2b** precursor is unknown, phen was used for the diimine coordination reaction to give **2c** in order to simplify the system. The proposed reaction scheme is shown in Scheme 2.8.

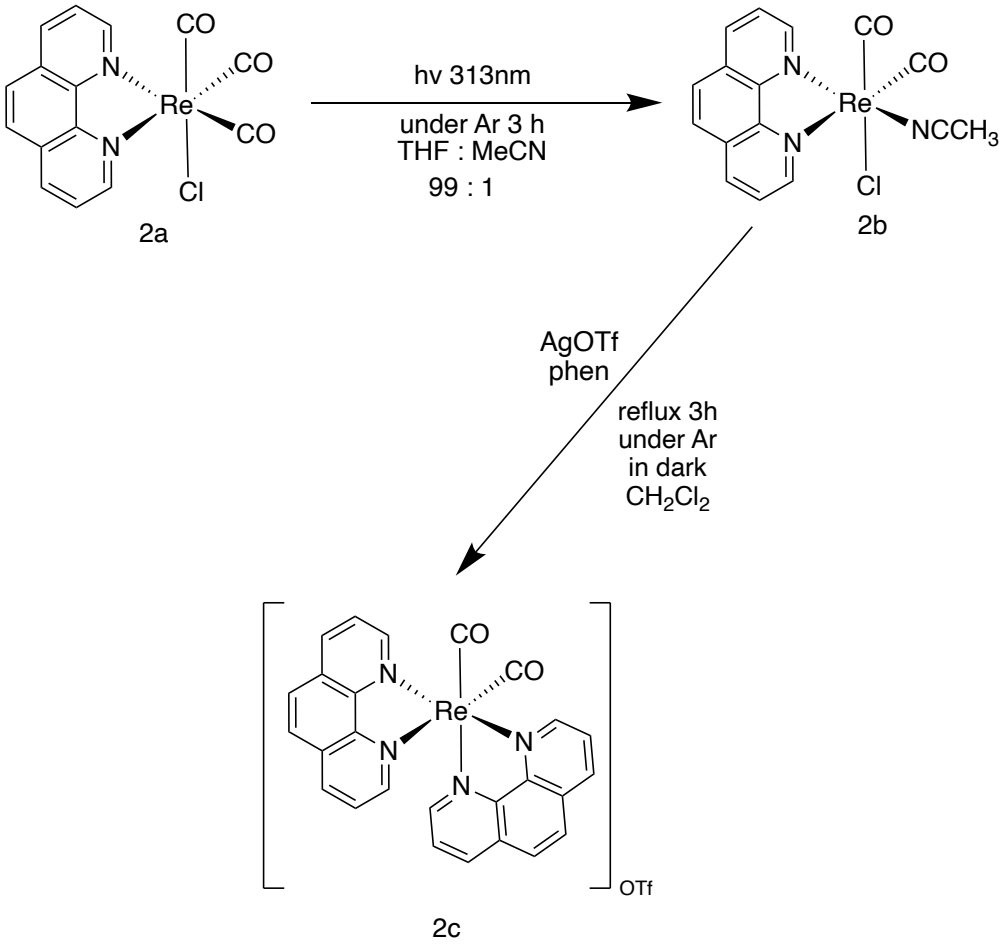

Scheme 2.8 The proposed reaction scheme for the Direct CO substitution-cis,cis isomer route.

The formation of *cis,cis*-[(Cl)(CH_3CN)Re($CO)_2$(bpy)] was performed following similar synthetic condition in the literature,[43] and is detailed in experiment Section 4.2.10. All the steps were followed by FTIR, ^{1}H NMR and HRMS measurements.

2.3.5.2.1. FTIR measurement

FTIR measurements were used to monitor the reaction. The UV irradiation of [(Cl)Re($CO)_3$(phen)] for three hours gave a black solution, that after purification CH_2Cl_2/hexane afforded a red solid. The solid was analysed by FTIR and the spectrum (Figure 2.22-a) showed the strong absorption at 1911 and 1830 cm^{-1} corresponding to the desired *cis,cis*-[(Cl)(CH_3CN)Re($CO)_2$(phen)]. It is also possible to observe a small

signal at 2023 cm^{-1}, indicating that some starting material is still present. The crude product was refluxed in presence of AgOTf and phen ligand for three hours. The FTIR spectrum (Figure 2.22-b) obtained after 3h shows absorption at 1927 and 1844 cm^{-1}, relative to the [(Cl)(OTf)Re$(CO)_2$(phen)](**2b'**) intermediate. The reaction was then refluxed for further 12h in CH_3OH. The FTIR spectrum (Figure 2.22-c) after this time only afforded in CH_2Cl_2 under reflux 3 hours and simple purification will show the appearance 1921 and 1846 cm^{-1}, corresponding to the formation of the desired *cis*-[Re$(CO)_2(phen)_2$] (**2c**). It is also possible to observe the appearance of signals at 1913 and 1832 cm^{-1}, that matches with the reported *cis,cis*-[$(CH_3CN)_2$Re$(CO)_2$(phen)] (**2b"**).

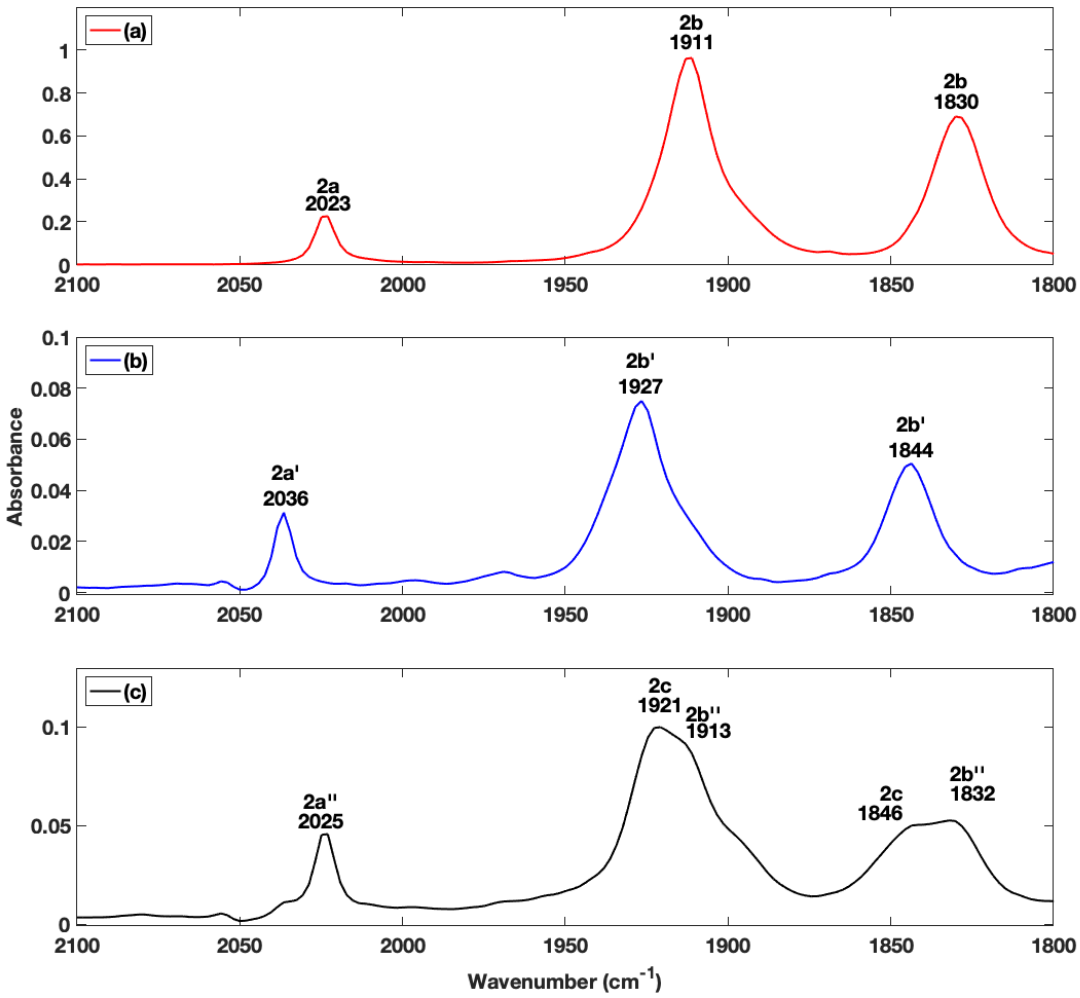

Figure 2.22 The IR spectra of Direct CO substitution-cis, cis isomer route in each step. Formation of *cis, cis*-[(Cl)(CH_3CN)Re($CO)_2$(phen)] (a). Formation of *cis,cis*-[(OTf)(CH_3CN)Re($CO)_2$(bpy)] (b). Formation of bis-diimine complex (c).

2.3.5.2.2. ^{1}H NMR measurement

The system was also analysed by ^{1}H NMR spectroscopy. Similar to the FTIR data, it is possible to observe the formation of *cis,cis*-[(Cl)(CH_3CN)Re($CO)_2$(bpy)] after irradiation of[(Cl)Re($CO)_3$(phen)] (Figure 2.23-a). Then the final complex *cis*-[Re($CO)_2$(phen)$_2$] (**2c**) was also analysed by ^{1}H NMR spectroscopy.(Figure 2.23-b) However, a complex mixture of compounds was found, that included the characteristic signal of the product at 9.93 ppm. It is also possible to observe residual phenanthroline

starting material and possibly the *cis,cis*-[$(CH_3CN)_2Re(CO)_2$(phen)] (**2b"**).

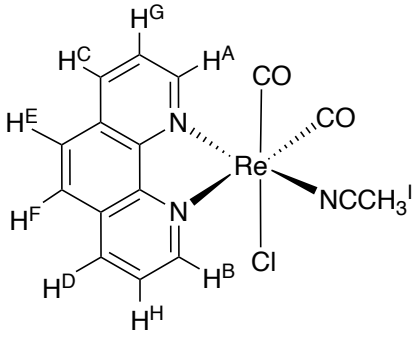
H^G
H^C
H^A
CO
H^E
N
CO
Re
NCCH3^I
H^F
N
Cl
H^D
H^B
H^H

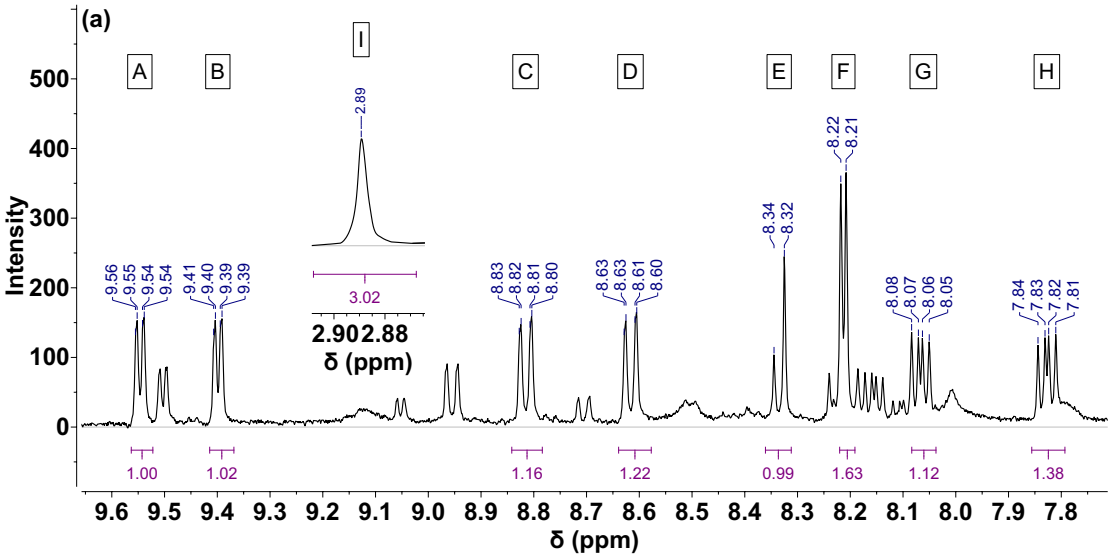
(a)
A
B
I
C
D
E
F
G
H
Intensity
500
400
300
200
100
0
2.89
3.02
2.902.88
δ (ppm)
9.56
9.55
9.54
9.54
9.41
9.40
9.39
9.39
8.83
8.82
8.81
8.80
8.63
8.63
8.61
8.60
8.34
8.32
8.22
8.21
8.08
8.07
8.06
8.05
7.84
7.83
7.82
7.81
1.00
1.02
1.16
1.22
0.99
1.63
1.12
1.38
9.6 9.5 9.4 9.3 9.2 9.1 9.0 8.9 8.8 8.7 8.6 8.5 8.4 8.3 8.2 8.1 8.0 7.9 7.8
δ (ppm)

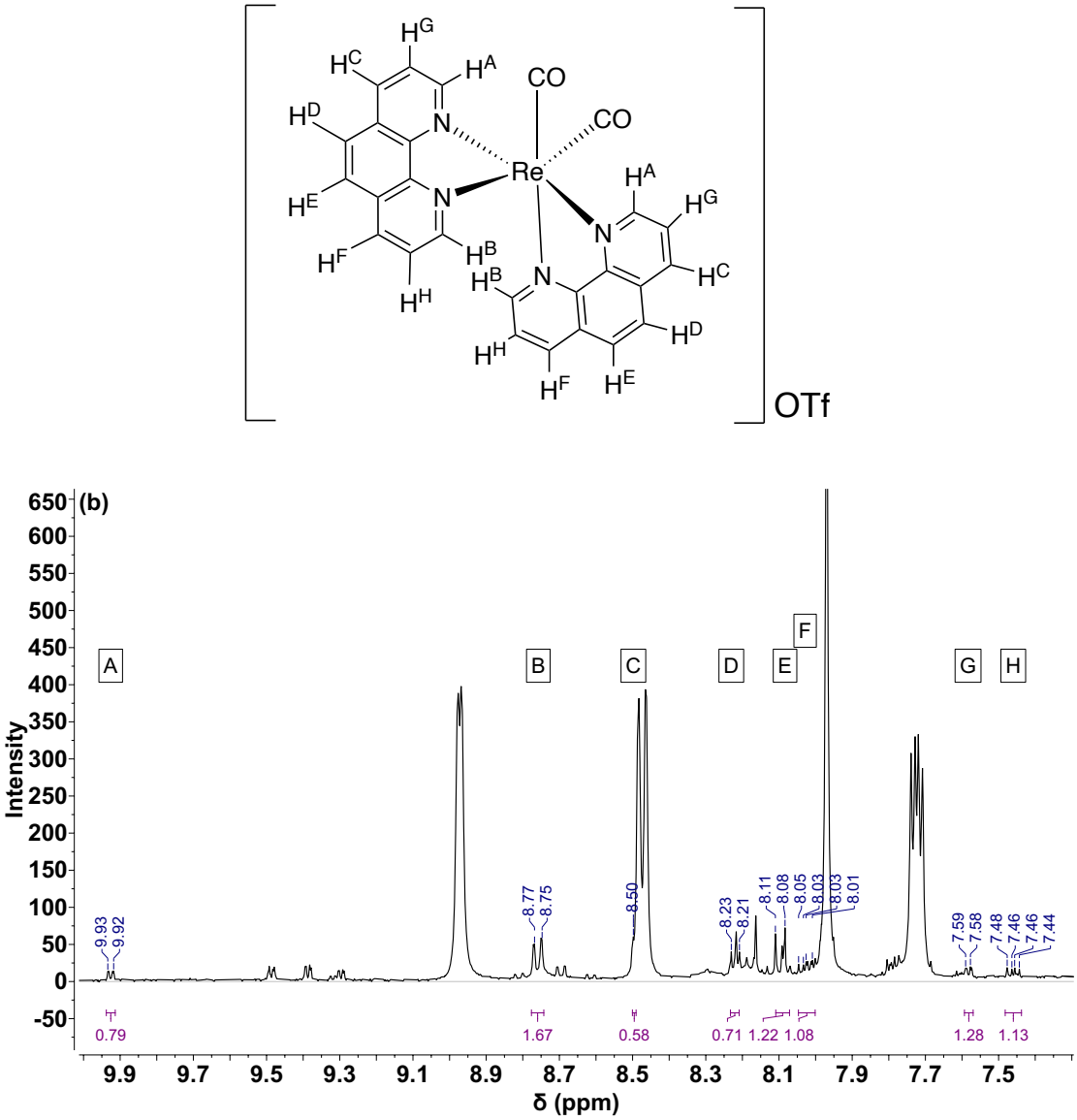

Figure 2.23 The ^{1}H NMR spectra of Direct CO substitution-cis, cis isomer route in each step. Formation of *cis,cis*-[(Cl)(CH_3CN)Re($CO)_2$(bpy)] (spectrum (a)) and the final formation bis-diimine complex (spectrum (b))

2.3.5.2.3. HRMS measurement

In order the further confirm the structure of the Rhenium bis-diimine dicarbonyl complex prepared, HRMS was obtained for *cis*-[Re($CO)_2$(phen)$_2$]OTf. The HRMS

shows a peak with 603.0825 m/z relative to the ion (M^+) which matches the mass of $[Re(CO)_2(phen)_2]^+$ (calc. 603.0825, error. 1.20 ppm). The HRMS of *cis, cis*-$[(Cl)(CH_3CN)Re(CO)_2(phen)]$ was not obtained due to the low stability of the complex in polar solvents.

2.3.5.2.4. Conclusion of Direct CO substitution-cis, cis isomer route

The direct CO substitution-cis, cis isomer route success to make Rhenium dicarbonyl bis-diimine complexes form cis, cis- $[(Cl)(CH_3CN)Re(CO)_2(phen)]$ precursor. Due to phen ligand reactivity, under 40 ˚C, reflux was not providing enough energy to complete the reaction in coordinate reaction. Therefore, we observed *cis, cis*-$[(OTf)(CH_3CN)Re(CO)_2(phen)]$ in IR measurement. The reaction continued in CH_3OH at higher temperature 80 ˚C, which we see the formation on cis-$[Re(CO)_2(phen)_2]OTf$. IR, NMR and HRMS show their peak and consistent with the literature.[58] Also, two possible complex *cis*, *cis*- $[(CH_3CN)_2Re(CO)_2(phen)]$ and *fac*-$[(CH_3CN)Re(CO)_2(phen)]$ were observed, but still need these results need further investigated to confirm.

2.4. Conclusion

This chapter could be concluded in three parts: general synthetic route to make $[Re(CO)_2(dppp2)_2]PF_6$, attempted alternative synthesis route to make $[Re(CO)_2(dppp2)_2]PF_6$ and invented new synthesis route for synthesizing dicarbonyl bis-diimine complexes.

In the first part of this work, the dppp2 ligand was synthesized. During the synthesis of dppp2 ligand, intermediate of the reaction was observed and characterized by ^1H NMR, ^{13}C NMR and HRMS. After that, two new intermediate complexes

[(OTf)Re(CO)$_3$(dppp2)] and [(CH$_3$CNRe(CO)$_3$(dppp2)]OTf as precursors have been successfully synthesized. Both complexes had characterized by FTIR, UV-Vis, ^{1}H NMR, ^{19}F NMR and HRMS. Also, emission measurements have been done. Furthermore, both intermediate complexes were attempted to be used as precursors to obtain [Re(CO)$_2$(dppp2)$_2$]$^+$ by using the "melting method". Only [(CH$_3$CN)Re(CO)$_3$(dppp2)]OTf melting with dppp2 ligand gave the desired product [Re(CO)$_2$(dppp2)$_2$]PF$_6$ with low yield and characterized by FTIR ^{1}H NMR, ^{19}F NMR and HRMS. The characterization showed that melting reaction resulted in one of the isomers of the complex.

In the second part of this work, an alternative synthesis route had been attempted. Two new complexes [(OTf)Re(CO)$_3$(phdo)] and [(CH$_3$CNRe(CO)$_3$(phdo)]OTf have been successfully synthesized to be used as precursors, and were characterized by FTIR, UV-vis, ^{1}H NMR, ^{19}F NMR, HRMS and emission spectroscopy. Both intermediate complexes were attempted to be used as precursors to obtain [Re(CO)$_2$(phdo)$_2$]$^+$ by using the "melting method". Unfortunately, none of the complexes led to the desired product.

In the third part of this work, due to the limitation of the "melting method", a new synthesis route for dicarbonyl bis-diimine complexes was investigated. Therefore, two new synthesis routes were proposed: Facial-meridianal isomerization route and direct CO substitution route. The result shows the Facial-meridianal isomerization route successfully synthesized dicarbonyl bis-diimine complex. However, instead of the proposed mixed ligand complex, the route yielded [Re(CO)$_2$(bpy)$_2$]$^+$ via *mer*-[(Cl)Re(CO)$_3$(bpy)] and *cis*,*cis*-[(Cl)(CH$_3$CN)Re(CO)$_3$(bpy)] as precursors. On the other hand, the direct CO substitution route led successfully to the dicarbonyl bis-

diimine complex. The route yielded $[Re(CO)_2(phen)_2]^+$ via *cis*,*cis*-$[(Cl)(CH_3CN)Re(CO)_3(phen)]$ as precursor step. Overall, both routes can successfully synthesize dicarbonyl bis-diimine complex, but the yields were very low, and the reaction conditions need further investigation.

2.5. Future work

In the future, further investigation of $[Re(CO)_2(diimine)_2]^+$ could be investigated. The negative results of some of the melting reactions could be further investigated using protection group on phdo ligand to make them survive melting reaction conditions. According to the literature, [82, 83] the melting point of phdo after adding a protection group can increase its melting point to 270 °C above with no mention of decomposition. The addition of the protection group could be added by organic synthesis or electrochemistry synthesis.[82, 83] The synthesis of $[Re(CO)_2(phdo)_2]^+$ as precursors will open up of dppz like complexes.

Secondly, we could further develop the two new synthesis routes presented in this chapter. The improvement could be explored in a few directions. We could improve the photoreaction for better yield. For example, we could use photo-flow-reactors to reduce the opportunity for complex decomposition by high energy UV lamp. Also, we could use CCl_3CN as a solvent ligand to produce *cis*,*cis*-$[(OTf)(CCl_3CN)Re(CO)_2(diimine)]$ precursors. In the literature it has been shown[84] that CCl_3CN has the poor coordinating ability compare to CH_3CN, which can provide a better leaving group for attaching the second diimine ligand.[84] Moreover, the OTf ligand exchange step becomes the new step which not done in the same pot, may help to attach mixed diimine ligands. It is because that can reduce the opportunity for the stronger coordinating ability diimine ligand replace the weaker coordinating ability diimine ligand.

Finally, the photophysics of different bis-diimine complex could be investigated further as they show potential in many areas. Unfortunately, planned TRIR measurement was not possible due to the instrument being down and not operating at the time complexes were produced. For example, $[Re(CO)_2(dppp2)_2]^+$, if we are able to get the pure complex in the future and probing the photophysics by TRIR and emission of the complex may further understand the system of $[Re(CO)_2(diimine)_2]^+$, to see how different diimine ligand affect the photophysics.

3. Chapter 3

Probing temperature effect on the photochemistry and photophysics of $[Re(CO)_4(4,4'\text{-}R_2\text{-}bpy)]PF_6$ in CH_2Cl_2 and CH_3CN

3.1. Introduction

3.1.1. Rhenium(I) tetracarbonyl diimine complexes

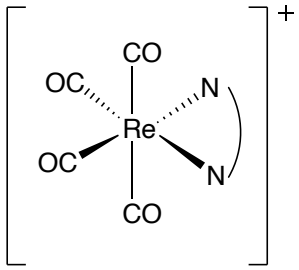

Figure 3.1 The structure of $[Re(CO)_4(N,N)]^+$ (N,N = diamine ligand)

Rhenium tetracarbonyl diimine complexes are a group of Rhenium carbonyl complexes that have not been as widely investigated. The most common structure is $[Re(CO)_4(N,N)]^+$ (where N,N is diimine ligand). The structure is shown in Figure 3.1. The studies to date have focused on complexes with bipyridine and phenazine ligands.[46, 47, 85, 86]

3.1.1.1. Synthesis of $[Re(CO)_4(N,N)]^+$

The synthesis of $[Re(CO)_4(N,N)]^+$ is relatively simple and the can be made by reacting $Re(CO)_5X$ (where X is Cl or Br) with Ag(OTf) to give $Re(CO)_5(OTf)$. This can be further reacted with target diimine ligand (N,N) to give $[Re(CO)_4(N,N)]^+$. The reaction conditions require the reaction to be carried out in the dark and under an inert atmosphere. The temperature required for the reaction depends on the nature of the diimine ligand.[46, 47, 85, 86] The reaction scheme is shown in Scheme 3.1

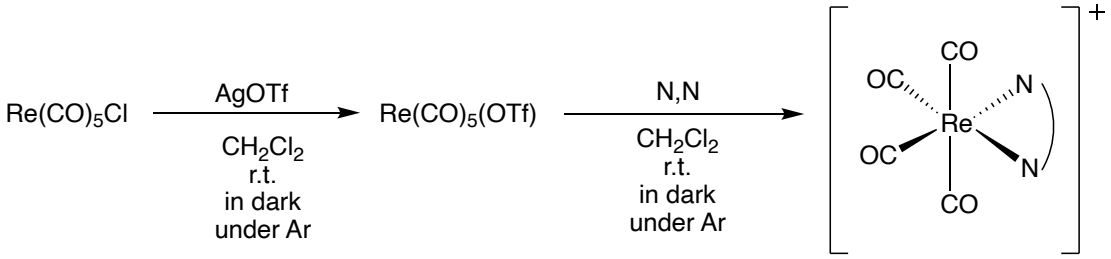

Scheme 3.1 the reaction of Synthesis of $[Re(CO)_4(N,N)]^+$

3.1.1.2. FTIR spectra of $[Re(CO)_4(N,N)]^+$

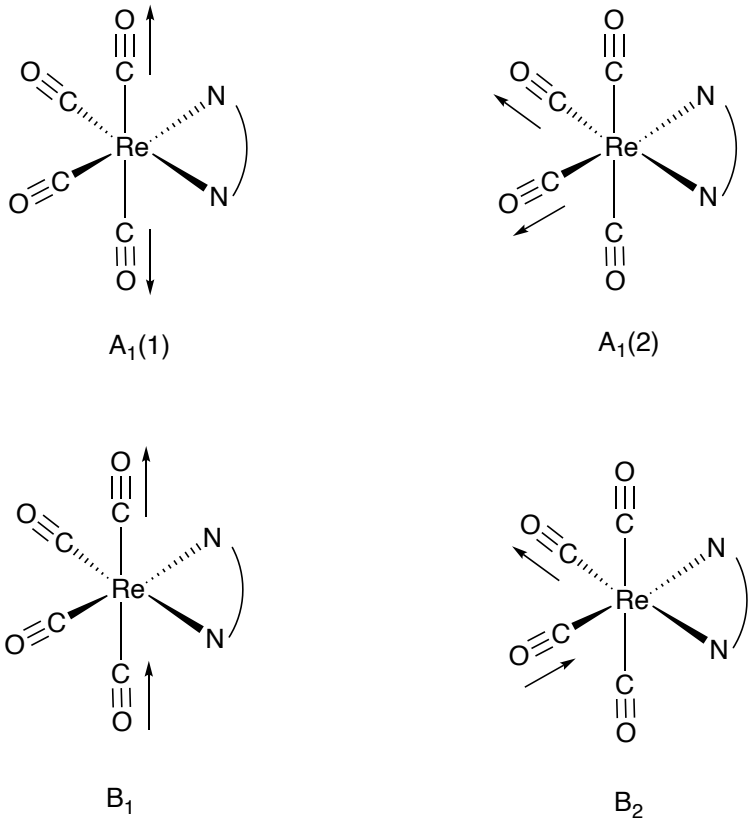

Figure 3.2 Different infrared ν(CO) modes of $[Re(CO)_4(N,N)]^+$

The infrared spectra of Rhenium tetracarbonyl diimine complexes contain four infrared bands consistent with the binding modes $A_1(1)$, $A_1(2)$, B_1 and B_2, as shown in Figure 3.2. For $[Re(CO)_4(bpy)]^+$, the ground state infrared bands in the ν(CO) region are observed at 1969, 2011, 2029, and 2123 cm^{-1}, corresponding to the B_2, $A_1(2)$, B_1 and

$A_1(1)$ modes respectively.[46, 47, 85]

3.1.1.3. ^{1}H NMR spectra of $[Re(CO)_4(N,N)]^+$

The ^{1}H NMR of the diimine ligand will shift to a higher position, but it will have a similar pattern as the chromophore ligand itself because the electron density is donating to the metal centre, which will deshield the protons. Furthermore, the tetracarbonyl complex will not affect the ligand symmetry too much, and the ^{1}H NMR will show the peak symmetry as a pure ligand.[46, 47, 85, 86]

3.1.1.4. Photochemistry and photophysics of $[Re(CO)4(N,N)]^+$

In papers spanning from 1990 to 1992, Shaver *et al.* investigated the photophysics of a number of Rhenium tetracarbonyl complexes.[86, 87] In their report it was shown that $[Re(CO)_4(bpym)]BF_4$ (bpym = 2,2-bipyrimidine) had vastly different properties compared to its tricarbonyl relatives. They found that tetracarbonyl complex had high emission energies, long lifetimes and that the excited states had powerful oxidant properties. Shaver suggested that exchanging one of the axial ligands from Cl to a strong field CO ligand will decrease the non-radiative decay pathway. Furthermore, they also investigated several other complexes, including $[Re(CO)_4(bpy)]^+$ (bpy = 2,2'-bipyridine), $[Re(CO)_4(dmb)]^+$ (dmb = 4,4'-dimethyl-2,2'-bipyridine) and $[Re(CO)_4(phen)]^+$ (phen = 1,10-phenanthroline), showed that changing the diimine ligand can vastly change the photophysical properties of the complex.[86, 87]

In 2000, Bernhard *et al*. conducted the TRIR measurements of $[Re(N,N)(CO)_4]^+$ (where N,N = 2,2'-bipyridine (bpy), 4,4'-dimethyl-2,2'-bipyridine (dmb), or 1,10-phenanthroline (phen)) in 1,2-dichloroethane (DCE). [88] The tetracarbonyl complex was probed following excitation at 355 nm. It was found that there was a formation of a

unique excited state that was assigned as a mixture of both MLCT character and LC excited state character, followed by the dissociation of a single CO ligand to form a *fac*–$[Re(CO)_3(N,N)(solvent)]^+$ complex. The bands corresponding to the $A_1(2)$, B_1 and B_2 modes shifted slightly to a higher energy, while the bands of the $A_1(1)$ mode shifted to a slightly lower energy. The characteristic shift to lower energy for an LC state (< 10 cm^{-1}) was thought to be counteracted by the larger shift to a higher energy of the MLCT state (> 40 cm^{-1}). This shift of the bands was attributed with the mixed ^{3}LC and ^{3}MLCT state for all three complexes. Bernhard *et al.* also showed the long-lived excited states that underwent photodissoiciation of a CO ligand and all show in the mixed ^{3}LC and ^{3}MLCT excited state.[88] The TRIR of $[Re(phen)(CO)_4]^+$ from Bernhard *et al* is shown in Figure 3.3

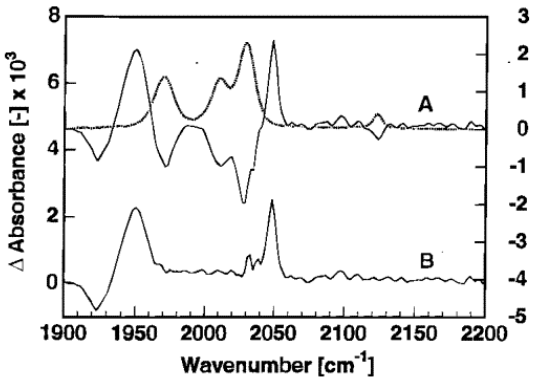

Figure 3.3 The IR spectrum of the photoproduct of $[Re(CO)_4(phen)]^+$ in DCE reported by Bernhard et al. The ground state spectrum is shown for comparison (A, dotted line) with the calculated photoproduct spectrum shown as (B). It is adapted from the reference[88].

3.1.1.4.1. Photochemistry and photophysics of $[Re(CO)_4(bpy)]^+$

More recently work in our group,[46] investigated the photophysics of $[Re(CO)_4(bpy)]^+$ by performing ns-TRIR and ps-TRIR measurement of $[Re(CO)_4(bpy)]PF_6$ in CH_2Cl_2 and CH_3CN following a 355 nm excitation. It was reported that in both solvents the

complex shows in two major excited states, which are State I and State II (ILCT/MLCT). Also, the photoproduct formation $[Re(CO)_3(bpy)(solvent)]^+$ was found and the data is shown in Figure 3.4

Solvent	Nature of State	Band Position (cm^{-1})	τ
CH_2Cl_2	State I	2067, 1966, 1973	100 ($\pm$ 10) ns
	ILCT/MLCT	2113, 2040, 2020, 1986	2.9 ($\pm$ 0.3) μs
	$[Re(CO)_3(bpy)(CH_2Cl_2)]$	2054, 1955	-
CH_3CN	State I	2111, 2060, 2037, 2009	160 ($\pm$ 30) ns
	ILCT/MLCT	2112, 2039, 2010, 1983	2.1 ($\pm$ 0.4) μs
	$[Re(CO)_3(bpy)(CH_3CN)][PF_6]$	2039, 1938	-

Figure 3.4 The ns-TRIR and ps-TRIR measurement of $[Re(CO)4(bpy)]PF_6$ in CH_2Cl_2 and CH_3CN. It is adapted from the reference[46].

Reynolds's also reported that the luminescence spectroscopy in CH_2Cl_2 and CH_3CN shows emission spectra. It has been assigned with the strong vibronic character at 449 and 479 nm, along with the broader, structureless region at lower energy (ca. 507 nm) consistent with a mixed ^{3}ILCT/^{3}MLCT state. The emission shown in Figure 3.5.

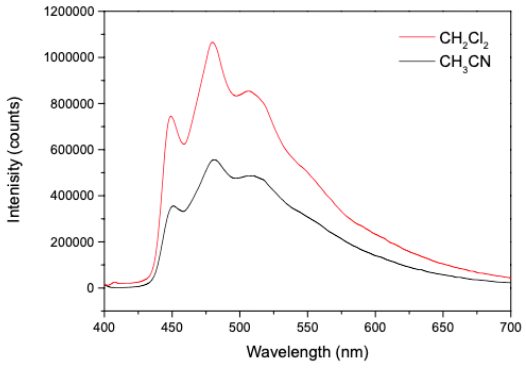

Figure 3.5 The emission spectra of $[Re(CO)4(bpy)]PF_6$ in CH_2Cl_2 and CH_3CN. It is adapted from the reference[46].

Furthermore, combining all spectroscopy data and TD-DFT calculations, Reynolds reported that following excitation, a high energy singlet is seen to decay and populate two mixed excited states, State I and State II, this is observed to occur on the picosecond timescale. State I was shown to decay on the nanosecond timescale. The TD-DFT calculations suggest that this state has both ^{3}ILCT and ^{3}MLCT nature, where the ^{3}MLCT is resulted from a charge transfer from the rhenium onto the bipyridine ligand. In comparison, the State II excited state decays on the microsecond timescale and results in the photodissociation of a CO ligand. The TD-DFT calculations have identified that this state also has both ^{3}ILCT and ^{3}MLCT nature, however, the ^{3}MLCT results from charge transfer from the rhenium onto the axial CO ligands.[46] The process that occurs is illustrated in Figure 3.6

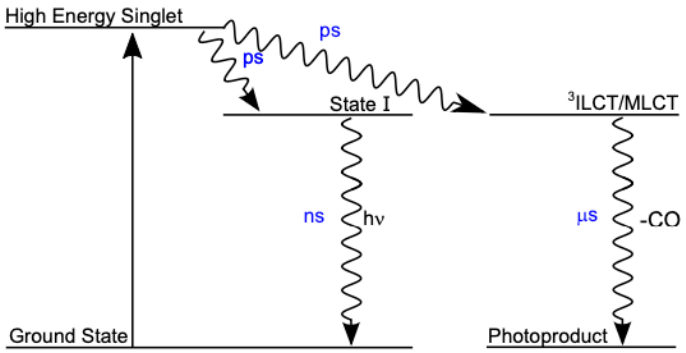

Figure 3.6 An illustration of the photophysical and photochemical processes that occur for [Re(CO)4(bpy)]PF_6 following 355 nm excitation. It is adapted from the reference[46].

3.1.1.4.2. The effect of temperature on photochemistry and photophysics

More recently, our group reported[85] the temperature dependent ns-TRIR measurement of [$Re(CO)_4(bpy)$]PF_6 in CH_2Cl_2 and CH_3CN following a 355 nm excitation.

In the study, TRIR results were reported in CH_2Cl_2 every five degrees from 5 to 35 ˚C.

At all temperatures, the same excitation profile was observed with State I, State II and the CO loss photoproduct. There were no new peaks observed at low or high temperature. Also, analysis of the single point kinetics showed no large dependence on temperature for either the decay of State I, State II or the growth of the photoproduct. The TRIR spectra in CH_2Cl_2 were reproduced and shown in Figure 3.7

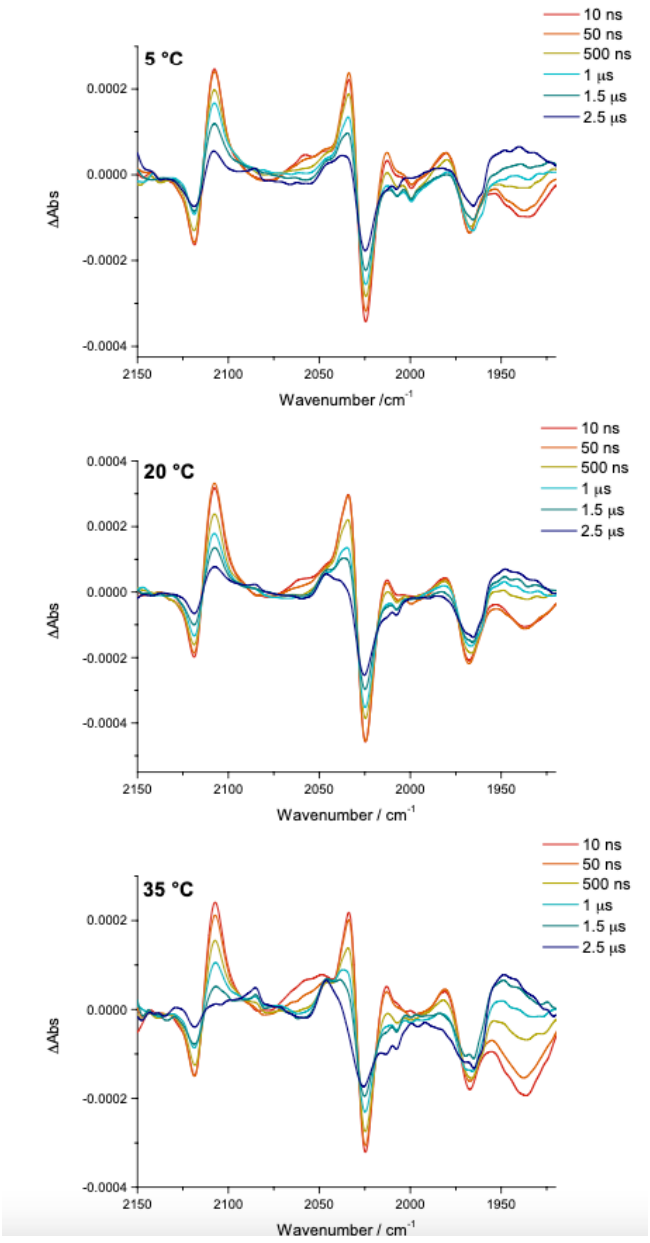

Figure 3.7 The TRIR data of temperature dependent ns-TRIR measurement of $[Re(CO)4(bpy)]PF_6$ in CH_2Cl_2. It is adapted from the reference[85].

On the other hand, the experiments carried out in CH_3CN from 15 to 55 ˚C every ten degrees, at all temperatures, showed slightly different temperature dependence even though the same profiles were observed, namely State I, State II and the CO loss photoproduct. There were no new peaks observed at low or high temperature. However, compared to the CH_2Cl_2 experiment, there is a much clearer increase in photoproduct production at higher temperatures. Also, analysis of the single point kinetics shows that the lifetime of decay of 'State I' increases with temperature, with the shortest lifetime at 15 °C (130 ± 64 ns) and the longest at 55 °C (326 ± 53 ns). The lifetime of decay of 'State II' decreases with temperature, with the shortest lifetime at 55 °C (2.97 ± 0.11 μs) and the longest at 15 °C (5.71 ± 0.52 μs). The growth of the photoproduct appears to have no trend with temperature. The TRIR in CH_3CN are reproduced in Figure 3.8

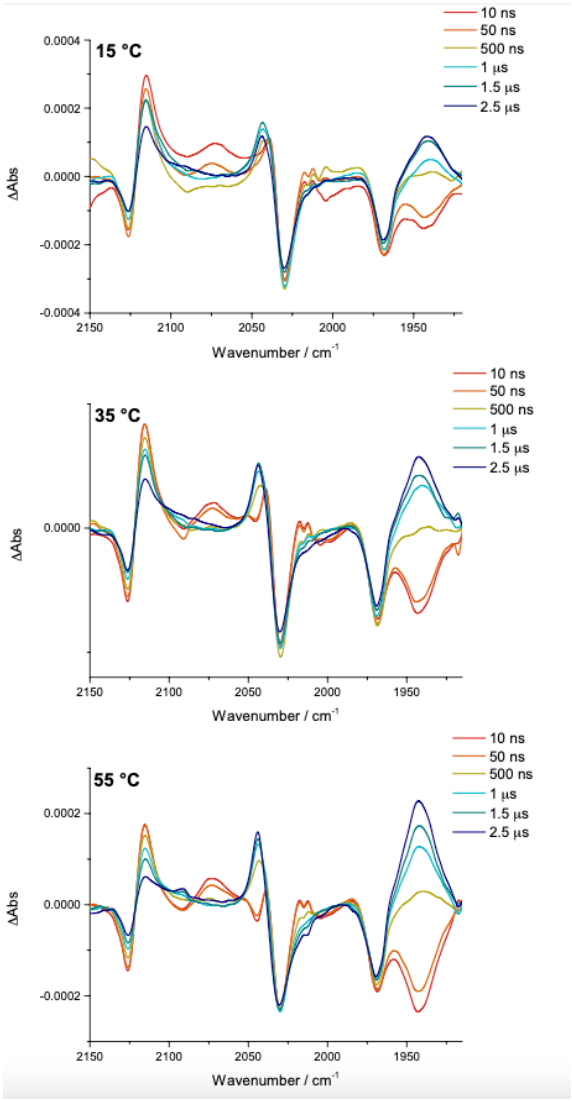

Figure 3.8 The TRIR data of temperature dependent ns-TRIR measurement of $[Re(CO)4(bpy)]PF_6$ in CH_3CN. It is adapted from the reference[85].

Furthermore, Garwood's also reported the temperature dependent emission measurement of $[Re(CO)_4(bpy)]PF_6$ in CH_2Cl_2 and CH_3CN. The emission in CH_2Cl_2 clearly decreases as the temperature increases. There is little to no change in the shape of the emission spectra upon a change in temperature, implying that there is no increased production of any other state. On the other hand, the results in CH_3CN showed at lower temperatures, the emission is like the emission seen in CH_2Cl_2. As the temperature increases, there appears to be a change in the shape of the emission spectra.

The spectra exhibited increasing ^{3}MLCT character, as shown by the broadening of the spectra and the centring of emission around 550 nm. The strong vibronic character at 449 and 479 nm associated with the ^{3}ILCT appears to weaken. This change would support observations of increased production of the photoproduct, as the photoproduct is produced from the MLCT state. The intensity of the emission also decreases as the temperature increases. The emission spectra are shown in Figure 3.9

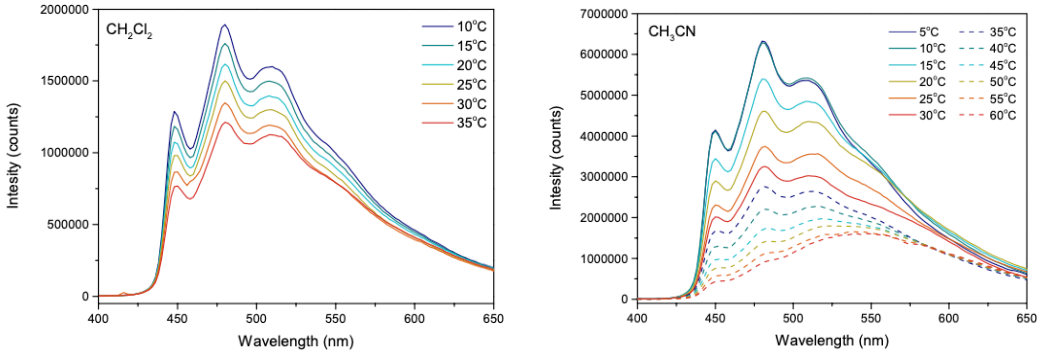

Figure 3.9 Temperature dependent emission measurement of [Re(CO)4(bpy)]PF_6 in CH_2Cl_2 and CH_3CN. It is adapted from the reference[85].

3.1.1.4.3. Photochemistry and photophysics of $[Re(CO)_4(4,4'\text{-}R_2\text{-}bpy)]^+$ (R= NH_2, CH_3, Br or CF_3)

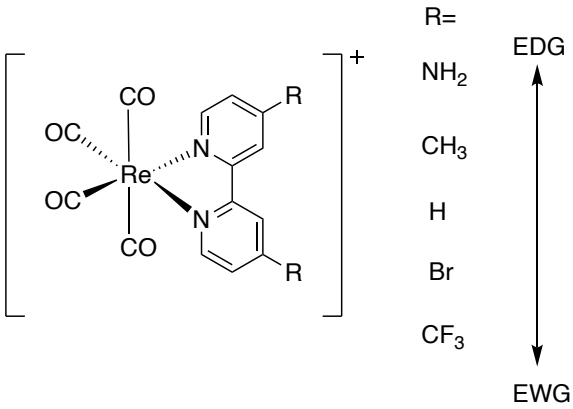

Figure 3.10 The structure of $[Re(CO)_4(4,4'\text{-}R_2\text{-}bpy)]^+$ (R= NH_2, CH_3, H Br or CF_3) with electron Donation groups (EDG) and electron withdrawing groups(EWG) order.

The ns-TRIR measurement of $[Re(CO)_4(4,4'\text{-}R_2\text{-}bpy)]^+$ (R= NH_2, CH_3, Br or CF_3) (Figure 3.10 in CH_2Cl_2 have also been investigated.[47] It is reported that the complex is shown similar excited state pathway as $[Re(CO)_4(bpy)]PF_6$ which are State I, State II and photoproduct, with the exception of NH_2 and CF_3. When the substituent is NH_2, the relaxation pathway only shows state I and II mixed together with fast decay and photoproduct peak. On the other hand, when the substituent is CF_3. only the state II and the photoproduct peak are shown. Also, it was found that with an electron donating group (EDG) on the bpy ligand, CO loss was more likely to occur. Where electron withdrawing groups were present, CO loss became a much less favoured pathway.[47] The ns-TRIR spectra of $[Re(CO)_4(4,4'\text{-}R_2\text{-}bpy)]^+$ (R= NH_2, CH_3, Br or CF_3) in CH_2Cl_2 are shown in Figure 3.11.

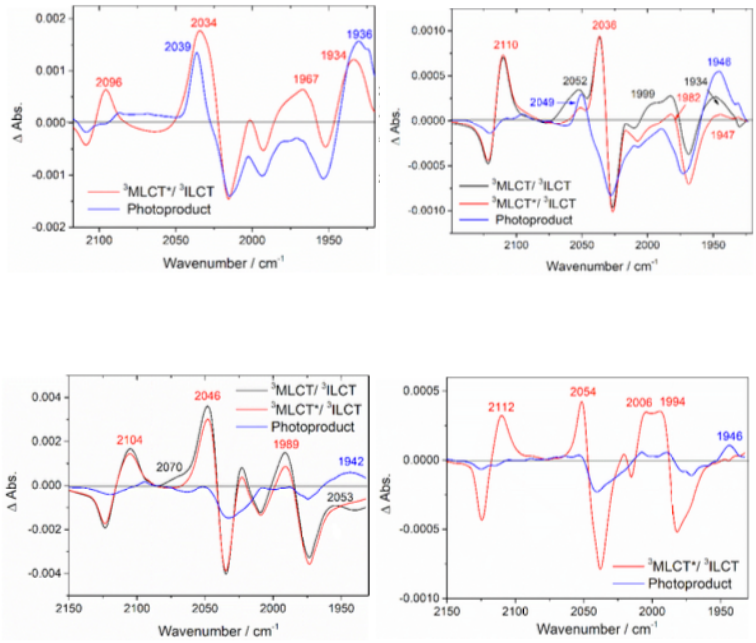

Figure 3.11 The ns-TRIR spectra of $[Re(CO)_4(4,4'\text{-}R_2\text{-}bpy)]^+$ (R= NH_2(top left), CH_3(top right), Br(bottom left) or CF_3 (bottom right) in CH_2Cl_2. It is adapted from the reference[47]

Again, the emission spectra of $[Re(CO)_4(4,4'\text{-}R_2\text{-}bpy)]^+$ (R= NH_2, CH_3, Br or CF_3) in

CH_2Cl_2 were reported. The result shows NH_2 and CF_3 substituents show more ^{3}MLCT structure, whereas substituents are CH_3 or Br show similar to $[Re(CO)_4(bpy)]PF_6$. Also, the electron-donating groups have less emission than electron-withdrawing groups. The spectra shown in Figure 3.12

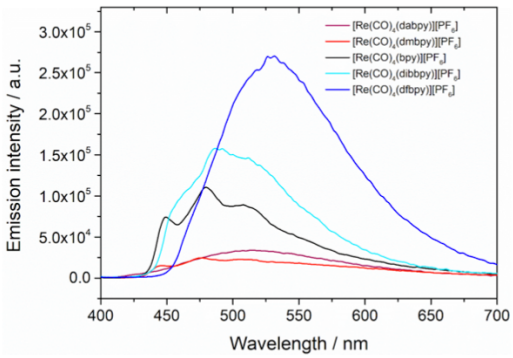

Figure 3.12 The emission spectra of $[Re(CO)_4(4,4'\text{-}R_2\text{-}bpy)]^+$ (R= NH_2, CH_3, H, Br or CF_3) in CH_2Cl_2. It is adapted from the reference[47]

3.2. Aim

The aim of the work described in this Chapter is to further examine the effect of temperature on the photochemistry and photophysics of $[Re(CO)_4(diimine)]^+$ complexes in CH_2Cl_2 and CH_3CN, particularly focusing on complexes with derivatives containing electron-withdrawing groups (EWGs) and electron-donating groups (EDGs). We have used the following strategy to address the aims above:

- Synthesize the complexes $[Re(CO)_4(4,4'\text{-}R_2\text{-}bpy)]PF_6$ (R= NH_2, CH_3, H, Br or CF_3) with the bpy derivatives as ligands.
- Probe the photochemistry and photophysics of $[Re(CO)_4(4,4'\text{-}R_2\text{-}bpy)]PF_6$ at various temperatures (10, 15, 20, 25, 30 and 35 ˚C) using emission spectroscopy in CH_2Cl_2

- Probe the photochemistry and photophysics of $[Re(CO)_4(4,4'\text{-}R_2\text{-}bpy)]PF_6$ at various temperatures (15, 25, 35, 45, 55 and 65 ˚C) using emission spectroscopy in CH_3CN.

3.3. Results and Discussion

3.3.1. Synthesis of $[Re(CO)_4(4,4'\text{-}(R)_2\text{-}bpy)]PF_6$ (R= NH_2, CH_3, H, Br or CF_3)

$[Re(CO)_4(4,4'\text{-}(R)_2\text{-}bpy)]PF_6$ (R= NH_2, CH_3, H, Br or CF_3) was prepared by the procedure previously described in the group[46, 47] and detailed in the experimental Section 4.2.11 to 4.2.15.

3.3.1.1. FTIR characterization

The complexes were analysed by FTIR in CH_2Cl_2 and CH_3CN. The spectra are shown in Figure 3.13. The results show a similar trend in both solvents. The derivatives containing EDGs were red-shift compared to the original bpy ligand, while the derivatives containing EWGs showed a blue-shift compared to the original bpy ligand. Therefore, the energy order for the vibrations on the complexes is from lower energy as stronger in the electron-donating ability of the ligand, which gives the order: (donating) NH_2 - CH_3 - H - Br - CF_3 (withdrawing). This happens because of changes in the metal centre electronic density. The electron-donating substituted group will increase the electronic donation to the metal centre from the bpy ligand, causing a CO bond relaxation. On the other hand, the electron-withdrawing substituted group will decrease the electron donation by the bpy ligand, causing the CO bond to be shortened. The result in CH_2Cl_2 is consistent with Wu's report.[47]

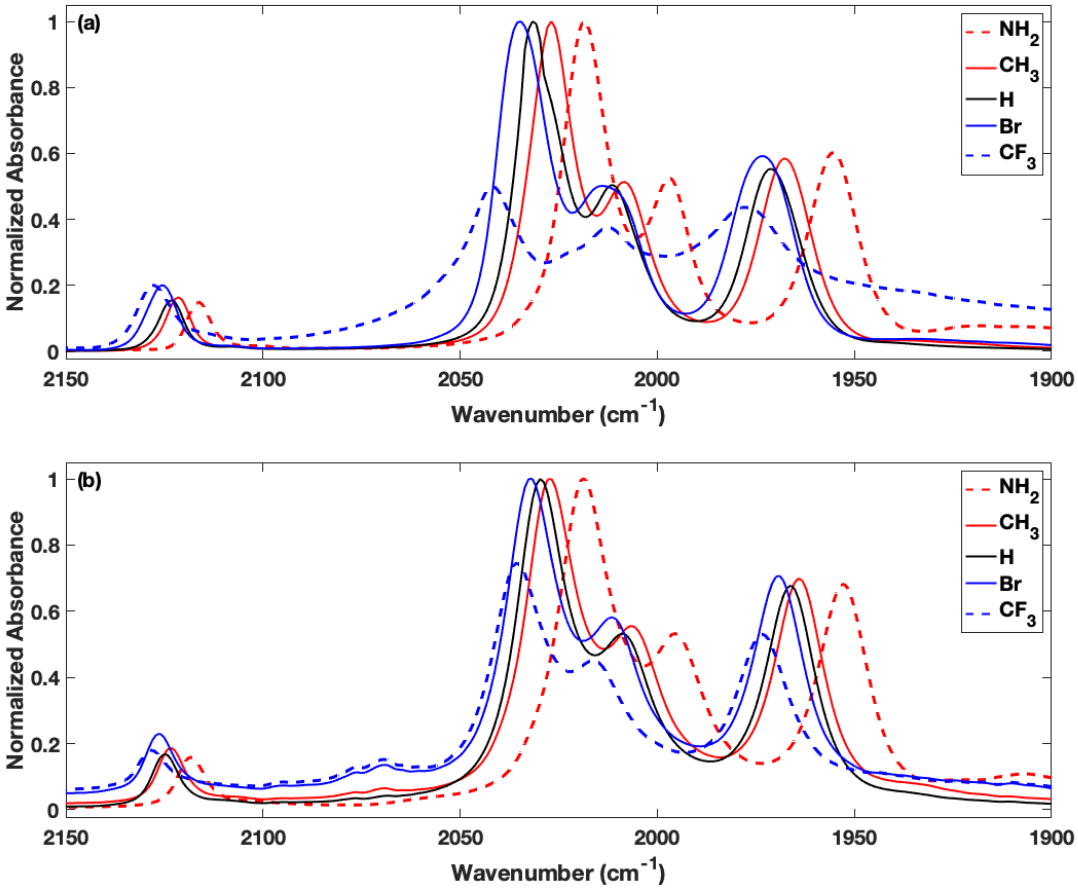

Figure 3.13 The FTIR spectra of $[Re(CO)_4(4,4'\text{-}(R)_2\text{-bpy})]PF6$ (R= NH_2, CH_3, H, Br or CF_3) in CH_2Cl_2 (a) and CH_3CN (b).

3.3.1.2. UV-vis measurement

The complexes were also analysed by UV-vis spectroscopy in CH_2Cl_2 and CH_3CN. The spectra are shown in Figure 3.14. The results in CH_2Cl_2 are consistent with Wu's and Reynolds's data.[46, 47] The results shows that in CH_3CN all complexes show a blue-shift for all transitions compared to CH_2Cl_2.[46]

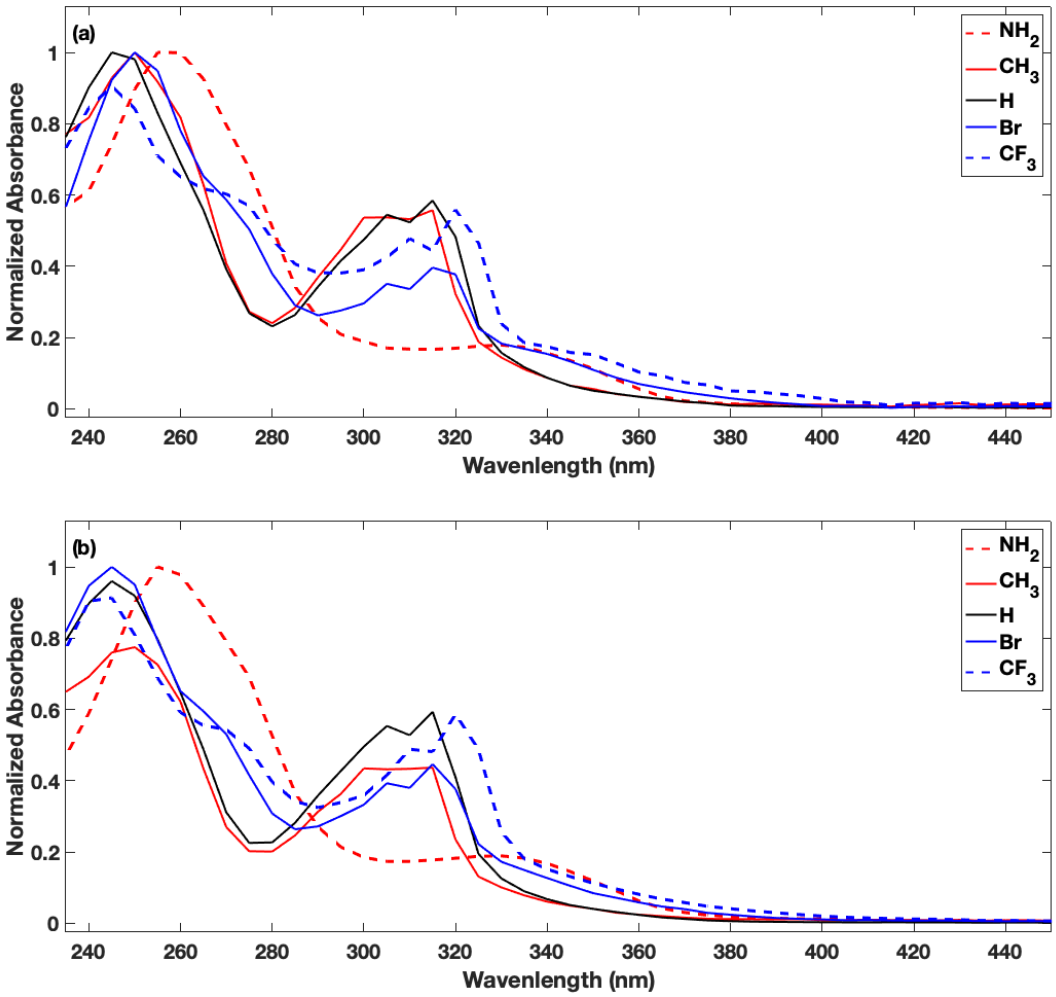

Figure 3.14 The UV-vis spectra of [Re(CO)$_4$(4,4'-(R)$_2$-bpy)]PF6 (R= NH_2, CH_3, H, Br or CF_3) in CH_2Cl_2 (a) and CH_3CN (b).

3.3.1.3. Temperature independent emission measurement

The complexes were also analysed by emission spectroscopy in CH_2Cl_2 and CH_3CN. The spectra are shown in Figure 3.15. The result in CH_2Cl_2 is consistent with Xu's data.[47] The results show that in CH_3CN all complexes show a red-shift for all emissions compared to CH_2Cl_2 data[47] and the EWG derivatives having to larger red-shift than the EDG derivatives. Also, the complex in CH_3CN shows more ^{3}MLCT emission structure. For the ^{3}MLCT emission structure at about 500 nm, we can see the EDG derivatives

having higher energy than EWG derivatives.

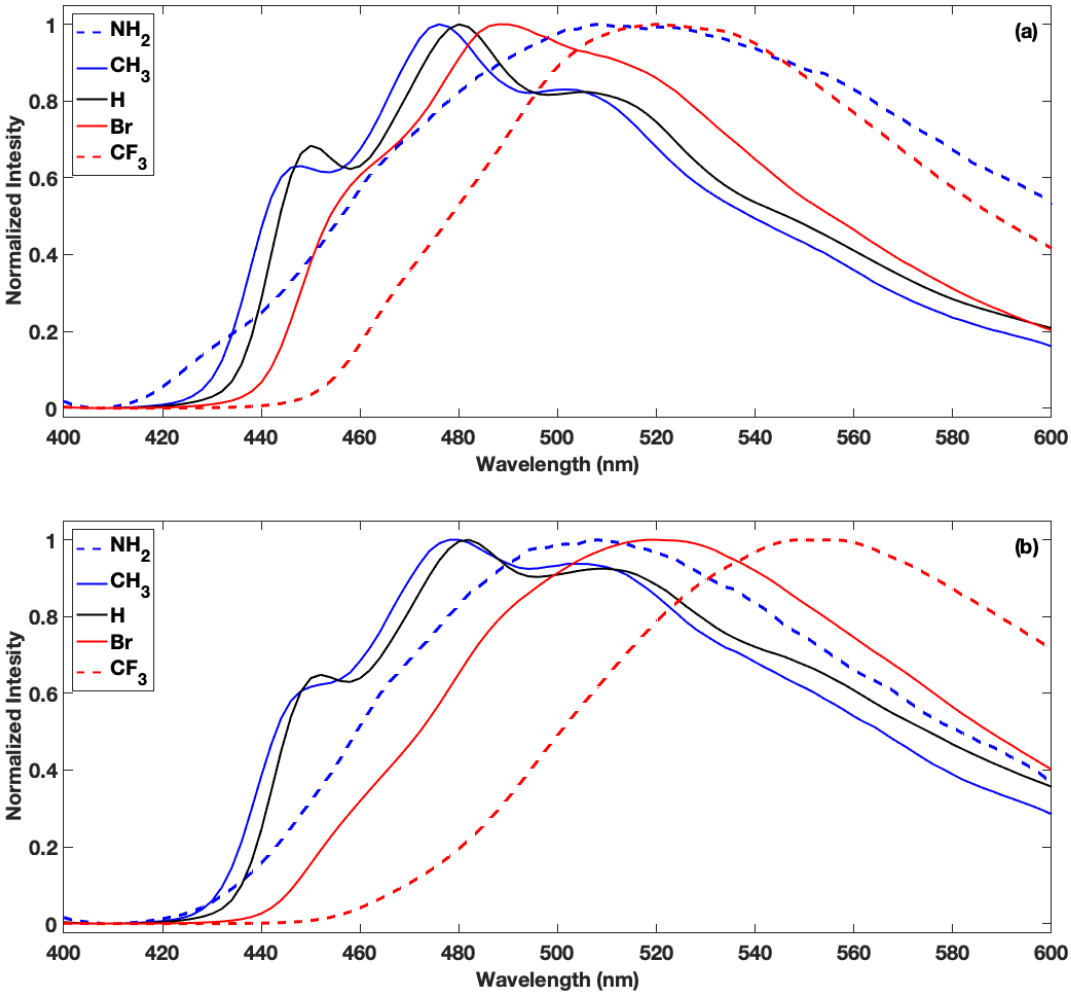

Figure 3.15 The emission spectra of $[Re(CO)_4(4,4'\text{-}(R)_2\text{-bpy})]PF6$ (R= NH_2, CH_3, H, Br or CF_3) in CH_2Cl_2 (a) and CH_3CN (b).

3.3.2. Temperature Dependent Emission and lifetime measurement in CH_2Cl_2

3.3.2.1. $[Re(CO)_4(4,4'\text{-}(H)_2\text{-bpy})]PF_6$ complex (3)

Temperature dependent emission measurement of $[Re(CO)_4(4,4'\text{-}(H)_2\text{-bpy})]PF_6$ in CH_2Cl_2 was repeated from reference[85]. For the non-substituted $[Re(CO)_4(4,4'\text{-}(H)_2\text{-bpy})]PF_6$ the emission shows maxima at 450, 480 and 510 nm at room temperature (25

°C), and the resolved shape of the emission suggests a mixed ^{3}ILCT and ^{3}MLCT excited state. The highest emission intensity was observed at the lowest temperature (15 °C), and then intensity gradually decreased with increasing temperature (Figure 3.16-a). Whilst no emission shift was observed with the increase in temperature and the ratio of the emission at 480 and 510 nm decreased with increasing temperature. The intensity changes trend is shown in Figure 3.16-b. The results showed an apparent linear decrease within the analysed temperature range, with an overall decrease of 1.6 times-fold. These results suggest that by increasing temperature, the population of ^{3}ILCT (higher energy) tend to populate ^{3}MLCT (lower energy) excited state.

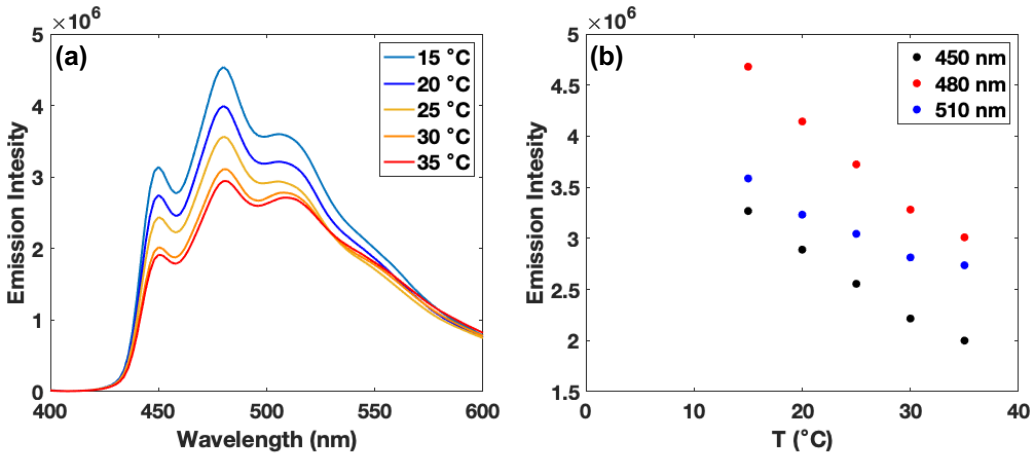

Figure 3.16 The emission spectra of Complex 3 in CH_2Cl_2 at various temperatures (a) and the intensity trend with various temperatures (b).

The lifetime measurement was found to be biexponential decay in all measured temperatures. The fast decay (τ_1) remains constant in all measured temperatures, but the slow decay (τ_2) decreases linearly with increasing temperature. The lifetime shows there are two states of emission.[89] The fast decay could count as 'state I' and the slow decay count as 'state II', because the slow decay affected by temperature which indicates the state of CO dissociation. Also, the TRIR result of complex 3 show state I

had faster decay and state II had slower decay. Moreover, the lifetime of fast and slow decay close with TRIR result of the lifetime of state I and II by previously described in the group.[85] The lifetime trend with temperature is shown in Figure 3.17

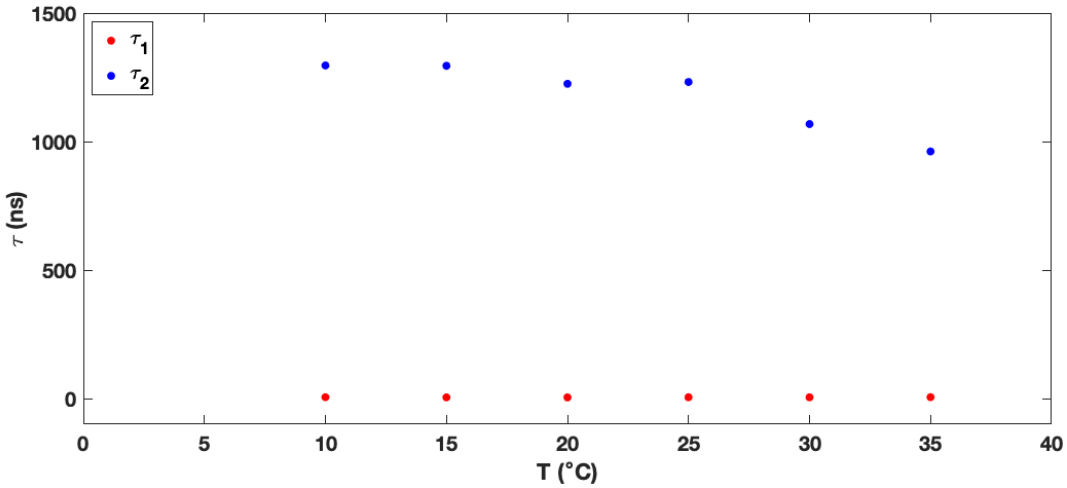

Figure 3.17 The trend of lifetime decay with increasing temperature of Complex 3 in CH_2Cl_2. The fast decay (τ_1, red), and the slow decay (τ_2, blue).

Concluded the emission and the lifetime results of Complex 3 in CH_2Cl_2 and compare it with the result previously described in the group, which shows that the state I and II is a mixed ^{3}ILCT/^{3}MLCT state. Also, the state II corresponding to CO dissociation and the ratio of population of ^{3}ILCT and ^{3}MLCT state tend to get closer with increased temperature which indicates that ^{3}ILCT state tends to populate ^{3}MLCT state with increased temperature. Therefore, in higher temperature (30 and 35˚C), it leads to more CO dissociation (τ_2 drop); however, the CH_2Cl_2 has the poor coordinating ability, which this could be the reason of CO dissociation at lower temperature (10 to 25 ˚C) was not effective (τ_2 constant). Also, the emission intensity decreased in lower temperature (15 to 25 ˚C) because ^{3}MLCT is a non-emission state.

3.3.2.2. $[Re(CO)_4(4,4'\text{-}(NH_2)_2\text{-}bpy)]PF_6$ Complex (1)

For the $[Re(CO)_4(4,4'\text{-}(NH_2)_2\text{-}bpy)]PF_6$ the emission wavelength maximum is at 506 nm at room temperature (25 °C), and the shape of the curve shows a ^{3}MLCT excited state emission structure. The emission spectra at different temperatures is shown in Figure 3.18-a. It is possible to observe a small red-shift in the emission with increasing temperature, passing from 506 nm at 10 °C to 524 nm at 35 °C. In addition, it is possible to observe that the intensity decreased gradually with increasing temperature. The intensity trend is shown in Figure 3.18-b. The results showed an apparent linear decrease within the analysed temperature range, with an overall decrease of 2.6 times-fold. These results suggest that increasing temperature could lead to more CO dissociation.

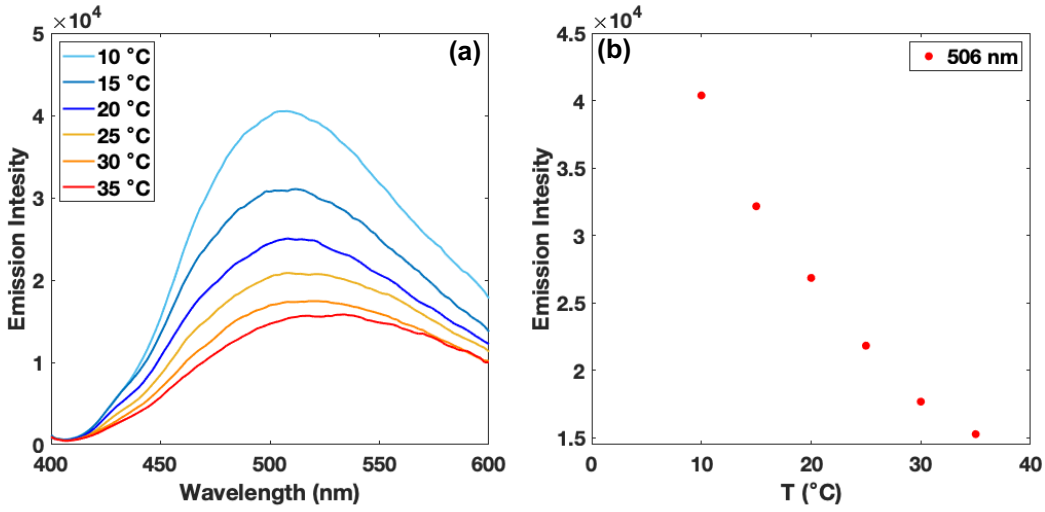

Figure 3.18 The emission spectra of Complex 1 in CH_2Cl_2 at various temperatures (a) and the intensity trend with various temperatures (b).

The lifetime measurement was found to be biexponential decay in all measured temperatures. The fast decay (τ_1) remains constant in all measured temperatures, but the slow decay (τ_2) decreases linearly with increasing temperature. The lifetime shows

there are two states of emission.[89] The fast decay could count as 'state I' and the slow decay count as 'state II', because the slow decay was affected by temperature, which indicates the state of CO dissociation. The lifetime trend with temperature is shown in Figure 3.19

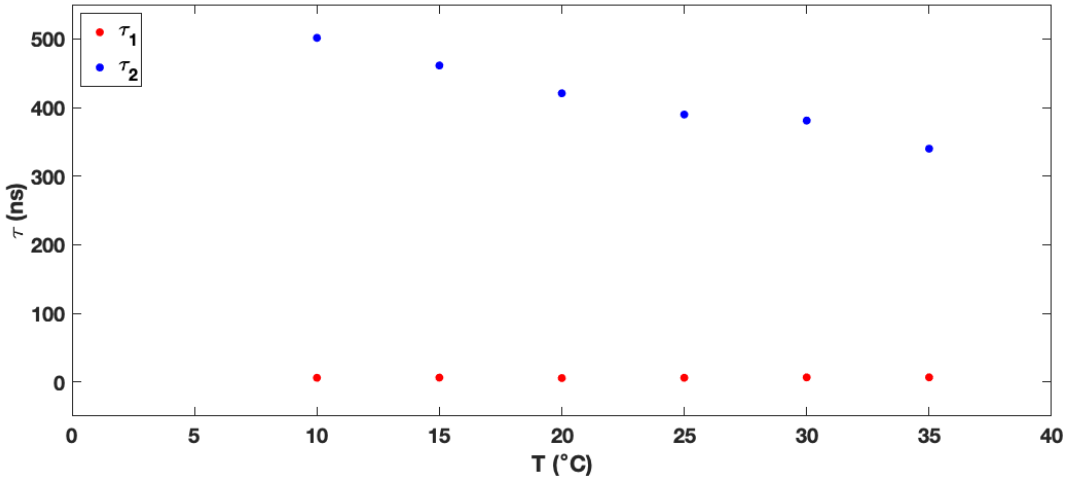

Figure 3.19 The trend of lifetime decay with increasing temperature of Complex 1 in CH_2Cl_2. The fast decay (τ_1, red), and the slow decay (τ_2, blue).

Concluded the emission and the lifetime results of Complex 1 in CH_2Cl_2 and comparing it with the result previously described in the group, it is shown that the state I and II is a mixed ^{3}ILCT/^{3}MLCT state, but it tends more towards ^{3}MLCT character. This is the reason why there are less emissions compared to complex 3 because ^{3}MLCT is a non-emission state. Wu's results show that complex 1 tends to do CO dissociation, therefore there is more CO dissociation with increased temperature which provides more energy to go over the reaction barriers.

3.3.2.3. $[Re(CO)_4(4,4'\text{-}(CH_3)_2\text{-bpy})]PF_6$ Complex (2)

For the $[Re(CO)_4(4,4'\text{-}(CH_3)_2\text{-bpy})]PF_6$, the emission shows maxima at 446, 476 and 508 nm at room temperature (25 °C), and the resolved shape of the emission suggests a

mixed ^{3}ILCT and ^{3}MLCT excited state. The emission spectra are shown in Figure 3.20-a. Also, for the emission energy, no shift was observed with increasing temperature, however the ratio of the peak at 476 and 506 decreased with increasing temperature. At the lowest temperature (10 °C), the highest intensity decreased gradually with increasing temperature. The intensity trend is shown in Figure 3.20-b. The results showed an apparent linear decrease within the analysed temperature range, with an overall decrease of 2.2 times-fold. These results suggest that by increasing temperature, the population of ^{3}ILCT (higher energy) state tends to populate ^{3}MLCT (lower energy) excited state.

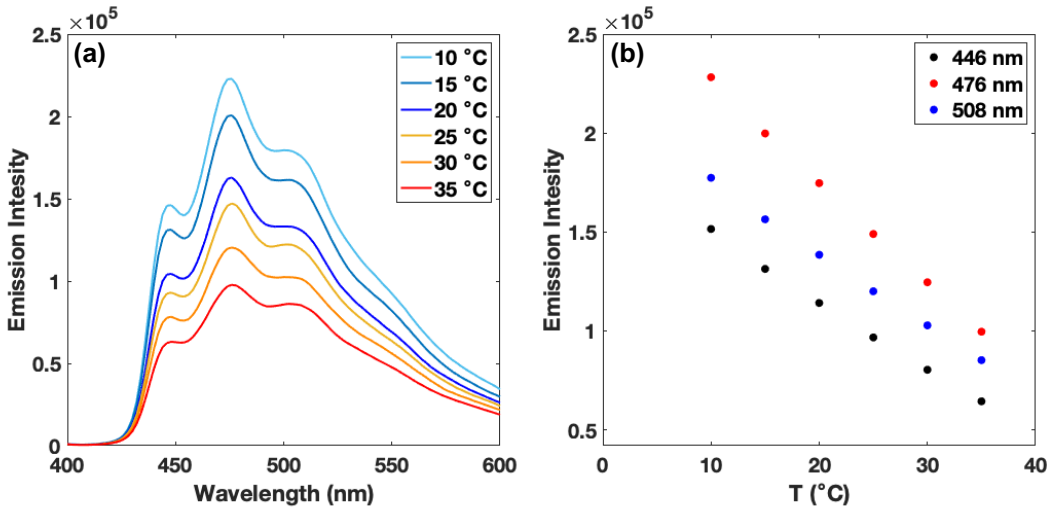

Figure 3.20 The emission spectra of Complex 2 in CH_2Cl_2 at various temperatures (a) and the intensity trend with various temperatures (b).

The lifetime measurement was found to be biexponential decay in all measured temperatures. The fast decay (τ_1) remains constant in all measured temperatures, but the slow decay (τ_2) decreases linearly with increasing temperature. The lifetime shows there are two states of emission.[89] The fast decay could count as 'state I' and the slow decay count as 'state II', because the slow decay affected by temperature which indicates the state of CO dissociation. Also, the TRIR result of complex 2 previously

described in the group shows state I had faster decay and state II had slower decay. The lifetime trend with temperature is shown in Figure 3.21.

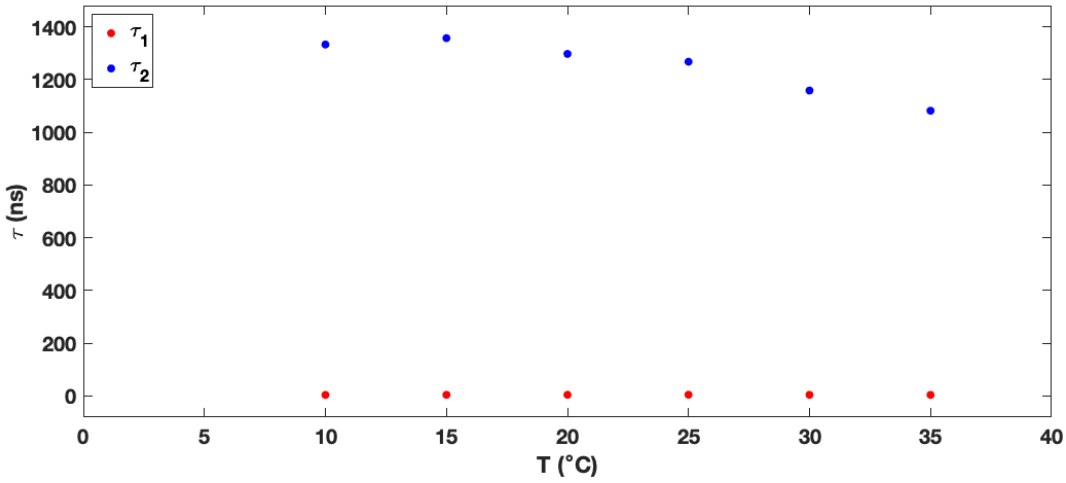

Figure 3.21 The trend of lifetime decay with increasing temperature of Complex 2 in CH_2Cl_2. The fast decay (τ_1, red), and the slow decay (τ_2, blue)

Concluded the emission and the lifetime results of Complex 2 in CH_2Cl_2 and comparing it with the result previously described in the group, it has been shown that the state I and II is a mixed ^{3}ILCT/^{3}MLCT state. Also, the state II corresponding to CO dissociation and the ratio of population of ^{3}ILCT and ^{3}MLCT tend to get closer with increased temperature, which indicates that ^{3}ILCT tends to populate ^{3}MLCT with increased temperature. Therefore, higher temperature (25 to 35˚C) leads to more CO dissociation (τ_2 drop); however, the CH_2Cl_2 having poor coordinating ability could be the reason why CO dissociation at lower temperature (10 to 20 ˚C) was not effective (τ_2 constant). Also, the emission intensity decreased at lower temperature (10 to 20 ˚C) because ^{3}MLCT is a non-emission state. The complex 2 has similar result compared to complex 3 in CH_2Cl_2, but complex 2 shows trend to do more CO dissociation. Therefore, complex 2 shows less emission lifetime and larger drop of emission intensity compared to complex 3.

3.3.2.4. $[Re(CO)_4(4,4'\text{-}(Br)_2\text{-}bpy)]PF_6$ Complex (4)

For the $[Re(CO)_4(4,4'\text{-}(Br)_2\text{-}bpy)]PF_6$ the emission shows maxima at 460, 488 and 516 nm at room temperature (25 °C), and the shape of the curve shows a mixed ^{3}ILCT and ^{3}MLCT excited state emission structure. The emission spectra are shown in Figure 3.22-a). Also, for the emission energy, no shift was observed with increasing temperature, and the ratio at 488 and 516 nm slightly decreased with increasing temperature. At the lowest temperature (10 °C), the highest intensity decreased very slowly with increasing temperature. The intensity trend is shown in Figure 3.22-b. The results showed an apparent linear decrease within the analysed temperature range, with an overall decrease of 1.1 times-fold. These results suggest that by increasing temperature, the population of ^{3}ILCT (higher energy) tends to populate ^{3}MLCT (lower energy) excited state.

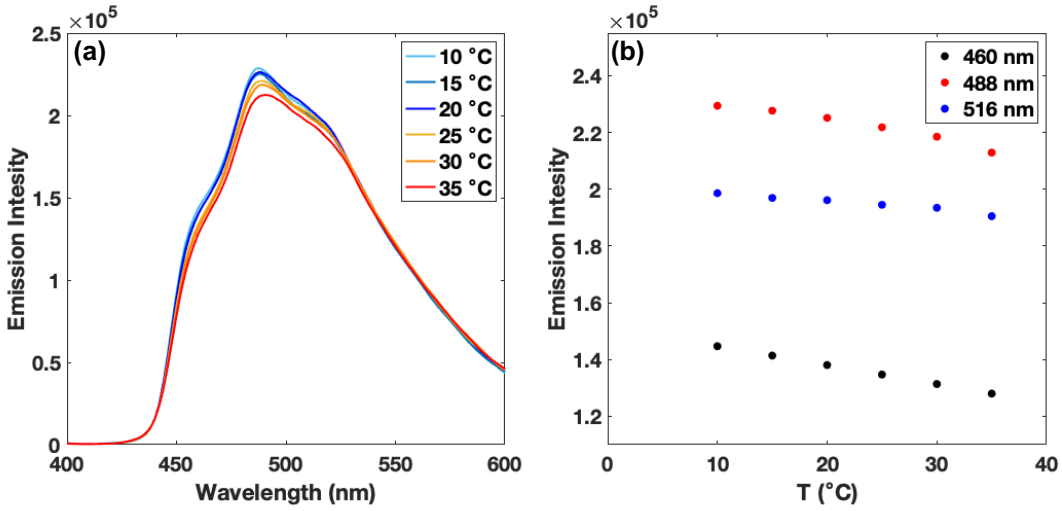

Figure 3.22 The emission spectra of Complex 4 in CH_2Cl_2 at various temperatures (a) and the intensity trend with various temperatures (b).

The lifetime measurement was found to be biexponential decay in all measured temperatures. The fast decay (τ_1) and slow decay (τ_2) remains constant in all measured

temperatures. The lifetime shows that there are two states of emission.[89] The fast decay could count as 'state I' and the slow decay count as 'state II' because the TRIR result of complex 4 previously described in the group shows state I had faster decay and state II had slower decay. The lifetime trend with temperature is shown in Figure 3.23

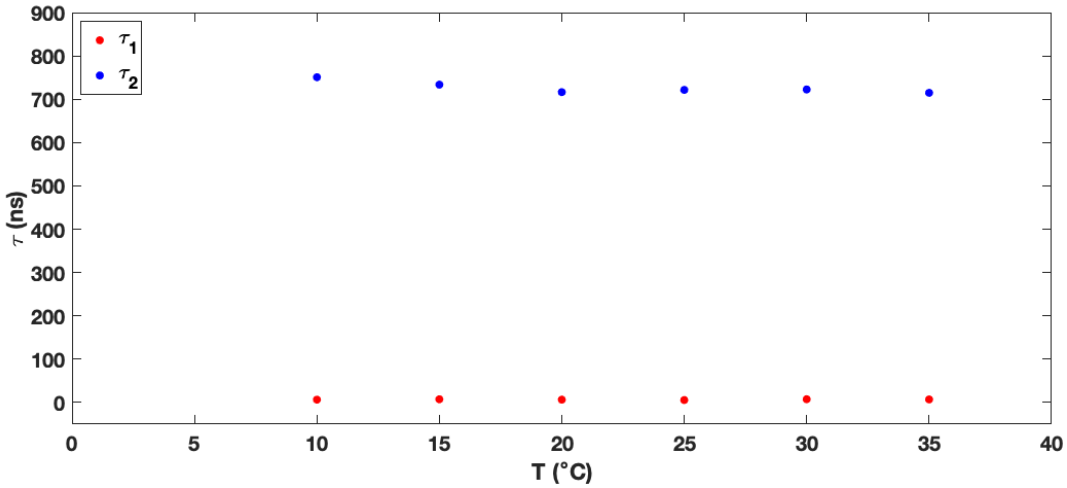

Figure 3.23 The trend of lifetime decay with increasing temperature of Complex 4 in CH_2Cl_2. The fast decay (τ_1, red), and the slow decay (τ_2, blue)

Concluded the emission and the lifetime results of Complex 4 in CH_2Cl_2 and compare it with the result previously described in the group, which show that the state I and II is a mixed ^{3}ILCT/^{3}MLCT state. The ratio of population of ^{3}ILCT and ^{3}MLCT tend to get closer with increased temperature, which indicates that ^{3}ILCT state tends to populate ^{3}MLCT state with increased temperature and Wu's Thesis reported Complex 4 tends to do emission than CO dissociation.[47] Therefore, the emission intensity decreased may only be due to more ^{3}MLCT population which it is a non-emission state.

3.3.2.5. $[Re(CO)_4(4,4'\text{-}(CF_3)_2\text{-bpy})]PF_6$ Complex (5)

For the $[Re(CO)_4(4,4'\text{-}(CF_3)_2\text{-bpy})]PF_6$ the emission shows maxima at 520 nm at room temperature (25 °C), and the shape of the curve shows a ^{3}MLCT excited state emission

structure. The emission spectra are shown in Figure 3.24-a. Also, for the emission energy, no shifts were observed with increasing temperature. At the lowest temperature (10 °C), the highest intensity decreased slowly with increasing temperature. The intensity trend is shown in Figure 3.24-b. The results showed an apparent linear decrease within the analysed temperature range, with an overall decrease of 1.1 times-fold.

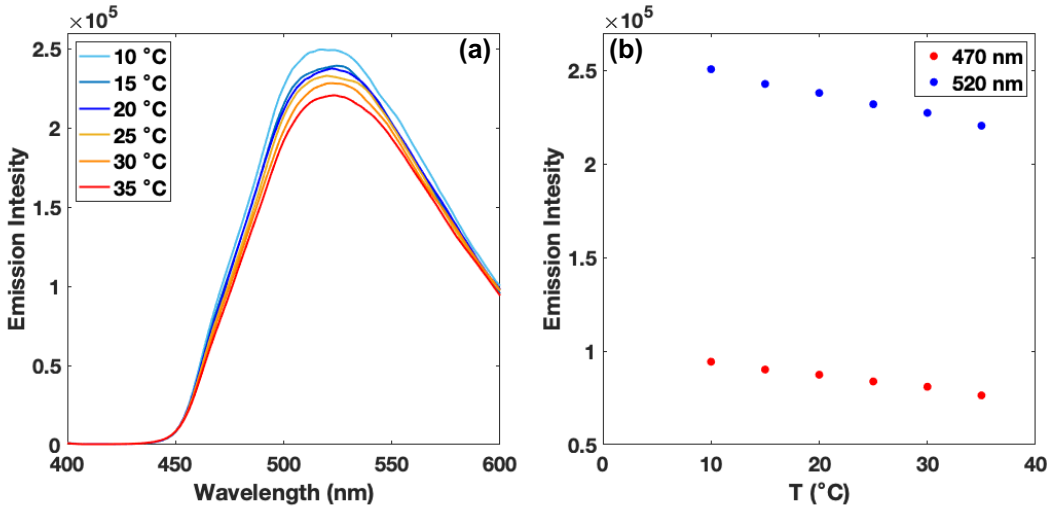

Figure 3.24 The emission spectra of Complex 5 in CH_2Cl_2 at various temperatures (a) and the intensity trend with various temperatures (b).

The lifetime measurement was found to be biexponential decay in all measured temperatures. The fast decay (τ_1) and slow decay (τ_2) remains constant in all measured temperatures, The lifetime shows there are two states of emission.[89] The fast decay could count as 'state I' and the slow decay count as 'state II'. Also, two decay lifetime are closer compared to other derivatives The lifetime trend with temperature is shown in Figure 3.25.

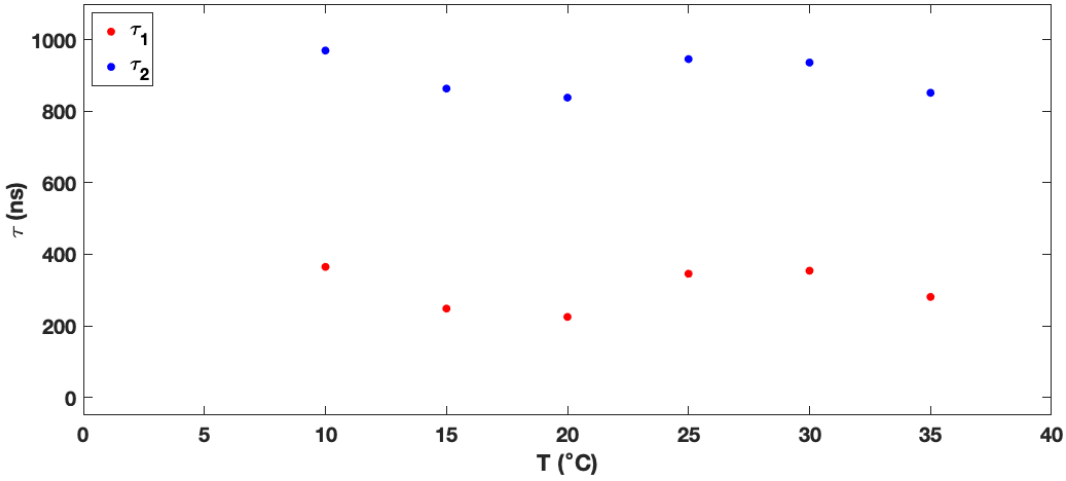

Figure 3.25 The trend of lifetime decay with increasing temperature of Complex 5 in CH_2Cl_2. The fast decay (τ_1, red), and the slow decay (τ_2, blue)

Concluded the emission and the lifetime results of Complex 5 in CH_2Cl_2 and compare with the result previously described in the group, which show that the state I and II is a mixed ^{3}ILCT/^{3}MLCT state. Complex 5 may tend to populate in the state I because the difference of lifetime of fast and slow decay became smaller. Therefore, complex 5 does not tend to undergo CO dissociation, which is consistent as reported in Wu's report. The emission intensity decrease may stem from the fact that the population of ^{3}MLCT in state 1 increases with increased temperature.

3.3.3. Temperature Dependent Emission and lifetime measurement in CH_3CN

3.3.3.1. $[Re(CO)_4(4,4'\text{-}(H)_2\text{-bpy})]PF_6$ complex (3)

Temperature dependent emission measurement of $[Re(CO)_4(4,4'\text{-}(H)_2\text{-bpy})]PF_6$ in CH_3CN was repeated from reference[85].

For the non-substituted $[Re(CO)_4(4,4'\text{-}(H)_2\text{-bpy})]PF_6$ the emission shows maxima at 452, 482, and 512 nm at room temperature (25 °C), and the shape of the curve shows

mixed ^{3}ILCT and ^{3}MLCT excited state emission structure. The emission spectra are shown in Figure 3.26-a. Also, the energy was red-shifted with increasing temperature. The ratio of the peak at 482 and 512 nm is changed, and the shape of the curve from 55 ^{o}C started to change from mixed ^{3}ILCT and ^{3}MLCT excited state emission structure to more like ^{3}MLCT excited state emission structure. At the lowest temperature (25 ^{o}C), the highest intensity decreased sharply with increasing temperature up to 55 ^{o}C, and then the intensity decreased gradually with increasing temperature from 45 to 65 ^{o}C. The intensity trend is shown in Figure 3.26-b. The apparent linear decrease within the analysed temperature range, with an overall decrease 3.3 times-fold. These results suggest that by increasing temperature, the population of ^{3}ILCT (higher energy) trend to populate ^{3}MLCT (lower energy) excited state.

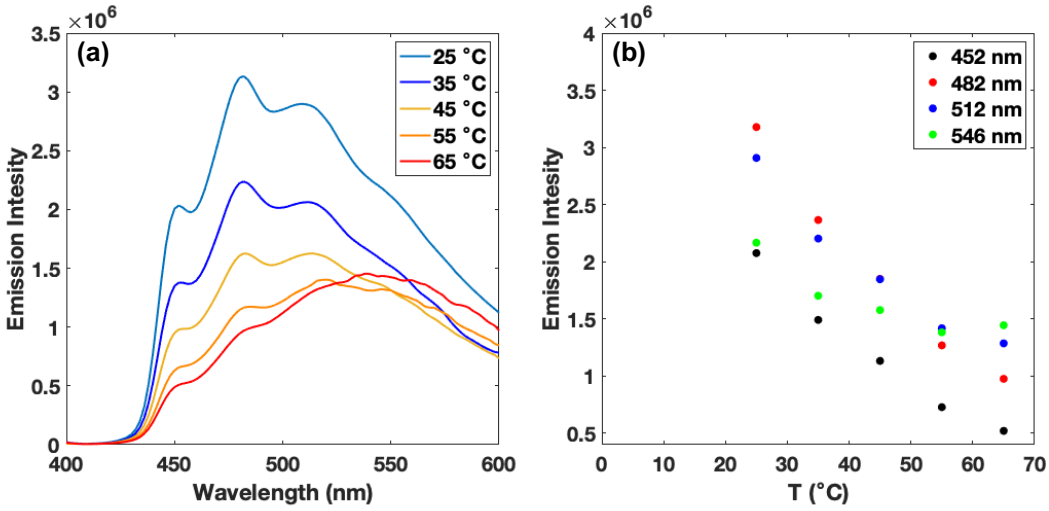

Figure 3.26 The emission spectra of Complex 3 in CH_3CN at various temperatures (a) and the intensity trend with various temperatures (b).

In CH_3CN, the lifetime measurement was found to be biexponential decay in all measured temperatures. The fast decay (τ_1) remains constant in all measured temperatures, but the slow decay (τ_2) decreases linearly with increasing temperature. The lifetime shows there are two states of emission;[89] The fast decay as 'state I' and the

slow decay as ‘state II’, because the slow decay was affected by temperature, which indicate the state of CO dissociation. Also, the TRIR result of complex 3 previously described in the group shows state I had faster decay and state II had slower decay. The trend is shown in Figure 3.27

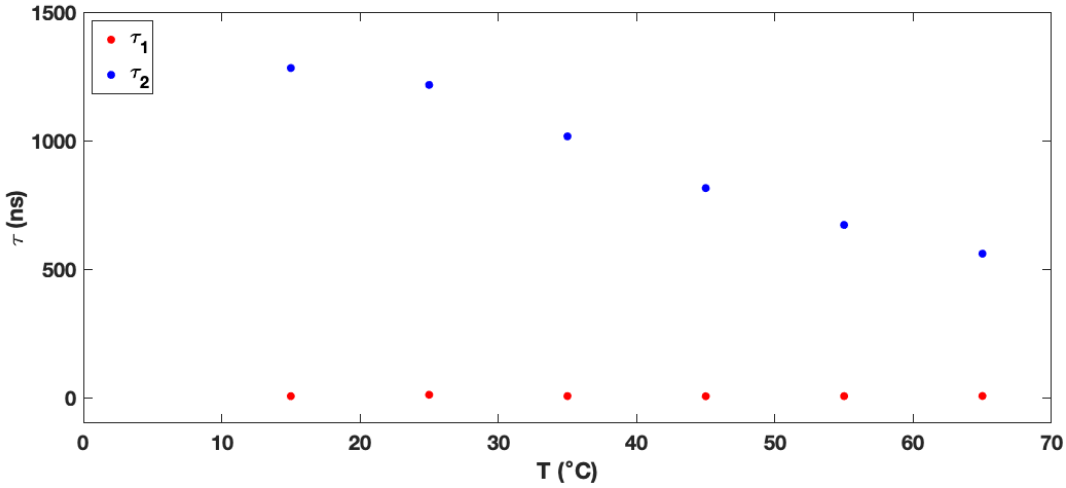

Figure 3.27 The trend of lifetime decay with increasing temperature of Complex 3 in CH_3CN. The fast decay (τ_1) is a red , and the slow decay (τ_2) is a blue .

Concluded the emission and the lifetime results of Complex 3 in CH_3CN and compare it with the result previously described in the group, which shows that the state I and II is a mixed ^{3}ILCT/^{3}MLCT state. Also, the state II corresponding to CO dissociation and the ratio of population of ^{3}ILCT and ^{3}MLCT tends to get closer with increased temperature, which indicates that ^{3}ILCT tends to populate ^{3}MLCT with increased temperature. Therefore, increased temperature leading to more CO dissociation (τ_2 drop).

3.3.3.2. $[Re(CO)_4(4,4'\text{-}(NH_2)_2\text{-bpy})]PF_6$ Complex (1)

For the $[Re(CO)_4(4,4'\text{-}(NH_2)_2\text{-bpy})]PF_6$ the emission wavelength maximum is at 504 nm at room temperature (25 ˚C), and the shape of the curve shows a ^{3}MLCT excited

state emission structure. The emission spectra are shown in Figure 3.28-a. At the lowest temperature (15 ˚C), the highest intensity decreased sharply with increasing temperature up to 45 ˚C, and then the intensity increased slowly with increasing temperature from 55 to 65 ˚C. The intensity trend is shown in Figure 3.28-b. The decrease within the analysed temperature range, with an overall decrease of 6.2 times-fold.

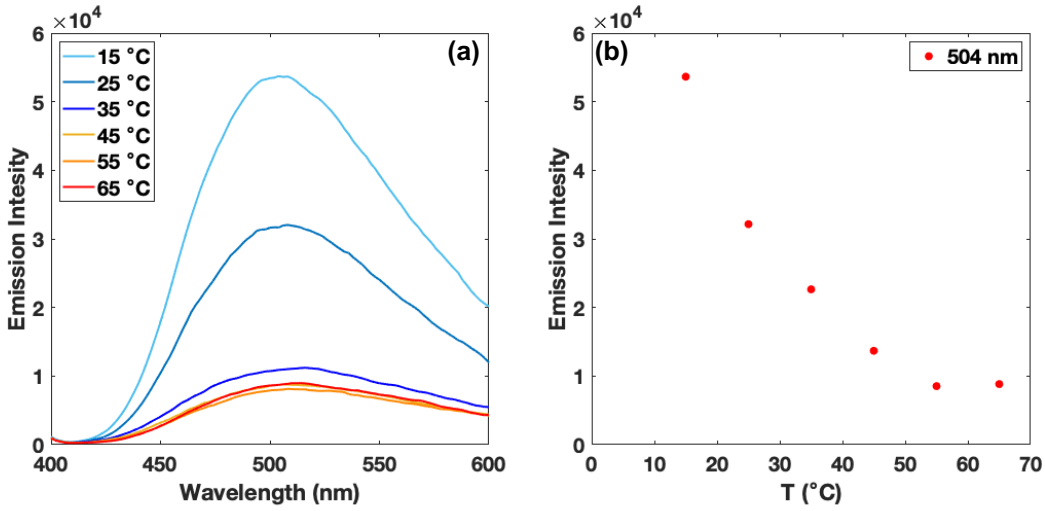

Figure 3.28 The emission spectra of Complex 1 in CH_3CN at various temperatures (a) and the intensity trend with various temperatures (b)

In CH_3CN, the lifetime measurement was found to be biexponential decay in all measured temperatures. The fast decay (τ_1) remains constant in all measured temperatures, but the slow decay (τ_2) decreases linearly with increasing temperature. The lifetime shows there are two states of emission.[89] The fast decay could count as 'state I' and the slow decay count as 'state II', because the slow decay affected by temperature which indicates the state of CO dissociation. the trend is shown in Figure 3.29.

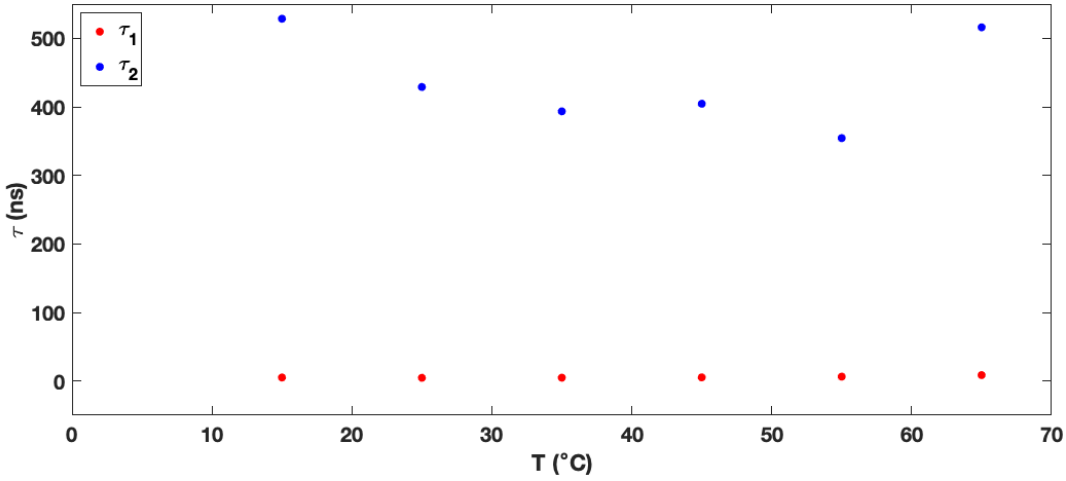

Figure 3.29 The trend of lifetime decay with increasing temperature of Complex 1 in CH_3CN. The fast decay (τ_1) is a red, and the slow decay (τ_2) is a blue.

Concluded the emission and the lifetime results of Complex 1 in CH_3CN and compare it with the result previously described in the group which show that the state I and II is a mixed ^{3}ILCT/^{3}MLCT state but a more ^{3}MLCT character. This is the reason of there is less emission compared to Complex 3 because ^{3}MLCT is a non-emission state. Increasing temperature tends to do more CO photodissociation. Also, the result shows the reaction barriers are lower because the intensity and slow decay drop more intensively in emission and lifetime measurement. Therefore, at a higher temperature at 55 and 65 ^{o}C, the photoproducts concentration increased more in the solution, leading to increase intensity, and the slow decay at the 65 ^{o}C resulted in an un-trend.

3.3.3.3. $[Re(CO)_4(4,4'\text{-}(CH_3)_2\text{-bpy})]PF_6$ Complex (2)

For the $Re(CO)_4(4,4'\text{-}(CH_3)_2\text{-bpy})]PF_6$ the emission maximum is at 446, 476, and 510 nm at room temperature (25 ^{o}C), and the shape of the curve shows mixed ^{3}ILCT and ^{3}MLCT excited state emission structure. The emission spectra are shown in Figure 3.30-a. Also, the energy was red-shifted with increasing temperature. The ratio of the peak

at 476 and 510 nm is decreased, and the shape of the curve from 45 °C started to change from mixed ^{3}ILCT and ^{3}MLCT excited state emission structure to more like ^{3}MLCT excited state emission structure. At the lowest temperature (15 °C), the highest intensity decreased sharply with increasing temperature up to 35 °C, and then the intensity decreased gradually with increasing temperature from 45 to 65 °C. The intensity trend is shown in Figure 3.30-b. The apparent linear decrease within the analysed temperature range, with an overall decrease 7.0 times-fold. These results suggest that by increasing temperature, the population of ^{3}ILCT (higher energy) trend to populate ^{3}MLCT (lower energy) excited state.

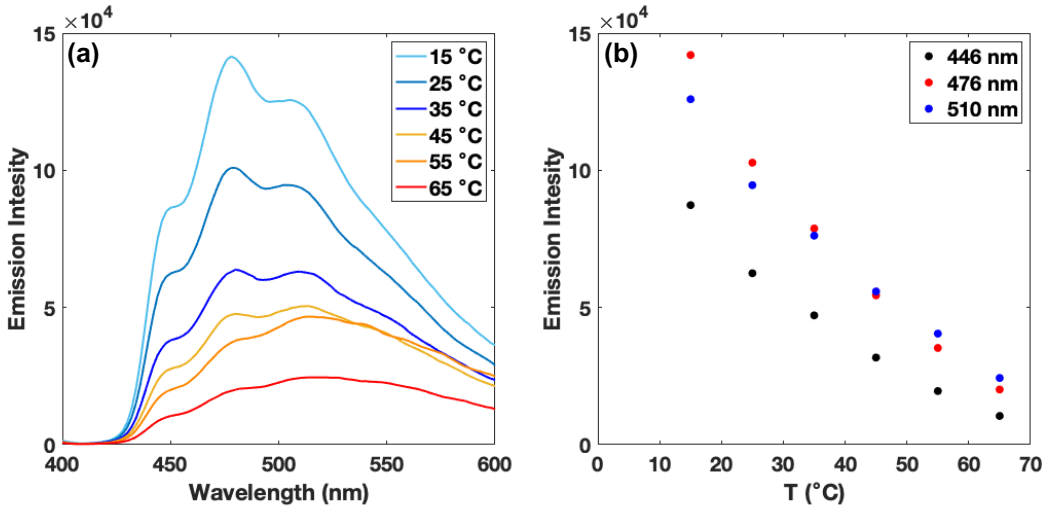

Figure 3.30 The emission spectra of Complex 2 in CH_3CN at various temperatures (a) and the intensity trend with various temperatures (b)

In CH_3CN, the lifetime measurement was found to be biexponential decay in all measured temperatures. The fast decay (τ_1) remains constant in all measured temperatures, but the slow decay (τ_2) decreases linearly with increasing temperature. The lifetime shows there are two states of emission.[89] The fast decay could count as 'state I' and the slow decay count as 'state II', because the slow decay affected by temperature which indicates the state of CO dissociation. The trend is shown in Figure

3.31.

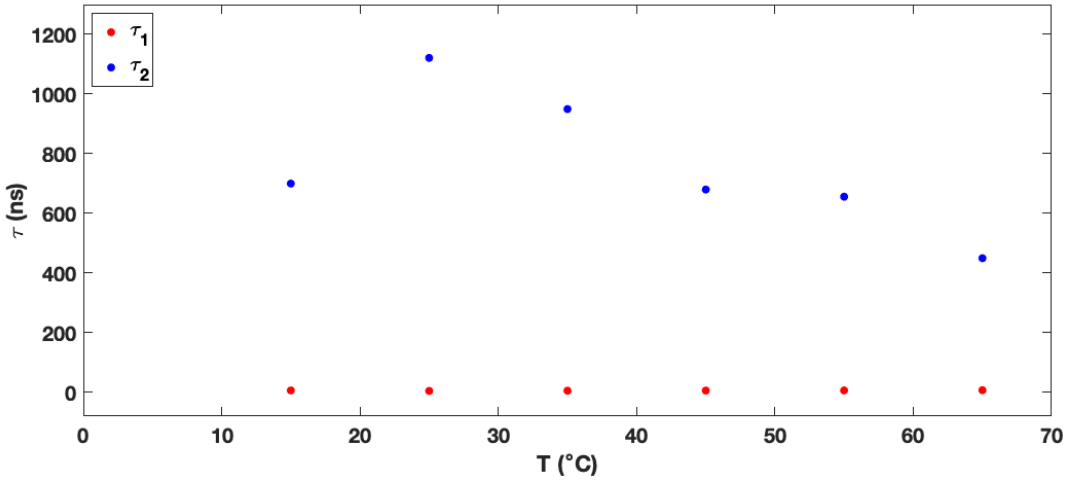

Figure 3.31 The trend of lifetime decay with increasing temperature of Complex 2 in CH_3CN. The fast decay (τ_1) is a red, and the slow decay (τ_2) is a blue.

Concluded the emission and the lifetime results of Complex 2 in CH_3CN and compare it with the result previously described in the group which shows that the state I and II is a mixed ^{3}ILCT/^{3}MLCT state but a more ^{3}MLCT character. The complex 2 populated in a mixed ^{3}ILCT and ^{3}MLCT excited state after excitation, but increasing temperature, the population of ^{3}ILCT tends to populate the ^{3}MLCT excited state. At 55 and 65 °C, the complex shows more ^{3}MLCT excited state than the mixed states, which leads to more CO photodissociation. Also, the reaction barriers are lower because the intensity and slow decay drop more intensively in emission and lifetime measurement.

3.3.3.4. [Re(CO)$_4$(4,4'-(Br)$_2$-bpy)]PF$_6$ Complex (4)

For the Re(CO)$_4$(4,4'-(Br)$_2$-bpy)]PF$_6$ the emission maximum is at 524 nm at room temperature (25 °C), and the shape of the curve shows mostly ^{3}MLCT excited state emission. The emission spectra are shown in Figure 3.32-a. Also, the energy remained with increasing temperature, and the ratio of the peak at 488 and 524 nm decreased with

increased temperature. At the lowest temperature (15 °C), the highest intensity decreased gradually with increasing temperature. After 45 °C, the intensity of 522 nm decreased more than the intensity of 492 nm. The intensity trend is shown in Figure 3.32-b. The decrease within the analysed temperature range, with an overall decrease 2.1 times-fold.

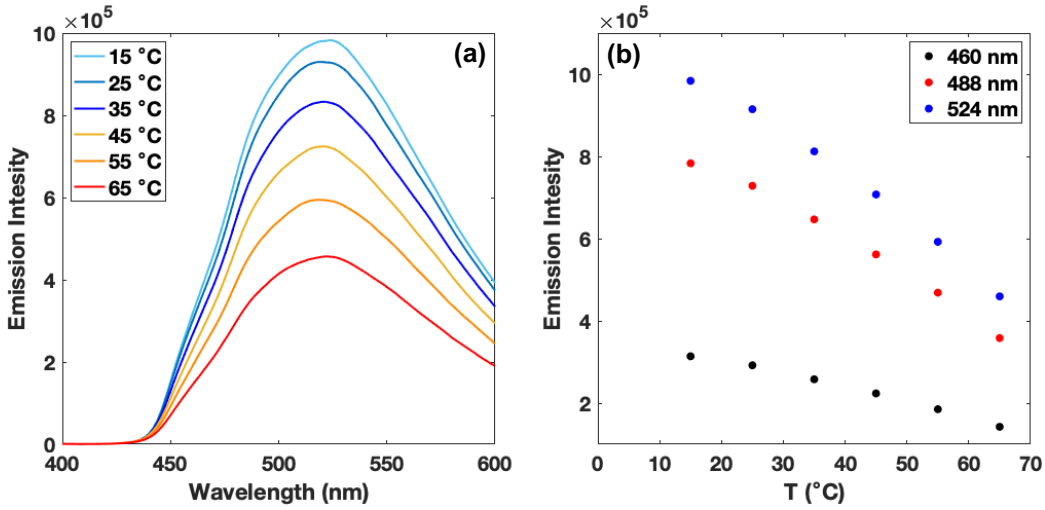

Figure 3.32 The emission spectra of Complex 4 in CH_3CN at various temperatures (a) and the intensity trend with various temperatures (b)

In CH_3CN, the lifetime measurement was found to be biexponential decay in all measured temperatures. The fast decay (τ_1) remains constant in all measured temperatures, but the slow decay (τ_2) decreases linearly with increasing temperature. The lifetime shows there are two states of emission.[89] The fast decay could count as 'state I' and the slow decay count as 'state II', because the slow decay affected by temperature which indicates the state of CO dissociation. the trend is shown in Figure 3.33.

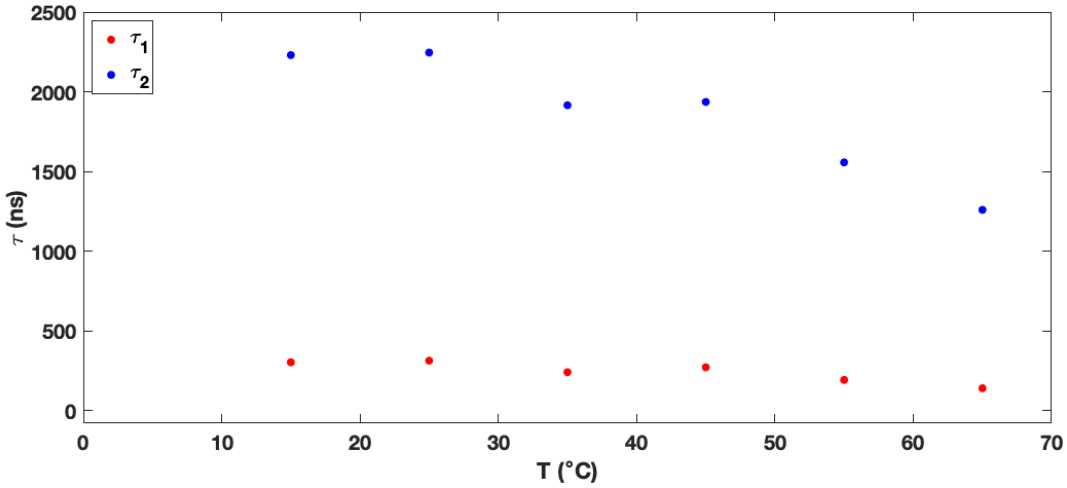

Figure 3.33 The trend of lifetime decay with increasing temperature of Complex 4 in CH_3CN. The fast decay (τ_1) is a red, and the slow decay (τ_2) is a blue.

Concluded the emission and the lifetime results of Complex 4 in CH_3CN and compare it with the result previously described in the group, which shows that the state I and II is a mixed ^{3}ILCT/^{3}MLCT state. The ratio of population of ^{3}ILCT and ^{3}MLCT tends to get closer with increased temperature, which indicates that ^{3}ILCT tends to populate ^{3}MLCT with increased temperature. Therefore, there is more CO dissociation with increased temperature.

3.3.3.5. $[Re(CO)_4(4,4'\text{-}(CF_3)_2\text{-bpy})]PF_6$ Complex (5)

For the $Re(CO)_4(4,4'\text{-}(CF_3)_2\text{-bpy})]PF_6$ the emission maximum is at 550 nm at room temperature (25 °C), and the shape of the curve shows a ^{3}MLCT excited state emission structure. The emission spectra are shown in Figure 3.34-a. Also, the energy shows slightly blue-shifted with increasing temperature. At the lowest temperature (15 °C), the highest intensity decreased gradually with increasing temperature. The intensity trend is shown in Figure 3.34-b. The decrease within the analysed temperature range, with an overall decrease 1.3 times-fold.

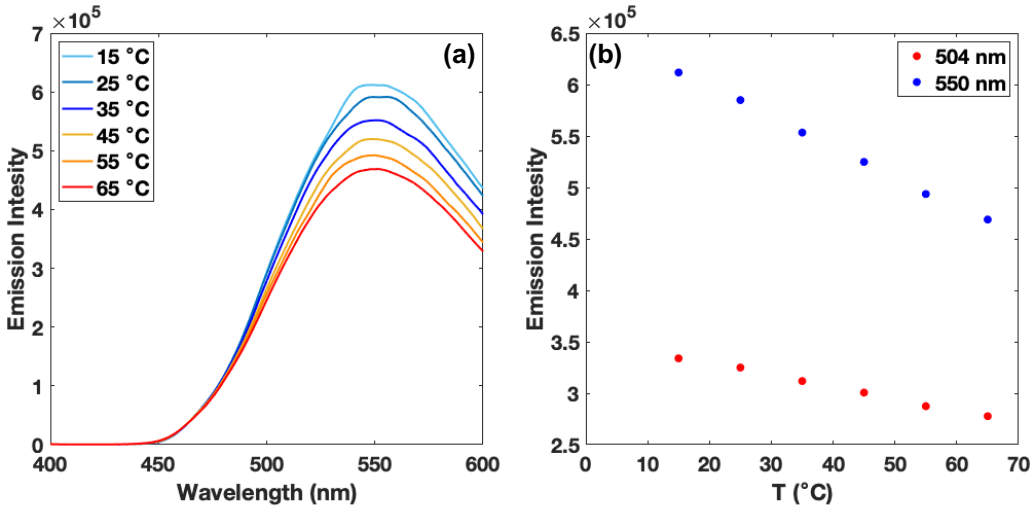

Figure 3.34 The emission spectra of Complex 5 in CH_3CN at various temperatures (a) and the intensity trend with various temperatures (b)

In MeCN, the lifetime measurement was found to be biexponential decay in all measured temperatures. The fast decay (τ_1) and slow decay (τ_2) remains constant in all measured temperatures, The lifetime shows there are two states of emission.[89] The fast decay could count as 'state I' and the slow decay count as 'state II'. Also, two decay lifetime are closer compared to other derivatives. The trend is shown in Figure 3.35

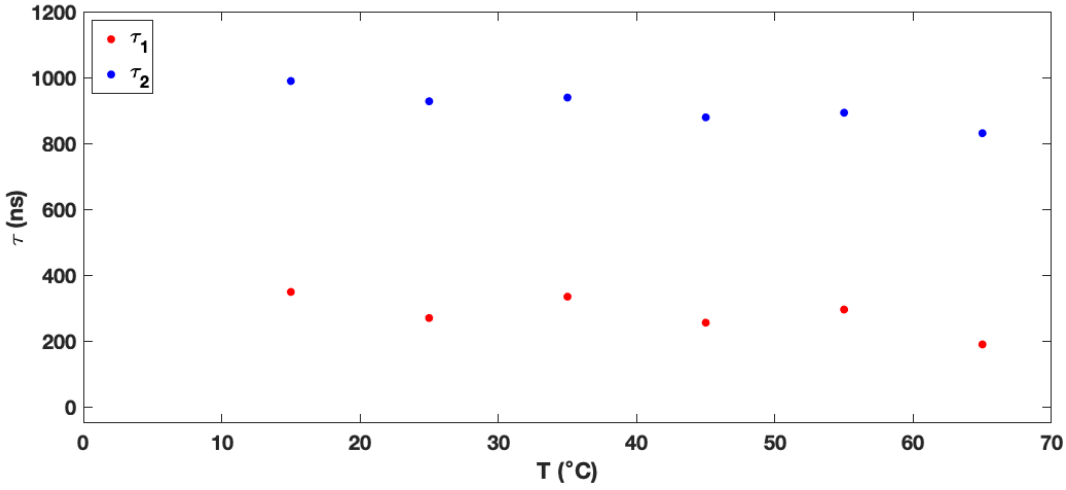

Figure 3.35 The trend of lifetime decay with increasing temperature of Complex 5 in CH_3CN. The fast decay (τ_1) is a red, and the slow decay (τ_2) is a blue.

Concluded the emission and the lifetime results of Complex 5 in CH_3CN and compare with the result previously described in the group, which shows that the state I and II is a mixed ^{3}ILCT/^{3}MLCT state. Complex 5 may tend to populate in state I because the difference of lifetime data of fast and slow decay of Complex 5 became smaller. Therefore, complex 5 does not tend to do CO dissociation which consistent with Wu's report. The emission intensity decreased may be due to the population of ^{3}MLCT in the state I increased with increasing temperature which ^{3}MLCT is a non-emission state.

3.3.4. The photophysic and photochemistry of $[Re(CO)_4(4,4'\text{-}R_2\text{-}bpy)]^+$

This section is going to conclude the photophysics of $[Re(CO)_4(4,4'\text{-}R_2\text{-}bpy)]^+$ (R= NH_2, CH_3, H, Br or CF_3) from the result and comparing it with the results previously described in the group.

The excited state plays a role in CO photodissociation, the complex need to populate in state II to do the dissociation.[46, 47, 85] Also, in state II which is a mixed ^{3}ILCT/^{3}MLCT state, it needs to go through the ^{3}MLCT state to complete the reaction. Therefore, when increasing temperature, the emission result shows, in both solvent CH_3CN and CH_2Cl_2, all the complexes will tend to populate ^{3}MLCT from ^{3}ILCT (the ratio of the peaks decreased). Although, the energy barrier is affected by the solvent, in which case CH_2Cl_2 is a higher barrier than CH_3CN, the energy barrier between ^{3}ILCT and ^{3}MLCT can be overcome by increased temperature. This is the one of the reasons why emission intensity decreases in both solvents, since ^{3}MLCT becomes more populated, and it is a non-emission state. The other reasons of decreased intensity is the complex lost their concentration due to CO dissociation to form the photoproduct *fac*-$[Re(CO)3(4,4'\text{-}R_2\text{-}bpy)(solvent)]^+$. Also, the formation of the photoproduct is the reason of the emission

energy red shifted and the emission lifetime (slow decay) shows decreased. However, in CH_2Cl_2 the CO dissociation is not favourable. This comes up to second explanation.

In general, the complexes in CH_3CN are more favourable to do CO photodissociation than in CH_2Cl_2. The reason may be due to the different mechanism in CH_3CN and CH_2Cl_2. CH_2Cl_2 is the poor coordinating ability ligands, the complex in CH_2Cl_2 needs more energy to overcome the reaction barrier to complete the dissociation. On the other hand, CH_3CN has the better coordinating ability, therefore, the complex in CH_3CN needs less energy to overcome the reaction barrier. When increasing temperature, in CH_3CN, it can be much easier to overcome the barrier to do more CO photodissociation. Therefore, by increasing the temperature in both solvents, the complex tends to populate ^{3}MLCT which can process dissociation, but still need to overcome the second reaction barrier to complete the reaction. This is the reason why CH_2Cl_2 is not favourable for CO dissociation.

Furthermore, the different substituents can enhance or inhibit the temperature effect and CO dissociation. The explanation is that the substituents on the bpy ligand affect the energy of the ^{3}MLCT state and the higher ^{3}MLCT state energy more favourable to do CO dissociation. The peak of ^{3}MLCT state for EDG (NH_2) has the higher energy in emission and then following the trend to CH_3 and the last with EWG (CF_3) which has the lower energy in emission. Also, the substituents may affect the population between ^{3}ILCT and ^{3}MLCT. Therefore, when the substituent is NH_2 which has the higher ^{3}MLCT state energy, increased temperature and when the solvent is CH_2Cl_2, still showing the drop of emission intensity and lifetime also, the red-shifted on emission energy, which indicates enhancing on CO dissociation. On the other hand, when the substituent is CF_3 which has the lower ^{3}MLCT state energy, increased temperature and

when the solvent is CH_3CN still show less emission intensity drop and constant lifetime which indicates inhibiting CO dissociation.

The proposed equilibrium scheme and energy diagram are shown in Scheme 3.2 and Figure 3.36

$$^3ILCT \rightleftharpoons {}^3MLCT \rightleftharpoons photoprodcuts + CO_{(g)}$$

Scheme 3.2 The proposed equilibrium relationship between ^{3}ILCT and ^{3}MLCT state and photoproducts

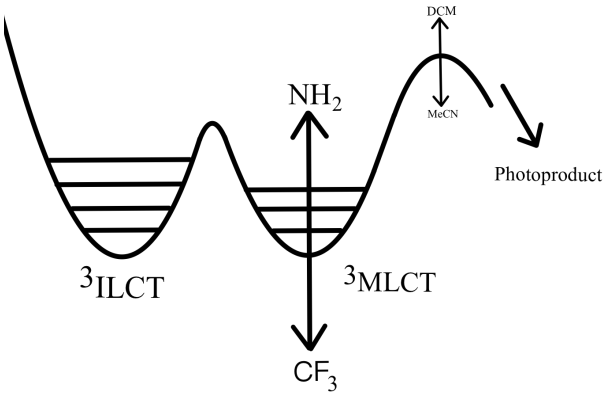

Figure 3.36 The proposed energy diagram of $[Re(CO)4(4,4'\text{-}R_2\text{-}bpy)]^+$ ($R=NH_2$, CH_3, H, Br, CF_3).

3.4. Conclusion

The five complexes $[Re(CO)_4(4,4'\text{-}R_2\text{-}bpy)]^+$ ($R=NH_2$, CH_3, H, Br, CF_3) have been probed by FTIR, UV-vis and emission spectroscopy in CH_2Cl_2 and CH_3CN. In addition, the complexes of the temperature dependence of the emission were monitored by using lifetime measurements in CH_2Cl_2 and CH_3CN. The result of those measurements shows that the CO photodissociation reaction of the complexes may have two reaction barriers, the first barriers is between in state II ^{3}ILCT and ^{3}MLCT state and the second barriers is in the ^{3}MLCT state and the photoproduct. The temperature and the solvent affected

both barriers. The substituents on the bpy ligand affected the energy of ^{3}MLCT state which will enhance or inhibited the temperature effect and CO dissociation.

3.5. Future work

There are many things could be done in the future. Firstly, the TRIR measurement of the complex $[Re(CO)_4(4,4'\text{-}R_2\text{-}bpy)]^+$ (R=NH_2, CH_3, H, Br, CF_3) in CH_3CN still needs to be done. It is because the measurement could provide more insight in the excited state and further investigate the result of this chapter. Also, temperature dependent TRIR measurement in CH_2Cl_2 and CH_3CN needs to be attempted which can provide more knowledge on the temperature effect on the photochemistry and photophysic of the complexes. Moreover, the DFT calculation could be done in the future for all five complexes to give more support on the TRIR and emission measurement.

4. Chapter 4

Experimental

This Chapter describes the techniques, apparatus and chemicals which have been used for the work presented in this Thesis together with the description of synthetic procedures and materials.

4.1. Materials

All chemicals were used as supplied. Rhenium chloride pentacarbonyl, 2,3-Diaminopyridine, 2,2-bipyridine, 4,4'-dimethyl-2,2'-bipyridine, 4,4'-Bis(trifluoromethyl)-2,2'-bipyridine, silver trifluoromethanesulfonate (AgOTf) and ammonium hexafluorophosphate (NH_4PF_6) were obtained from Sigma Aldrich. 4,4'-dibromo-2,2'-bipyridine and 4,4'-diamino-2,2'-bipyridine were obtained from Flurochem. 1,10-phenanthroline-5,6-dione (phdo) and 1,10-phenanthroline were obtained from VWR international and were used without further purification.

Solvents for general experimental use, namely hexane, toluene, ethyl acetate, acetone were obtained from Fischer Scientific. Dichloromethane, diethyl ether, tetrahydrofuran, ethanol, methanol, and acetonitrile were obtained from Sigma Aldrich. All used without further purification.

Solvents for NMR use. Chloroform-d, acetone-d_6, acetonitrile-d_3, dichloromethane-d_2 and dimethyl sulfoxide-d_6 supplied by Sigma Aldrich and again were used without further purification.

Solvents for emission use. Acetonitrile (anhydrous, 99.8 %) and dichloromethane

(anhydrous, ≥ 99.8 %) were obtained from Sigma Aldrich and were used without further purification.

4.2. Synthetic Procedures

4.2.1. Synthesis of dppp2 Ligand

Pyrido[2',3′:5,6]pyrazino[2,3-f][1,10]phenanthroline (dppp2)

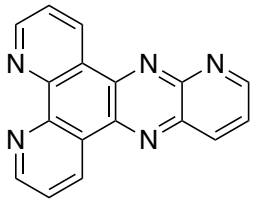

2,3-diaminopyridine (260 mg, 2.4mmol) and 1,10-phenanthroline-5,6-dione (500 mg, 2.4 mmol) were added in methanol (40 mL) to give a brown solution that was gently refluxed for about 3 h, then cooled to room temperature. The reaction solution was concentrated on a rotary evaporator. The brown precipitate was filtered was washed with cooled ethanol and recrystallized from chloroform. The product was obtained as a yellow powder.

Yield: 507mg (75%). ^{1}H NMR (400 MHz, DMSO) δ 9.51 (dd, *J* = 8.1, 1.8 Hz, 1H), 9.46 (dd, *J* = 8.1, 1.8 Hz, 1H), 9.39 (dd, *J* = 4.0, 1.9 Hz, 1H), 9.26 – 9.19 (m, 2H), 8.80 (dd, *J* = 8.5, 1.9 Hz, 1H), 8.05 (dd, *J* = 8.5, 4.0 Hz, 1H), 8.00 – 7.90 (m, 2H). ESI-HRMS m/z: 284.0933 (calc. 284.0931) $C_{17}H_{10}N_5$ ($M+H^+$).

4.2.1.1. The pale beige precipitate —— the intermediate

9,14-dihydropyrido[2',3':5,6]pyrazino[2,3-*f*][1,10]phenanthroline-8b,14a-diol

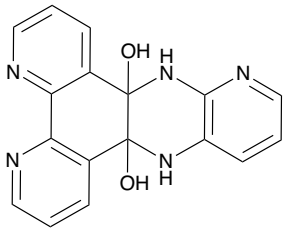

2,3-diaminopyridine (208 mg, 1.9mmol) and 1,10-phenanthroline-5,6-dione (400 mg, 1.9 mmol) were added in CH_3CN (40 mL) to give a brown solution that was gently refluxed for about 3 hours, then cooled to room temperature. The brown solid precipitate was filtered off and the product was obtained as a pale beige powder.

Yield:529 mg (87%). ^{1}H NMR (400 MHz, DMSO) δ 8.63 (ddd, *J* = 8.4, 4.7, 1.7 Hz, 2H), 8.12 (d, *J* = 8.3 Hz, 2H), 7.42 (td, *J* = 8.1, 4.7 Hz, 2H), 7.36 (dd, *J* = 4.9, 1.6 Hz, 1H), 7.31 (s, 1H), 6.80 (s, 1H), 6.75 (s, 1H), 6.44 (dd, *J* = 7.6, 4.9 Hz, 1H), 5.96 (s, 1H), 5.90 (s, 1H). ESI-HRMS m/z: 320.1141(calc. 320.1142) $C_{17}H_{13}N_5O_2$ ($M+H^+$).

4.2.2. Synthesis of *fac*-[(Cl)Re(CO)$_3$ (dppp2)]

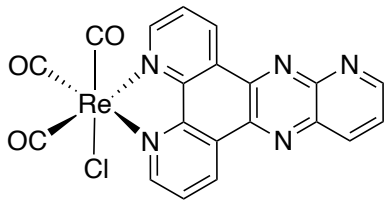

$Re(CO)_5Cl$ (255 mg, 0.7 mmol) and dppp2 (200mg, 0.7 mmol) were added to dry toluene (40mL), and the mixture was refluxed under Ar with stirring for 4h in the dark. After that, the solution was cooled to room temperature, and a yellow-brown solid was collected by suction filtration. The crude product was washed with ice toluene (3x10mL) and dried in the open air under suction yielding the final product as a yellow-brown powder.

Yield: 383mg (98%). ^{1}H NMR (400 MHz, d-DMSO): δ 9.51 (dd, J = 8.1, 1.8 Hz, 1H),

9.46 (dd, J = 8.1, 1.8 Hz, 1H), 9.39 (dd, J = 4.0, 1.9 Hz, 1H), 9.22 (m, 2H), 8.80 (dd, J = 8.5, 1.9 Hz, 1H), 8.05 (dd, J = 8.5, 4.0 Hz, 1H), 7.95 (m,2H). FTIR (CH_2Cl_2), ν(CO): 2025(s), 1924(s), 1901(s). ESI-HRMS m/z: 611.9817 (calc. 611.9844) $C_{20}H_9ClN_5NaO_3Re$ ($M+Na^+$).

4.2.3. Synthesis of *fac*-[(OTf)Re(CO)$_3$(dppp2)]

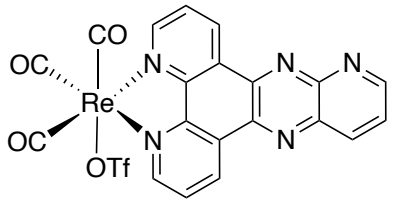

fac-[(Cl)Re(CO)$_3$(dppp2)] (350 mg, 0.6 mmol) and AgOTf (160mg, 0.6 mmol) were dissolved in dry CH_2Cl_2, and the solution was refluxed under Ar with stirring for 12h in the dark. After that, the solution was cooled to room temperature and filtered off the AgCl precipitate by gravity filtration. The clear solution (CH_2Cl_2 solvent) was removed under vacuum until about 5-10 mL left. Excess hexane was added to the solution to form brown solid, and the solid was collected following suction filtration. The crude product was washed with hexane (3x10mL) and dried in the open air under suction yielding the final product as an orange-brown powder.

Yield: 304 mg (72%). ^{1}H NMR (400 MHz, CD_2Cl_2) δ 10.05 (dd, J = 8.2, 1.5 Hz, 1H), 9.95 (dd, J = 8.3, 1.5 Hz, 1H), 9.53 (m, 3H), 8.87 (dd, J = 8.6, 1.9 Hz, 1H), 8.15 (m,2H), 8.05 (dd, J = 8.5, 4.1 Hz, 1H); ^{19}F NMR (376 MHz, CD_2Cl_2): δ -77.71. FTIR (CH_2Cl_2), ν(CO): 2038(s), 1938(s), 1919(s).

4.2.4. Synthesis of *fac*-[(CH$_3$CN)Re(CO)$_3$(dppp2)]OTf

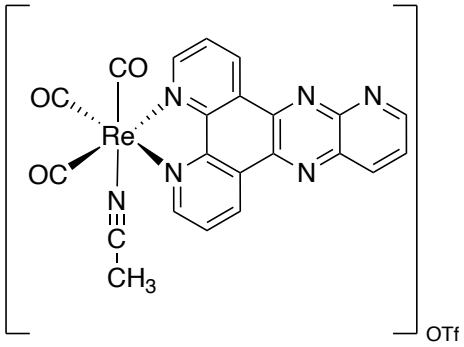

fac-[(Cl)Re(CO)$_3$(dppp2)] (300mg, 0.5mmol) and AgOTf (130mg, 0.5mmol) were dissolved in dry CH_2Cl_2, and the solution was refluxed under Ar with stirring for 12h in the dark. After that, the solution was cooled to room temperature and filtered off the AgCl precipitate by gravity filtration. The clear solution (CH_2Cl_2 solvent) was removed under a vacuum. The solid was dissolved in MeCN (40mL) and stirred for 30min. Then, the solvent was removed under a vacuum until about 5-10 mL was left. Excess diethyl ether was added to the solution and stirred until it crushed the brown solid. The solid was collected by suction filtration. The crude product was washed with diethyl ether (3x10mL) and dried in the open air under suction. The final product was obtained as a yellow-brown powder.

Yield 296 mg (80%). ^{1}H NMR (400 MHz, CD_2Cl_2): δ 9.99 (m, 2H), 9.75 – 9.70 (m, 1H), 9.44 (dd, J = 5.3, 1.5 Hz, 1H), 9.32 (dd, J = 5.3, 1.5 Hz, 1H), 9.08 (dd, J = 8.5, 1.8 Hz, 1H), 8.22 (m, 2H), 7.97 (dd, J = 8.3, 5.3 Hz, 1H), 2.53 (s, 1H)(CH_3CN). ^{19}F NMR (376 MHz, CD_2Cl_2): δ -78.93. FTIR (CH_2Cl_2), ν(CO): 2042(s), 1948(b). ESI-HRMS m/z: 595.0520 (calc. 595.0523) $C_{22}H_{12}N_6O_3Re$ (M^+).

4.2.5. Synthesis of *cis, trans*-$[Re(CO)_2(dppp2)_2]PF_6$

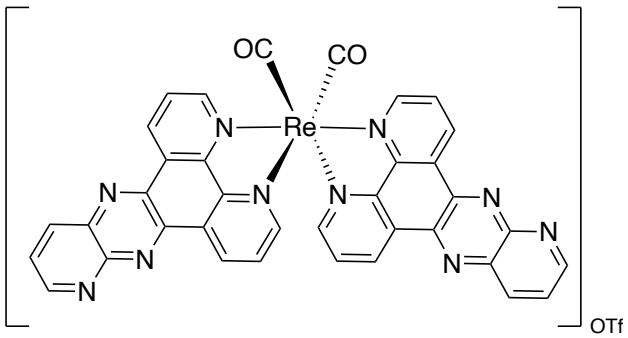

fac-$[(CH_3CN)Re(CO)_3(dppp2)]OTf$ (200mg, 0.27mmol) and a large excess of dppp2 were added in a heavy walled reaction tube with a stir bar. The tube was capped with a septum and purged with Ar. The mixture was heated to 270 ^oC while stirring for ca. 4 h. The resulting black solid product was cooled and then dissolved in CH_3CN and NH_4PF_6 added, and the solution was stirred 30 min. The solution was concentrated by removing the solvent under a vacuum until about 5-10 mL was remaining. Excess diethyl ether was added to the solution resulting in precipitation of a brown solid. The product was initially purification using column chromatography (alumina) using CH_2Cl_2:CH_3CN (3:7). The resulting solid was recrystallized from CH_2Cl_2 and diethyl ether. The final product was obtained as a brown solid.

Yield 7.9mg (3.0%). ^1H NMR (400 MHz, CD_3CN) δ 10.06 – 10.00 (m, 2H), 9.90 (d, *J* = 8.2 Hz, 1H), 9.83 (dd, *J* = 8.2, 1.3 Hz, 1H), 9.64 (d, *J* = 8.3 Hz, 1H), 9.56 (d, *J* = 7.9 Hz, 1H), 9.46 (ddd, *J* = 14.3, 4.0, 1.9 Hz, 2H), 8.87 (dd, *J* = 8.7, 1.9 Hz, 1H), 8.78 (dd, *J* = 8.5, 1.9 Hz, 1H), 8.21 (dd, *J* = 8.3, 5.4 Hz, 2H), 8.12 – 8.02 (m, 2H), 7.94 (d, *J* = 4.7 Hz, 2H), 7.69 (dd, *J* = 8.2, 5.4 Hz, 2H). ^{19}F NMR (376 MHz, CD_3CN) δ -72.03, -73.91. FTIR (CH_2Cl_2), ν(CO): 1924(s), 1854(s). ESI-HRMS m/z: 809.1143 (calc. 809.1166) $C_{36}H_{18}N_{10}O_2Re$ (M^+).

4.2.6. Synthesis of *fac*-[(Cl)Re(CO)$_3$(phdo)]

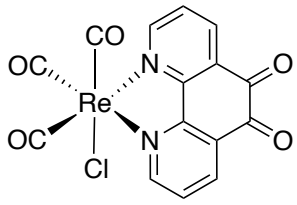

Phdo=1,10-phenanthroline-5,6-dione

$Re(CO)_5Cl$ (689 mg, 1.9mmol) and phdo (400 mg, 1.9mmol) were added to dry toluene (40mL), and the mixture was refluxed (4h) under Ar in the dark. The solution was cooled to room temperature producing a yellow-brown solid which was collected by suction filtration. The crude product was washed with ice toluene (3x10mL) and dried yielding final product as a red-brown powder.

Yield 892 mg (90%). ^{1}H NMR (400 MHz, CD_3CN) δ 9.23 (dd, *J* = 5.5, 1.5 Hz, 1H), 8.69 (dd, *J* = 8.0, 1.6 Hz, 1H), 7.85 (dd, *J* = 8.0, 5.5 Hz, 1H). FTIR (CH_3CN), ν(CO): 2024(s), 1924(s), 1905(s) and 1709(m)(phdo)

4.2.7. Synthesis of *fac*-[(OTf)Re(CO)$_3$(phdo)]

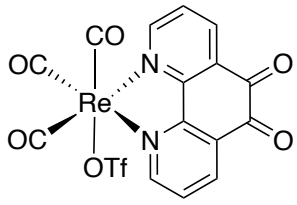

fac-[(Cl)Re(CO)$_3$ (phdo)] (200 mg, 0.39mmol) and AgOTf (100mg , 0.39mmol) were dissolved in dry CH_2Cl_2 (40 mL) and the solution was refluxed under Ar with stirring for 12h in the dark. AgCl filtered off after the solution was cooled to room temperature and solution concentrated to ca. 5-10 mL. The crude product was obtained following the addition of an excess hexane. The brown solid, and the solid was collected and

washed with hexane (3x10mL) yielding the final product as orange powder

Yield 78.7 mg (32%). ^{1}H NMR (400 MHz, CD_2Cl_2) δ 9.32 (dd, *J* = 5.5, 1.6 Hz, 2H), 8.80 (dd, *J* = 8.0, 1.6 Hz, 2H), 7.92 (dd, *J* = 8.0, 5.5 Hz, 2H); ^{19}F NMR (376 MHz, CD_2Cl_2) δ -77.51; FTIR (CH_2Cl_2), ν(CO):2041(s), 1944(s), 1924(s), 1705(m)(phdo).

4.2.8. Synthesis of *fac*-[(CH$_3$CN)Re(CO)$_3$(phdo)]OTf

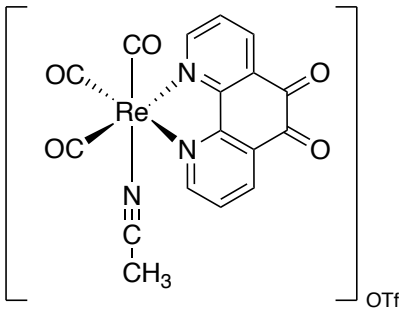

fac-[Re(CO)$_3$(phdo)Cl] (350mg, 0.68mmol) and AgOTf(175mg, 0.68mmol) were dissolved in dry CH_2Cl_2, and the solution was refluxed under Ar with stirring for 12h in the dark. AgCl filtered off after the solution was cooled to room temperature. A solid was obtained after removing the solvent and recrystallized from CH_3CN /diethyl ether. The resulting solid was washed with diethyl ether (3x10mL) yielding the final product was obtained as a red powder.

Yield:172mg (48%). ^{1}H NMR (400 MHz, CD_2Cl_2): δ 9.14 (dd, *J* = 5.5, 1.5 Hz, 2H), 8.80 (dd, *J* = 8.0, 1.5 Hz, 2H), 7.88 (dd, *J* = 8.0, 5.5 Hz, 2H), 2.25 (s, 3H (CH_3CN)). ^{19}F NMR (376 MHz, CD_2Cl_2): δ -79.29. FTIR (CH_2Cl_2), ν(CO): 2043(s), 1944(b), 1712(s)(phdo). ESI-HRMS m/z:522.0089 (calc. 522.0094) $C_{17}H_9N_3O_5Re$ (M^+).

4.2.9. Facial-meridianal isomerization route——Synthesis Rhenium (I) bis-diimine complex

In this section, a new synthetic approach was attempted, and the yield of the reaction was unfortunately low, therefore, there is no accurate yield present. The low yield also limited characterization and full purification on each step was not obtained.

4.2.9.1. Synthesis of *fac*-[(Cl)Re(CO)$_3$(bpy)]

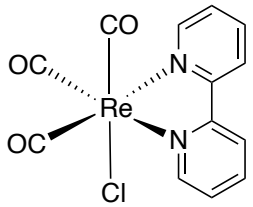

$Re(CO)_5Cl$ (150 mg) and bpy (75 mg) were added to dry toluene (40mL), and the mixture was refluxed under Ar with stirring for 4h in the dark. After that, the solution was cooled to room temperature, and a yellow-brown solid was collected by suction filtration. The crude product was washed with ice toluene (3x10mL) and dried in the open air with suction. The final product was obtained as a yellow powder (ca. 200 mg) and characterized as above.

4.2.9.2. Synthesis of *mer*-[(Cl)Re(CO)$_3$(bpy)]

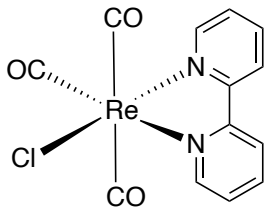

fac-[(Cl)Re(CO)$_3$(bpy)] (50mg) was dissolved in THF (250 ml) and irradiated by 400W medium pressure Hg lamp under Ar for 3 h. Removing the solvent under vacuum produced the crude product which was dissolved in CH_2Cl_2 and following removal of

insoluble black impurity allowed the isolation of the product as brown solid.

^{1}H NMR (400 MHz, THF) δ 9.48 (d, *J* = 5.6 Hz, 1H), 9.04 (d, *J* = 5.3 Hz, 1H), 8.61 (s, 1H), 8.53 – 8.46 (m, 1H), 8.17 (s, 1H), 7.80 (d, *J* = 7.9 Hz, 1H), 7.64 (d, *J* = 6.7 Hz, 1H), 7.30 (s, 1H). FTIR (CH_2Cl_2), ν(CO): 2048 (w), 1936(vs) and 1884(s) cm^{-1}.

4.2.9.3. Synthesis of *cis,cis*-[(Cl)(CH_3CN)Re($CO)_2$(bpy)]

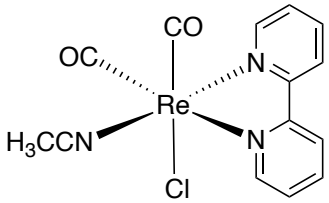

mer-[(Cl)Re($CO)_3$(bpy)] (ca. 10 mg) was dissolved in CH_3CN (40mL) under reflux for 30 minutes. The solution was concentrated, and excess diethyl ether was added. The impurity was removed by filtration and removal of the solvent yielded the product as red solid.

^{1}H NMR (400 MHz, Acetone) δ 9.19 (d, *J* = 5.6 Hz, 1H), 9.03 (d, *J* = 6.3 Hz, 1H), 8.61 (d, *J* = 8.5 Hz, 1H), 8.50 (d, *J* = 8.2 Hz, 1H), 8.22 (t, *J* = 7.9 Hz, 1H), 8.01 (t, *J* = 7.2 Hz, 1H), 7.70 (t, *J* = 6.5 Hz, 1H), 7.44 (t, *J* = 6.0 Hz, 1H), 2.83 (s, 3H). FTIR (CH_2Cl_2), ν(CO):1913(s) and 1830(s) cm^{-1}.

4.2.9.4. Synthesis of *cis*-[(Re(CO)$_2$(bpy)$_2$]OTf

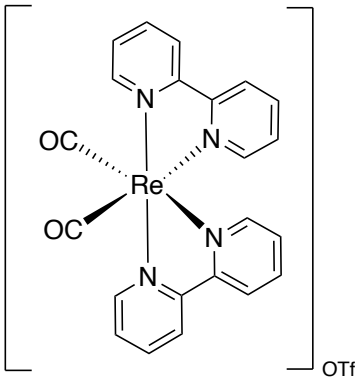

cis,cis-[(Cl)(CH$_3$CN)Re(CO)$_2$(bpy)] (ca. 10 mg) was dissolved in CH_2Cl_2 (40 mL). Excess of AgOTf and phdo ligand were added and the solution was refluxed 3h under Ar and in the dark. AgCl was filtered and the solution was concentrated, and excess hexane was added. A yellow impurity was removed by filtration and removal of the solvent yielded the product as red solid.

^{1}H NMR (400 MHz, CD_3CN) δ 9.45 (d, *J* = 5.0 Hz, 2H), 8.46 (d, *J* = 8.4 Hz, 2H), 8.39 (d, *J* = 8.2 Hz, 2H), 8.17 – 8.12 (m, 2H), 8.02 (t, *J* = 7.0 Hz, 2H), 7.64 – 7.60 (m, 2H), 7.41 (d, *J* = 4.8 Hz, 2H), 7.36 – 7.31 (m, 2H). FTIR (CH_2Cl_2), ν(CO):1917(s) and 1848(s) cm^{-1}. ESI-HRMS m/z: 555.0824 (calc. 555.0825) $C_{22}H_{16}N_4O_2Re$ (M^+).

4.2.10. Direct CO substitution route——Synthesis Rhenium (I) bis-diimine complex

In this section, a new synthetic approach was attempted, and the yield of the reaction was unfortunately low, therefore, there is no accurate yield present. The low yield also limited characterization and full purification on each step was not obtained.

4.2.10.1. Synthesis of *fac*-[(Cl)Re(CO)$_3$(phen)]

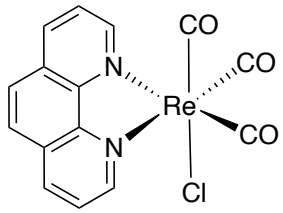

$Re(CO)_5Cl$ (150 mg) and phen (75 mg) were added to dry toluene (40mL), and the mixture was refluxed under Ar with stirring for 4h in the dark. After that, the solution was cooled to room temperature, and a yellow-brown solid was collected by suction filtration. The crude product was washed with ice toluene (3x10mL) and dried in the open air under suction. The final product was obtained as a yellow powder (ca. 155mg).

4.2.10.2. Synthesis of *cis,cis*-[(Cl)(CH_3CN)Re(CO)$_2$(phen)]

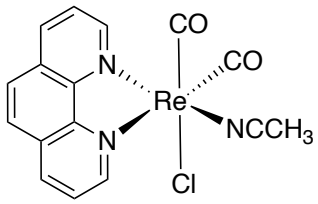

fac-[(Cl)Re(CO)$_3$(phen)] (50 mg) was dissolved in THF/CH_3CN(99:1, 250 mL) and immersion well photoreactor was used. The solution was irradiated by 400W medium pressure Hg lamp under Ar for 3 hours. The solution became black, and the solvent was removed under vacuum. The crude was dissolved in CH_2Cl_2 and excess hexane was added and the black impurity was removed. The solvent was removed under vacuum and the brown solid was recrystallised from CH_3CN and excess diethyl ether was added. A yellow impurity was removed and removal of solvent yielded the product was obtained as red solid.

^{1}H NMR (400 MHz, Acetone) δ 9.55 (dd, J = 5.4, 1.3 Hz, 1H), 9.40 (dd, J = 5.0, 1.4

Hz, 1H), 8.82 (dd, *J* = 8.1, 1.4 Hz, 1H), 8.62 (dd, *J* = 8.2, 1.4 Hz, 1H), 8.33 (d, *J* = 7.8 Hz, 1H), 8.21 (d, *J* = 4.0 Hz, 1H), 8.08 – 8.04 (m, 1H), 7.83 (dd, *J* = 8.1, 5.4 Hz, 1H), 2.89 (s, 3H). FTIR (CH_2Cl_2), ν(CO):1911(s) and 1830(s) cm^{-1}.

4.2.10.3. Synthesis of *cis*-[Re(CO)$_2$(phen)$_2$]OTf

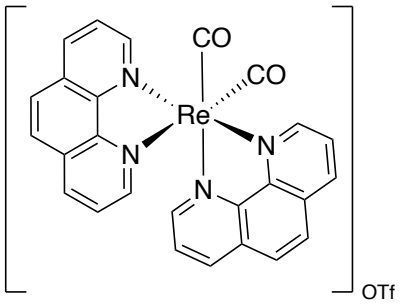

cis,cis-[(Cl)(CH_3CN)Re(CO)$_2$(phen)] (ca. 10 mg) was dissolved in CH_2Cl_2 (40 mL). Excess AgOTf and phen ligand were added and the solution was refluxed for 3 hours under Ar and in the dark. Removal AgCl was achieved by filtration and following removal the solvent the resulting mixture was dissolved in CH_3OH and refluxed 12 hours under Ar and in the dark. Removal of the solvent yielded the product was obtained as red solid.

^{1}H NMR (400 MHz, CD_3CN) δ 9.93 (d, *J* = 6.4 Hz, 2H), 8.76 (d, *J* = 8.3 Hz, 2H), 8.50 (s, 2H), 8.23 (s, 2H), 8.08 (s, 2H), 8.03 (dd, *J* = 9.0, 6.0 Hz, 2H), 7.58 (d, *J* = 5.3 Hz, 2H), 7.46 (dd, *J* = 8.2, 5.1 Hz, 2H). FTIR (CH_2Cl_2), ν(CO): 1921(s) and 1846(s) cm^{-1}. ESI-HRMS m/z: 603.0813 (calc. 603.0825) $C_{26}H_{16}N_4O_2Re$ (M^+).

4.2.11. Synthesis of $[Re(CO)_4(bpy)]PF_6$

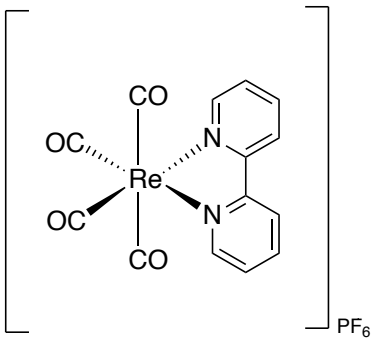

A mixture of $Re(CO)_5Cl$ (203mg, 0.5mmol) and AgOTf (128mg, 0.5mmol) in CH_2Cl_2 (40 ml) was stirred at room temperature for 12 hours under Ar and in the absence of light. Removal of AgCl was followed by the addition of 2,2'-bipyridine (bpy) (94mg, 0.6mmol) and the solution was stirred for a 24 hours under Ar and in the absence of light. Two-thirds of the reaction solution was removed under vacuum, and hexane (50 ml) was added to crash out the trifoliate analogue [Re(CO)4(bpy)][OTf]. [Re(CO)4(bpy)]OTf and NH_4PF_6 (350mg, 2 mmol) were dissolved in a H_2O/acetone (1:1) mixture, and stirred for 1 hour and then left to form a precipitate overnight. A yellow crystal was recovered.

Yield:113 (37%). ^{1}H NMR (400 MHz, CD_3CN) δ 9.02 (dd, *J* = 5.6, 1.3 Hz, 1H), 8.50 (dd, *J* = 8.3, 1.1 Hz, 1H), 8.31 (dd, *J* = 8.0, 1.6 Hz, 1H), 7.73 (dd, *J* = 5.6, 1.3 Hz, 1H). ^{19}F NMR (376 MHz, CD_3CN) δ -72.92 (d, *J* = 706.4 Hz) (PF_6). FTIR (CH_2Cl_2), ν(CO):2123(m), 2032(vs), 2011(s) and 1971(s) cm^{-1}. ESI-HRMS m/z: 455.0124 (calc. 445.0041) C14H8N2O4Re (M^+).

4.2.12. Synthesis of $[Re(CO)_4(4,4'\text{-}(NH)_2\text{-bpy})]PF_6$

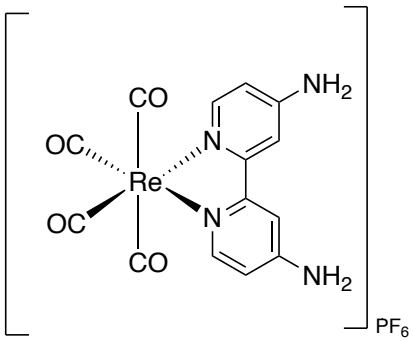

A solution of $Re(CO)_5Cl$ (203mg, 0.5mmol) and AgOTf (128mg, 0.5mmol) in CH_2Cl_2 (40 ml) was stirred at room temperature for 12 hours under Ar and in the absence of light. AgCl was removed and 4,4'-diamino-2,2'-bipyridine (4,4'-$(NH)_2$-bpy) (100mg, 0.6mmol) was added and the solution was stirred for a further 48 hours under Ar and in the absence of light. The solution was concentrated to two-thirds of the original reaction volume and hexane (50 ml) was added to crash out the trifoliate analogue [Re(CO)4(4,4'-$(NH)_2$-bpy)][OTf]. [Re(CO)4(4,4'-$(NH)_2$-bpy)][OTf] and NH_4PF_6 (350mg, 2 mmol) were dissolved in a H_2O/acetone (1:1) mixture, and stirred for 1 hour and then left to form a precipitate overnight. The yellow-brown solid was recrystalised from CH_2Cl_2 yielding the product was obtained as a yellow powder.

Yield 42 mg (13%). ^{1}H NMR (400 MHz, CD_3CN) δ 8.29 (d, *J* = 6.5 Hz, 2H), 7.33 (d, *J* = 2.5 Hz, 2H), 6.75 (dd, *J* = 6.5, 2.5 Hz, 2H), 5.88 (s, 4H). ^{19}F NMR (376 MHz, CD_3CN) δ -72.96 (d, *J* = 706.4 Hz) (PF_6). FTIR (CH_2Cl_2), ν(CO):2117(m), 2018(vs), 1997(s), and 1955(s) cm^{-1}. ESI-HRMS m/z:484.0290 (calc. 484.0259) $C_{14}H_{10}N_4O_4Re$ (M^+).

4.2.13. Synthesis of $[Re(CO)_4(4,4'\text{-}(CH_3)_2\text{-bpy})]PF_6$

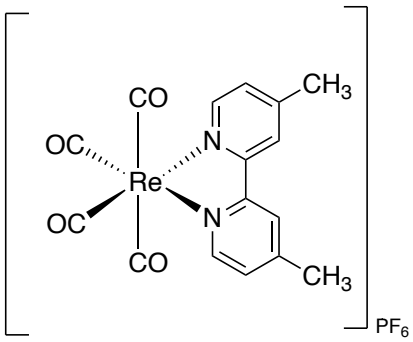

A solution of $Re(CO)_5Cl$ (203mg, 0.5mmol) and AgOTf (128mg, 0.5mmol) in CH_2Cl_2 (40 ml) was stirred at room temperature for 12 hours under Ar and in the absence of light. After removal of AgCl, 4,4'-dimethyl-2,2'-bipyridine (4,4'-$(CH_3)_2$-bpy))(97 mg, 0.6 mmol) was added in solution and the solution was stirred for a further 24 hours under Ar and in the absence of light. The solution was concentrated to two-thirds of the reaction solution was removed under vacuum, and hexane (50 ml) was added to crash out the trifoliate analogue $[Re(CO)_4(4,4'\text{-}(CH_3)_2\text{-bpy})][OTf]$. $[Re(CO)_4(4,4'\text{-}(CH_3)_2\text{-bpy})]OTf$ and NH_4PF_6 (350mg, 2 mmol) were dissolved in a H_2O/acetone (1:1) mixture, and stirred for 1 hour and then left to form a precipitate overnight. The precipitate was recrystallized from CH_2Cl_2 and hexane yielding the product as light yellow crystals.

Yield: 155mg (50%). ^1H NMR (400 MHz, CD_3CN) δ 8.82 (d, J = 5.8 Hz, 2H), 8.37 – 8.32 (m, 2H), 7.55 (ddd, J = 5.7, 1.8, 0.9 Hz, 2H), 2.60 (s, 6H). ^{19}F NMR (376 MHz, CD_3CN) δ -72.94 (d, J = 706.4 Hz) (PF_6). FTIR (CH_2Cl_2), ν(CO):2121(m), 2027(vs), 2008(s) and 1967(s) cm^{-1}. ESI-HRMS m/z: 482.0391 (calc. 482.0354) $C_{16}H_{12}N_2O_4Re$ (M^+).

4.2.14. Synthesis of $[Re(CO)_4(4,4'\text{-}(Br)_2\text{-}bpy)]PF_6$

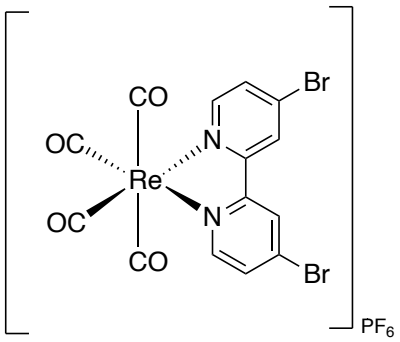

A solution of $Re(CO)_5Cl$(203mg, 0.5mmol) and AgOTf (128mg, 0.5mmol) in CH_2Cl_2 (40 ml) was stirred at room temperature for 12 hours under Ar and in the absence of light. 4,4'-Dibromo-2,2'-bipyridine (4,4'-$(Br)_2$-bpy) (188mg,0.6mmol) was added in solution after removal of AgCl. The solution was stirred for a 48 hours under reflux, Ar and in the absence of light. The solution was concentrated to two-thirds of the original reaction volume and hexane (50 ml) was added to generate $[Re(CO)_4(4,4'\text{-}(Br)_2\text{-}bpy)]OTf$. $[Re(CO)_4(4,4'\text{-}(Br)_2\text{-}bpy)]OTf$ and NH_4PF_6 (350mg, 2 mmol) were dissolved in a H_2O/acetone (1:1) mixture, and stirred for 1 hour and then left to form a precipitate overnight. The product was recrystalised from acetone and hexane (1:1) yielding the product was obtained as yellow crystals.

Yield:104mg (28%). ^1H NMR (400 MHz, CD_3CN) δ 8.81 (d, J = 6.0 Hz, 1H), 8.73 (d, J = 2.1 Hz, 1H), 7.94 (dd, J = 6.1, 2.1 Hz, 1H). ^{19}F NMR (376 MHz, CD_3CN) δ -72.97 (d, J = 706.4 Hz) (PF_6). FTIR (CH_2Cl_2), ν(CO):2125(m), 2036(vs), 2014(s) and1974(s) cm^{-1}. ESI-HRMS m/z: 610.8253 (calc. 610.8246) $C_{14}H_6Br_2N_2O_4Re$ (M^+).

4.2.15. Synthesis of $[Re(CO)_4(4,4'\text{-}(CF_3)_2\text{-bpy})]PF_6$

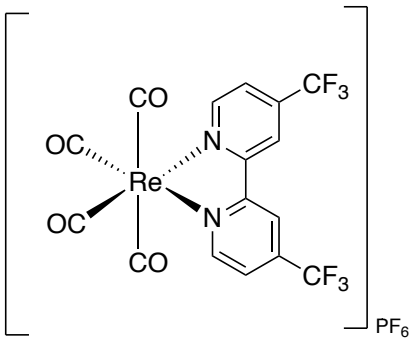

A solution of $Re(CO)_5Cl$ (203mg, 0.5mmol) and AgOTf (128mg, 0.5mmol) in CH_2Cl_2 (40 ml) was stirred at room temperature for 12 hours under Ar and in the absence of light. 4,4'-Bis(trifluoromethyl)-2,2'-bipyridine (4,4'-$(CF_3)_2$-bpy) (175mg, 0.6 mmol) was added in solution after removal of AgCl. The solution was stirred for a further 48 hours under reflux, Ar and in the absence of light. The solution was concentrated to two-thirds of the reaction solution and hexane (50 ml) was added to precipitate $[Re(CO)_4(4,4'\text{-}(CF_3)_2\text{-bpy})]OTf$. $[Re(CO)_4(4,4'\text{-}(CF_3)_2\text{-bpy})]OTf$ and NH_4PF_6 (350mg, 2 mmol) were dissolved in a H_2O/acetone (1:1) mixture, and stirred for 1 hour and then left to form a precipitate overnight yielding product was obtained as pale yellow crystals.

Yield: 76.8 mg (21%). ^1H NMR (400 MHz, CD_3CN) δ 9.26 (d, J = 5.8 Hz, 1H), 8.94 – 8.89 (m, 1H), 8.05 (dd, J = 5.9, 1.9 Hz, 1H). ^{19}F NMR (376 MHz, CD_3CN) δ -65.52 (CF_3), -72.97 (d, J = 706.3 Hz) (PF_6). FTIR (CH_2Cl_2), ν(CO):2128(m), 2042(vs), 2012(s) and 1978(s) cm^{-1}. ESI-HRMS m/z:590.9825 (calc. 590.4276) $C_{16}H_6F_6N_2O_4Re$ (M^+).

4.3. Other Experimental Techniques

4.3.1. FTIR Spectroscopy and UV-Vis Spectroscopy

FTIR measurements were made using a Thermo Nicolet FTIR spectrometer fitted with

a MCT detector. Spectra were recorded with either of 32 to 64 scans and a resolution of 2 cm^{-1}. An infrared solution cell (Harrick Corp.) with CaF_2 (2 x 25 mm) windows with a path length ca. 800 μm was typically used but the pathlength was altered depending on the concentration of the solution. UV/visible absorption spectra were taken using a Perkin Elmer Lambda 5 spectrometer in a quartz cuvette with 1 cm spacing.

4.3.2. Luminescence Spectroscopy

All emission and excitation spectra were taken on an Edinburgh Instrument FLS920 combined fluorescence lifetime and steady state spectrometer. The excitation source used for all steady state emission and excitation was a xenon (Xe) Arc lamp. All samples were taken using a quartz cuvette with a 1cm path length. All solutions exhibited absorbance of between 0.10-0.20 at the excitation wavelength. Emission lifetime experiments were run with a ps-diode laser (406 nm), with a freeze-pump-thaw degassed solution under Ar unless stated otherwise.

4.3.3. ^{1}H, ^{13}C and ^{19}F NMR Spectroscopy

^{1}H NMR spectra were recorded at 400 MHz in deuterated chloroform or deuterated methanol at room temperature using the JEOL ex400 NMR spectrometer. ^{13}C NMR spectra were recorded at 400 MHz in deuterated chloroform or deuterated methanol at room temperature using the JEOL ex400 NMR spectrometer. ^{19}F NMR spectra were recorded at 376 MHz in deuterated chloroform or deuterated methanol at room temperature using the JEOL ex400 NMR spectrometer. Shifts in peaks are due to changes in solvent were compared to literature values.

4.3.4. Mass Spectroscopy

All mass spectra were obtained with the Mass Spectrometry Service (University of Nottingham). Positive and negative ion electrospray mass spectra were recorded using an automated Micromass LCT spectrometer using ElectroSpray Ionisation. Measurements were performed in methanol or acetonitrile solutions.

5 Reference

1. P. A. Summers, J. A. Calladine, F. Ghiotto, J. Dawson, X.-Z. Sun, M. L. Hamilton, M. Towrie, E. S. Davies, J. McMaster, M. W. George and M. Schröder, *Inorg Chem*, 2016, **55**, 527-536.

2. C. D. Windle, M. W. George, R. N. Perutz, P. A. Summers, X. Z. Sun and A. C. Whitwood, *Chem. Sci.*, 2015, **6**, 6847-6864.

3. P. R. D. Murray, J. H. Cox, N. D. Chiappini, C. B. Roos, E. A. McLoughlin, B. G. Hejna, S. T. Nguyen, H. H. Ripberger, J. M. Ganley, E. Tsui, N. Y. Shin, B. Koronkiewicz, G. Qiu and R. R. Knowles, *Chem. Rev.*, 2022, **122**, 2017-2291.

4. A. Y. Chan, I. B. Perry, N. B. Bissonnette, B. F. Buksh, G. A. Edwards, L. I. Frye, O. L. Garry, M. N. Lavagnino, B. X. Li, Y. Liang, E. Mao, A. Millet, J. V. Oakley, N. L. Reed, H. A. Sakai, C. P. Seath and D. W. C. MacMillan, *Chem. Rev.*, 2022, **122**, 1485-1542.

5. A. Hagfeldt, G. Boschloo, L. Sun, L. Kloo and H. Pettersson, *Chem. Rev.*, 2010, **110**, 6595-6663.

6. M. Urbani, G. de la Torre, M. K. Nazeeruddin and T. Torres, *Chem. Soc. Rev.*, 2019, **48**, 2738-2766.

7. D. L. Ashford, M. K. Gish, A. K. Vannucci, M. K. Brennaman, J. L. Templeton, J. M. Papanikolas and T. J. Meyer, *Chem. Rev.*, 2015, **115**, 13006-13049.

8. S. Ardo and G. J. Meyer, *Chem. Soc. Rev.*, 2009, **38**, 115-164.

9. J.-F. Yin, M. Velayudham, D. Bhattacharya, H.-C. Lin and K.-L. Lu, *Coord. Chem. Rev.*, 2012, **256**, 3008-3035.

10. N. J. Lundin, A. G. Blackman, K. C. Gordon and D. L. Officer, *Angew. Chem. Int. Ed.*, 2006, **45**, 2582-2584.

11. C. Fan and C. Yang, *Chem. Soc. Rev.*, 2014, **43**, 6439-6469.

12. K. Y. Zhang, Q. Yu, H. Wei, S. Liu, Q. Zhao and W. Huang, *Chem. Rev.*, 2018, **118**, 1770-1839.

13. D. Parker, J. D. Fradgley and K.-L. Wong, *Chem. Soc. Rev.*, 2021, **50**, 8193-

8213.

14. R. Zhang and J. Yuan, *A.Chemical Research*, 2020, **53**, 1316-1329.

15. R. Horvath and K. C. Gordon, *Inorganica Chim. Acta*, 2011, **374**, 10-18.

16. A. E. Friedman, J. C. Chambron, J. P. Sauvage, N. J. Turro and J. K. Barton, *J. Am. Chem. Soc.*, 1990, **112**, 4960-4962.

17. P. Müller and K. Brettel, *Photochem Photobiol Sci*, 2012, **11**, 632-636.

18. D. M. Roundhill, in *Photochemistry and Photophysics of Metal Complexes*, ed. D. M. Roundhill, Springer US, Boston, MA, 1994, pp. 67-115.

19. D. M. Roundhill, in *Photochemistry and Photophysics of Metal Complexes*, ed. D. M. Roundhill, Springer US, Boston, MA, 1994, pp. 25-65.

20. D. M. Roundhill, in *Photochemistry and Photophysics of Metal Complexes*, ed. D. M. Roundhill, Springer US, Boston, MA, 1994, pp. 1-24.

21. R. Horvath, G. S. Huff, K. C. Gordon and M. W. George, *Coord. Chem. Rev.*, 2016, **325**, 41-58.

22. A. Kumar, S.-S. Sun and A. J. Lees, in *Photophysics of Organometallics*, ed. A. J. Lees, Springer Berlin Heidelberg, Berlin, Heidelberg, 2010, pp. 1-71.

23. S. Ernst and W. Kaim, *J. Am. Chem. Soc.*, 1986, **108**, 3578-3586.

24. T. Phillips, I. Haq, A. J. Meijer, H. Adams, I. Soutar, L. Swanson, M. J. Sykes and J. A. Thomas, *Biochemistry*, 2004, **43**, 13657-13665.

25. H. Takeda, K. Kokie, T. Morimoto, H. Inumaru. and O. Ishitani, *Advances in Inorganic Photochemistry* Elsevier Inc, USA, 2011.

26. H. D. Stoeffler, N. B. Thornton, S. L. Temkin and K. S. Schanze, *J. Am. Chem. Soc.*, 1995, **117**, 7119-7128.

27. E. Hevia, J. Pérez, V. Riera, D. Miguel, S. Kassel and A. Rheingold, *Inorg Chem*, 2002, **41**, 4673-4679.

28. A. Vlček, in *Photophysics of Organometallics*, ed. A. J. Lees, Springer Berlin Heidelberg, Berlin, Heidelberg, 2010, pp. 73-144.

29. J. V. Caspar and T. J. Meyer, *J. Phys. Chem.*, 1983, **87**, 952-957.

30. M. Boraghi and T. A. White, *Inorganica Chim. Acta*, 2021, **526**, 120528.

31. N. Mansour, S. Mehanna, M. A. Mroueh, H. Audi, K. Bodman-Smith, C. F. Daher, R. I. Taleb, M. El-Sibai and R. S. Khnayzer, *Euro. J. Inorg. Chem.*, 2018, **2018**, 2524-2532.

32. M. K. Kuimova, W. Z. Alsindi, J. Dyer, D. C. Grills, O. S. Jina, P. Matousek, A. W. Parker, P. Portius, X. Z. Sun, M. Towrie, C. Wilson, J. Yang and M. W. George, *Dalton Trans*, 2003, 3996-4006.

33. M. K. Kuimova, W. Z. Alsindi, A. J. Blake, E. S. Davies, D. J. Lampus, P. Matousek, J. McMaster, A. W. Parker, M. Towrie, X. Z. Sun, C. Wilson and M. W. George, *Inorg Chem*, 2008, **47**, 9857-9869.

34. B. Adams, G. E. Shillito, N. T. Lucas, M. W. George and K. C. Gordon, *Inorg Chem*, 2017, **56**, 12967-12977.

35. H. van der Salm, C. B. Larsen, J. R. McLay, M. G. Fraser, N. T. Lucas and K. C. Gordon, *Dalton Trans*, 2014, **43**, 17775-17785.

36. J. Dyer, W. J. Blau, C. G. Coates, C. M. Creely, J. D. Gavey, M. W. George, D. C. Grills, S. Hudson, J. M. Kelly, P. Matousek, J. J. McGarvey, J. McMaster, A. W. Parker, M. Towrie and J. A. Weinstein, *Photochem Photobiol Sci*, 2003, **2**, 542-554.

37. H. van der Salm, M. G. Fraser, R. Horvath, S. A. Cameron, J. E. Barnsley, X. Z. Sun, M. W. George and K. C. Gordon, *Inorg Chem*, 2014, **53**, 3126-3140.

38. J. Dyer, C. M. Creely, J. C. Penedo, D. C. Grills, S. Hudson, P. Matousek, A. W. Parker, M. Towrie, J. M. Kelly and M. W. George, *Photochem Photobiol Sci*, 2007, **6**, 741-748.

39. Q. Cao, C. M. Creely, E. S. Davies, J. Dyer, T. L. Easun, D. C. Grills, D. A. McGovern, J. McMaster, J. Pitchford, J. A. Smith, X. Z. Sun, J. M. Kelly and M. W. George, *Photochem Photobiol Sci*, 2011, **10**, 1355-1364.

40. S. Sato, T. Morimoto and O. Ishitani, *Inorg Chem*, 2007, **46**, 9051-9053.

41. K. Saita, Y. Harabuchi, T. Taketsugu, O. Ishitani and S. Maeda, *Phys. Chem. Chem. Phys.*, 2016, **18**, 17557-17564.

42. S. Sato, A. Sekine, Y. Ohashi, O. Ishitani, A. M. Blanco-Rodríguez, A. Vlček, Jr., T. Unno and K. Koike, *Inorg Chem*, 2007, **46**, 3531-3540.

43. S. Sato, Y. Matubara, K. Koike, M. Falkenström, T. Katayama, Y. Ishibashi, H. Miyasaka, S. Taniguchi, H. Chosrowjan, N. Mataga, N. Fukazawa, S. Koshihara, K. Onda and O. Ishitani, *Chem. Eur. J*, 2012, **18**, 15722-15734.

44. J. R. Schoonover and G. F. Strouse, *Chem. Rev.*, 1998, **98**, 1335-1356.

45. *Handbook of Instrumental Techniques for Analytical Chemistry*, 1997.

46. K. E. A. Reynolds, PhD Thesis, University of Nottingham, 2020.

47. X. Wu, PhD Thesis, University of Nottingham, 2019.

48. B. Wardle, *Principles and Applications of Photochemistry*, John Wiley & Sons Ltd, England, 2009.

49. M. Montalti, A. Credi, L. Prodi and M. T. Gandolfi, *Handbook of photochemistry*, CRC/Taylor & Francis, Boca Raton, 3rd edn., 2006.

50. G. D. Smith and R. A. Palmer, in *Handbook of Vibrational Spectroscopy*, eds. J. M. Chalmer and P. R. Griffiths, 2006, pp. 666-681.

51. C. Rödig and F. Siebert, in *Handbook of Vibrational Spectroscopy*, eds. J. M. Chalmer and P. R. Griffiths, 2006, pp. 682-695.

52. D. C. Grills and M. W. George, in *Handbook of Vibrational Spectroscopy*, eds. J. M. Chalmer and P. R. Griffiths, 2006, pp. 718-733.

53. G. Bistoni, *Chem. Sci.*, 2016, **7**, 1174-1184.

54. J. M. Butler, M. W. George, J. R. Schoonover, D. M. Dattelbaum and T. J. Meyer, *Coord. Chem. Rev.*, 2007, **251**, 492-514.

55. K. Schindler and F. Zobi, *Molecules*, 2022, **27**.

56. R. J. Fernández-Terán and L. Sévery, *Inorg Chem*, 2021, **60**, 1325-1333.

57. J. R. Shakirova, S. Nayeri, S. Jamali, V. V. Porsev, V. V. Gurzhiy, O. V. Levin, I. O. Koshevoy and S. P. Tunik, *ChemPlusChem*, 2020, **85**, 2518-2527.

58. H. Atallah, C. M. Taliaferro, K. A. Wells and F. N. Castellano, *Dalton Trans*,

2020, **49**, 11565-11576.

59. J. L. Smithback, J. B. Helms, E. Schutte, S. M. Woessner and B. P. Sullivan, *Inorg Chem*, 2006, **45**, 2163-2174.

60. S. Sato and O. Ishitani, *Coord. Chem. Rev.*, 2015, **282-283**, 50-59.

61. D. A. Kurtz, B. Dhakal, E. S. Donovan, G. S. Nichol and G. A. N. Felton, *Inorg Chem Communications*, 2015, **59**, 80-83.

62. K. Schindler, A. Crochet and F. Zobi, *RSC Advances*, 2021, **11**, 7511-7520.

63. D. A. Kurtz, K. R. Brereton, K. P. Ruoff, H. M. Tang, G. A. N. Felton, A. J. M. Miller and J. L. Dempsey, *Inorg Chem*, 2018, **57**, 5389-5399.

64. T. Auvray, B. Del Secco, A. Dubreuil, N. Zaccheroni and G. S. Hanan, *Inorg Chem*, 2021, **60**, 70-79.

65. I. M. Lorkovic, M. S. Wrighton and W. M. Davis, *Journal of the American Chemical Society*, 1994, **116**, 6220-6228.

66. F. Zobi, L. Kromer, B. Spingler and R. Alberto, *Inorg Chem*, 2009, **48**, 8965-8970.

67. U. Abram, R. Hübener, R. Alberto and R. Schibli, *Zeitschrift für anorganische und allgemeine Chemie*, 1996, **622**, 813-818.

68. S. Nasiri Sovari, I. Kolly, K. Schindler, Y. Cortat, S.-C. Liu, A. Crochet, A. Pavic and F. Zobi, *Journal*, 2021, **26**.

69. E. Schutte, J. B. Helms, S. M. Woessner, J. Bowen and B. P. Sullivan, *Inorg Chem*, 1998, **37**, 2618-2619.

70. K. Koike, J. Tanabe, S. Toyama, H. Tsubaki, K. Sakamoto, J. R. Westwell, F. P. A. Johnson, H. Hori, H. Saitoh and O. Ishitani, *Inorg Chem*, 2000, **39**, 2777-2783.

71. H. Tsubaki, A. Sekine, Y. Ohashi, K. Koike, H. Takeda and O. Ishitani, *J. Am. Chem. Soc.*, 2005, **127**, 15544-15555.

72. T. Morimoto, M. Ito, K. Koike, T. Kojima, T. Ozeki and O. Ishitani, *Chem. Eur. J*, 2012, **18**, 3292-3304.

73. N. Dyachenko, unpublished work.

74. P. A. Summers, B. S. Adams, N. Ibrahim, K. E. A. Reynolds, K. L. Fow, E. S. Davies, M. Towrie and M. W. George, *Vibr. Spectroscopy*, 2019, **100**, 86-92.

75. M. Pavlović, S. Nikolić, N. Gligorijević, B. Dojčinović, S. Aranđelović, S. Grgurić-Šipka and S. Radulović, *JBIC J. Biological Inorg. Chem.*, 2019, **24**, 297-310.

76. L. A. Saghatforoush, R. Mehdizadeh and F. Chalabian, *Trans. Metal Chem.*, 2010, **35**, 903-910.

77. M. H. Abraham and R. J. Abraham, *New Journal of Chemistry*, 2017, **41**, 6064-6066.

78. T. Hayashida, H. Kondo, J.-i. Terasawa, K. Kirchner, Y. Sunada and H. Nagashima, *J. Organometallic Chem.*, 2007, **692**, 382-394.

79. K. R. Cairns, W. Levason, G. Reid and W. Zhang, *Polyhedron*, 2021, **207**, 115367.

80. M. Kaplanis, G. Stamatakis, V. D. Papakonstantinou, M. Paravatou-Petsotas, C. A. Demopoulos and C. A. Mitsopoulou, *J. Inorg. Biochem.*, 2014, **135**, 1-9.

81. J. Shakeri, H. Farrokhpour, H. Hadadzadeh and M. Joshaghani, *RSC Advances*, 2015, **5**, 41125-41134.

82. W. Z. Antkowiak and A. Sobczak, *Tetrahedron*, 2001, **57**, 2799-2805.

83. B. Batanero and F. Barba, *Organic Letters*, 2005, **7**, 2567-2569.

84. T. A. Engesser, D. Kratzert and I. Krossing, *Zeitschrift für anorganische und allgemeine Chemie*, 2018, **644**, 652-656.

85. G. Garwood, PhD Thesis, University of Nottingham, 2022.

86. R. J. Shaver and D. P. Rillema, *Inorg Chem*, 1992, **31**, 4101-4107.

87. R. J. Shaver, D. P. Rillema and C. Woods, *J. Chem. Soc., Chemical Communications*, 1990, DOI: 10.1039/C39900000179, 179-180.

88. S. Bernhard, K. M. Omberg, G. F. Strouse and J. R. Schoonover, *Inorg Chem*, 2000, **39**, 3107-3110.

89. P. Coppens, J. Sokolow, E. Trzop, A. Makal and Y. Chen, *J. Phys. Chem. L.*, 2013, **4**, 579-582.